NASA-CR-204753

NASA Grant No. NAG8-963

Microstructural Development during Directional Solidification of Peritectic Alloys

Final Technical Report

Grant Period: October 1, 1993 - December 31, 1996

Principal Investigator: Dr. Thomas A. Lograsso

Institute for Physical Research and Technology
Iowa State University
Ames, Iowa 50011

Microstructural Development during Directional Solidification of Peritectic Alloys

Introduction

A thorough understanding of the microstructures produced through solidification in peritectic systems has yet to be achieved, even though a large number of industrially and scientifically significant materials are in this class. One type of microstructure frequently observed during directional solidification consists of alternating layers of primary solid and peritectic solid oriented perpendicular to the growth direction [1-10]. This layer formation is usually reported for alloy compositions within the two-phase region of the peritectic isotherm and for temperature gradient and growth rate conditions that result in a planar solid-liquid interface. Layered growth in peritectic alloys has not previously been characterized on a quantitative basis, nor has a mechanism for its formation been verified. The mechanisms that have been proposed for layer formation can be categorized as either extrinsic [1,4,10] or intrinsic [2,3,5,11] to the alloy system. The extrinsic mechanisms rely on externally induced perturbations to the system for layer formation, such as temperature oscillations, growth velocity variations, or vibrations. The intrinsic mechanisms approach layer formation as an alternative type of two phase growth that is inherent for certain peritectic systems and solidification conditions. Convective mixing of the liquid is an additional variable which can strongly influence the development and appearance of layers due to the requisite slow growth rate. The first quantitative description of layer formation is a model recently developed by Trivedi based on the intrinsic mechanism of cyclic accumulation and depletion of solute in the liquid ahead of the interface, linked to repeated nucleation events in the absence of convection [12]. The objective of this research is to characterize the layered microstructures developed during ground-based experiments in which external influences have been minimized as much as possible and to compare these results to the current the model. Also, the differences between intrinsic and externally influenced layer formation were explored.

The choice of alloy system is critical to a study of the formation of layered microstructures. The ideal system would have a well-characterized phase diagram, equal densities of both elements in the liquid state to minimize compositionally-driven convective flows, a low peritectic temperature to simplify directional solidification and the achievement of a high temperature gradient in the liquid, a broad composition range for the peritectic reaction, and a reasonable hardness at room temperature to facilitate handling and metallographic preparation. The In-Sn system was selected initially due to a very low peritectic temperature and the nearly equal densities of In and Sn in the liquid state. Since the In-rich peritectic reaction had apparently not been utilized previously for solidification research, experiments were conducted to check the phase diagram in the region of interest (see Section I and Reference 13). The alloys in this system proved to be difficult to handle and prepare in bulk form with the equipment available, so experiments were initiated with the Sn-Cd system. Layered microstructures had been observed previously in Sn-Cd alloys [2,5]. The solute element Cd is expected to be more dense in the liquid state than Sn, which should minimize convection when solidification occurs upward as was done for this research. A review of the phase diagram literature revealed a

discrepancy in the position of the peritectic phase field at the peritectic temperature. Directional solidification experiments confirmed the version in the most recently published phase diagram evaluation (see Section II and Reference 14). After selecting an intermediate alloy composition which yielded a reasonably regular layered microstructure, directional solidification experiments were conducted over a range of growth velocities (see Section III and Reference 15). The arrangement of the solid phases and other microstructural features were characterized, and the layer lengths and layer compositions were measured as a function of solidification distance. These experiments were then repeated for a range of alloy compositions and a limited number of growth velocities to investigate the effect of overall composition (see Section IV). Finally, these alloys were also solidified in the presence of temperature oscillations to study the interaction between the natural formation mechanism and external influences (see Section V).

References

1. N. J. W. Barker and A.Hellawell: *Met. Sci.*, 1974, vol. 8, pp. 353-356.
2. W. J. Boettinger: *Metall. Trans.*, 1974, vol. 5, pp. 2023-2031 .
3. A. P. Titchener and J. A. Spittle: *Acta Metall.*, 1975, vol. 23, pp. 497-502.
4. A. Ostrowski and E. W. Langer: in *Solidification and Casting of Metals*, The Metals Society, London, 1979, pp. 139-143.
5. H. D. Brody and S. A. David: in *Solidification and Casting of Metals*, The Metals Society, London, 1979, pp. 144-151.
6. D. J. Larson, R. G. Pirich, and W. R. Wilcox, Annual Report on Contract NAS8-32998, Marshall Space Flight Center, 1981.
7. B. C. Fuh: Ph.D. Dissertation, Iowa State University, Ames, IA, 1984.
8. B. F. Oliver and B. Kad: *J. Less-Common Met.*, 1991, vol. 168, pp. 81-90.
9. J. H. Lee and J. D. Verhoeven: *J. Cryst. Growth*, 1994, vol. 144, pp. 353-366.
10. J. W. Rutter, M. G. Julien, and G. R. Purdy: *Mater. Sci. and Technol.*, 1995, vol. 11, pp. 1233-1240.
11. M. Hillert: in *Solidification and Casting of Metals*, The Metals Society, London, 1979, pp. 81-87.
12. R. Trivedi: *Metall. and Mater. Trans. A*, 1995, vol. 26A, pp. 1583-1589.
13. K. L. Zeisler-Mashl and T. A. Lograsso: *J. Phase Equilibria*, 1995, vol. 16, pp. 516-519.
14. K. L. Zeisler-Mashl and T. A. Lograsso: *J. Phase Equilibria*, 1996, vol. 17, pp. 7-9.
15. K. L. Zeisler-Mashl and T. A. Lograsso: Accepted October 1996 for publication in *Metall. and Mater. Trans. A*.

Section I: Determination of the In-Rich Peritectic Region in the In-Sn System by Differential Scanning Calorimetry

Abstract

Phase compositions at the In-rich peritectic isotherm in the In-Sn phase diagram and related liquidus and solidus slopes were determined through differential scanning calorimetry. The resultant liquid composition at the peritectic temperature was essentially the same as reported in previous work [1,2], but the compositions of primary (In) and peritectic β were significantly higher in the solute element Sn than previously reported. These higher levels of Sn are most likely due to reduced microsegregation resulting from the very slow heating and cooling rates utilized in this work.

Unidirectional solidification in binary peritectic alloy systems yields a variety of microstructures, depending on such factors as imposed growth rate and temperature gradient and the overall alloy composition relative to the compositions at the peritectic isotherm [3,4]. In an ongoing program to characterize such microstructures and model their development, the In-Sn system was chosen for study, in part due to the relatively low temperature peritectic reaction in the In-rich region of the phase diagram. The research described in this note was driven by the need for accurate values of the phase compositions and liquidus and solidus slopes at the peritectic isotherm.

Alloys of the desired compositions were prepared by melting 20 g batches of In and Sn of 99.99% purity in graphite crucibles in air and chill-casting into buttons. A piece from each button, approximately 4 g in size, was rolled to a thickness of 1 mm, and disks of about 5 mm in diameter and weighing 130 mg were punched from the sheet. These disks were utilized for both compositional and thermal analysis. The alloys were allowed to equilibrate at room temperature for several weeks prior to analysis.

Alloy compositions were selected to extend past the range of the most recently published values for phase compositions at the peritectic isotherm of 10 at.% Sn (10.3 wt.% Sn) for the primary In-rich solid solution and 14 at.% Sn (14.4 wt.% Sn) for the liquid [5]. Thirteen samples were prepared with nominal compositions varying from 5.8 to 17.5 at.% Sn (6 to 18 wt.% Sn) in 1 at.% Sn (1 wt.% Sn) increments. It should be noted that compositions were determined in wt.% Sn and converted to at.% Sn using atomic mass values of 114.82 and 118.69 g/mole for In and Sn, respectively. Chemical analyses were conducted on five of the thirteen alloys to verify the Sn contents and to determine the levels of trace contaminants. The Sn contents were measured using inductively coupled plasma-atomic emission spectrometry (ICP-AES) to 95% confidence limits of better than ±0.1 at.% Sn (±0.1 wt.% Sn) by analyzing each sample solution six times with a standard solution run between each sample analysis. In addition, the Sn levels in three disks of a single composition were determined to evaluate alloy homogeneity; the measured Sn contents were the same. The ICP-AES analyses of the five alloys indicated that the actual

alloy compositions were an average of 0.1 at.% Sn (0.1 wt.% Sn) below the target compositions. As a consequence, all of the actual alloy compositions were assumed to be 0.1 at.% Sn (0.1 wt.% Sn) lower than the target compositions. The levels of the most likely contaminants, C, O, and N, were determined and found to be insignificant (less than 50 ppm by weight). Based on these results, the alloy compositions reported in Table 1 are representative of each alloy batch and reliable to within 0.1 at.% Sn (0.1 wt.% Sn).

Temperatures at the phase boundaries were acquired through differential scanning calorimetry (DSC) as follows. Samples were placed in Al pans with press-fit lids; the high malleability of the In alloys ensured good thermal contact. The sample temperature was measured with a type K thermocouple. A flowing N_2 atmosphere was employed during testing to prevent oxidation. Prior to analyzing samples of the various alloys, the DSC unit was calibrated against a sample of the pure In used to make the alloys which had been prepared by the same procedure; the temperature correction was negligible. The DSC unit and sample were equilibrated at a temperature approximately 10°C below the lowest temperature of interest for the given sample. The temperature was then increased at a rate of 0.1°C/min to a temperature approximately 10°C above the highest temperature of interest. A cooling cycle was then conducted at the same rate, and the complete heating/cooling cycle was repeated for comparison. From the resultant heat flow versus temperature plots, the onset temperatures were determined as the intersection of the tangent to the initial side of the peak with the baseline level. For cases where undercooling was evident ((In) and β liquidus boundaries), the onset temperature was defined as the highest temperature observed after the heat flow deviated from the baseline level. Solidus temperatures and the peritectic temperature were measured from the heating cycles, while liquidus temperatures and the peritectic temperature were obtained from the cooling cycles. Since the peritectic temperature is constant in a binary system, the error in temperature determination inherent to this procedure can be estimated from these values. The average of the measured peritectic temperatures at 95% confidence limits is within ±0.1°C of the true value. Assuming that the measurement distributions were similar for the other temperatures, error bars at 95% confidence limits were approximated for these temperatures by decreasing the number of measurements in the error equation.

The onset temperatures from both the first and second heating and cooling cycles are reported in Table 1. The phase transition represented by each onset temperature was assigned based on the assumption of a peritectic reaction similar to those reported previously [1,2,5]. The values determined for the peritectic temperature from both of the heating and cooling cycles are quite similar, which suggests that temperatures obtained from the different cycles can be directly compared without the application of any correction. The temperatures for the (In) liquidus, (In) solidus, and β liquidus also exhibit no significant differences between the two cycles. However, the β solidus temperatures obtained from the second heating cycle are lower in all cases than those obtained from the first heating cycle, which is consistent with the occurrence of microsegregation during the first cooling cycle. For this reason, only the values for the β solidus from the first heating cycle will be used to develop the experimental phase diagram. These β solidus temperatures and the averages of the temperatures for the (In) liquidus, (In) solidus, β liquidus, and peritectic isotherm are plotted in Figure 1. An additional point shown clearly in Figure 1 is that the peritectic reaction occurred at alloy compositions with lower Sn levels than allowed by the intersection of the peritectic isotherm and the (In) solidus, namely at 9.6, 10.6,

and 11.6 at.% Sn (9.9, 10.9, and 11.9 wt.% Sn). The detection of the peritectic reaction at these compositions is again related to microsegregation during solidification, which caused a small amount of liquid to be present at the peritectic temperature. The degree of microsegregation was apparently insufficient to affect the measurement of the temperatures at the (In) solidus, since no deviation in this boundary is evident at compositions close to the peritectic reaction.

Phase boundaries for the diagram were developed by fitting equations to the data in Table 1. Linear equations were used for the final version rather than second or third order polynomials, because extrapolations of the boundaries thus obtained were more correct and the closeness of fit was almost the same. Three other conditions were also applied to these equations in order to obey phase rules. 1). The (In) liquidus and solidus should meet at the equilibrium melting temperature of pure In. This condition was met by the fitted equations for the data, although at a temperature 0.5°C below the reported melting point [5]. 2). The (In) liquidus and β liquidus should cross at the peritectic temperature, which was accomplished by adjusting the equation for the β liquidus slightly. 3). The β liquidus and solidus should meet at the metastable melting point of pure In in the β form. Assuming that the metastable extensions of the β liquidus and solidus can be represented by straight lines, the equation for the β solidus was altered to intersect the β liquidus at 0% Sn. The resultant phase boundaries are included in Figure 1. Values at the peritectic isotherm and equations for the phase boundaries are reported in Table 2.

The phase boundaries determined in this work coincide in certain respects with those previously published by Evans and Prince [2] and by Okamoto [5], which is based in this region primarily on the work of Heumann and Alpaut [1]. The peritectic temperature and the value given by the (In) liquidus and β liquidus at the peritectic isotherm are quite similar (see Tables 2 and 3). However, the compositions of (In) and β at the peritectic temperature reported in the earlier work are significantly lower in Sn content. The most likely cause for these differences is the relative degree of chemical homogeneity in the solid during thermal analysis. The significantly lower heating and cooling rates employed in this work (0.1°C/min compared to 0.5 or 1°C/min) should have reduced the amount of microsegregation. Microsegregation during cooling has the effect of shifting the onset temperatures for solidus boundaries to lower compositions, as well as extending the compositional range over which the peritectic reaction is detected.

Acknowledgments

The authors would like to thank J. L. Amenson of the Materials Analysis and Research Laboratory at Iowa State University for running the DSC experiments. J. T. Wheelock of the Materials Preparation Center at Ames Laboratory cast and rolled the initial material; other MPC personnel performed the compositional analyses. This work was supported by the National Aeronautics and Space Administration under NASA Grants #NAG8-963 and #NAGW-2601 and was performed at Ames Laboratory. Ames Laboratory is operated for the U. S. Department of Energy by Iowa State University under contract No. W-7405-ENG-82.

References

1. T. Heumann and O. Alpaut: *J. Less-Common Metals*, 1964, vol. 6, pp. 108-117.

2. D. S. Evans and A. Prince: in *Alloy Phase Diagrams*, Elsevier Science Publishing Co., Inc., New York, 1983, pp. 389-394.

3. W. J. Boettinger: *Metall. Trans.*, 1974, vol. 5, pp. 2023-2031.

4. H. D. Brody and S. A. David: in *Solidification and Casting of Metals*, The Metals Society, London, 1979, pp. 144-151.

5. H. Okamoto: in *Phase Diagrams of Indium Alloys and Their Engineering Applications*, ASM International, Materials Park, OH, 1992, pp. 255-257.

Table 1. Transition Temperatures from DSC Data

Alloy Composition in At.% Sn (Wt.% Sn)	Temperatures from Heating Cycles (°C)			Temperatures from Cooling Cycles (°C)		
	(In) Solidus	Peritectic Temp.	β Solidus	(In) Liquidus	Peritectic Temp.	β Liquidus
5.7 (5.9)	149.2			149.9		
	148.9			149.4		
6.7 (6.9)	147.7			148.4		
	147.7			148.2		
7.7 (7.9)	146.3			147.6		
	146.3			147.5		
8.6 (8.9)	145.2			146.2		
	145.4			146.3		
9.6 (9.9)	143.9			145.1	140.2	
	143.7	139.9		145.1	140.3	
10.6 (10.9)	142.5			143.9	140.2	
	142.3	140.5		144.1	140.2	
11.6 (11.9)	141.4	140.6		143.0	140.2	
	141.1	140.6		143.2	140.2	
12.5 (12.9)	140.8	140.6		141.5	140.2	
	140.8	140.6	140.4	141.5	140.2	
13.5 (13.9)		140.5	139.9	141.0	140.2	
		140.7	138.3	141.0	140.0	
14.5 (14.9)			139.0			139.6
			138.3			139.6
15.5 (15.9)			137.7			138.6
			137.5			138.6
16.4 (16.9)			137.2			137.7
			136.5			137.8
17.4 (17.9)			136.4			136.8

Alloy Composition in At.% Sn (Wt.% Sn)	Temperatures from Heating Cycles (°C)			Temperatures from Cooling Cycles (°C)		
	(In) Solidus	Peritectic Temp.	β Solidus	(In) Liquidus	Peritectic Temp.	β Liquidus
			135.9			136.7

Table 2. Values for In-Sn Phase Diagram

Peritectic Isotherm	
Peritectic temperature	140.3°C
(In) composition	12.5 at.% Sn (12.9 wt.% Sn)
β composition	13.4 at.% Sn (13.75 wt.% Sn)
Liquid composition	13.9 at.% Sn (14.3 wt.% Sn)
Equations for Phase Boundaries	
(In) liquidus	T (°C) = 156.1 - 1.104C (wt.% Sn)
(In) solidus	T (°C) = 156.1 - 1.226C (wt.% Sn)
β liquidus	T (°C) = 154.6 - 0.9988C (wt.% Sn)
β solidus	T (°C) = 154.6 - 1.038C (wt.% Sn)

Table 3. Peritectic Isotherm Values from Literature

Value at Isotherm	**Heumann and Alpaut [1]**	**Evans and Prince [2]**
Peritectic temperature	143°C	141°C
(In) composition	10.0 at.% Sn	11.5 at.% Sn
β composition	12.0 at.% Sn	12.0 at.% Sn
Liquid composition	14.0 at.% Sn	14.0 at.% Sn

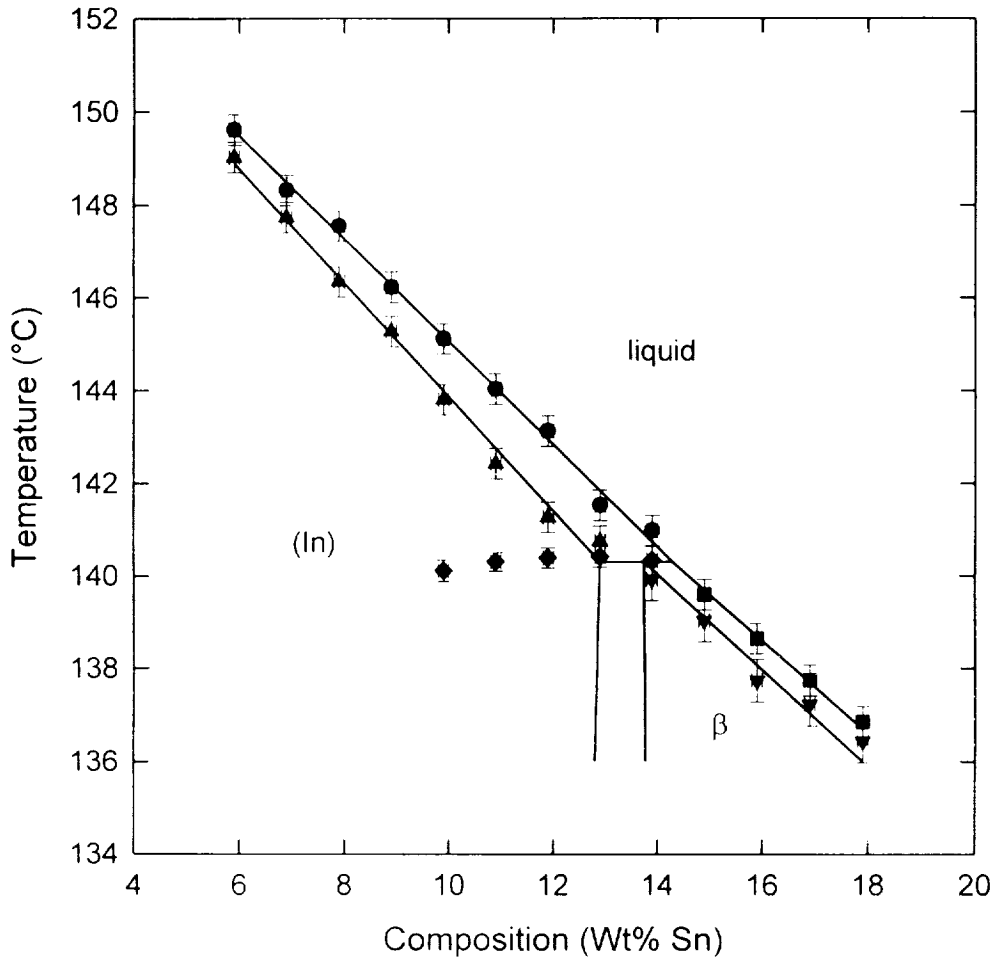

Figure 1. Section of the In-Sn phase diagram showing data from the first heating cycle for the β solidus (▼) and average values for the (In) liquidus (●), (In) solidus (▲), β liquidus (■), and peritectic isotherm (◆). The (In) and β solvus boundaries were drawn using the lower temperature data of Heumann and Alpaut [1].

Section II: Measurement of the Peritectic Phase Composition in the Sn-Cd System through Directional Solidification Techniques

As part of a research program aimed at characterizing and modeling the microstructures produced in binary peritectic alloy systems during directional solidification, recent efforts have focused on determining and verifying phase compositions at the peritectic isotherm in the Sn-Cd system. Previous work utilizing this system [1,2] referred to a phase diagram [3] which differs from the current evaluation [4] in the peritectic region (see Figure 1). The most significant difference between the two versions is the location of the β phase field. The lower Cd level of 1.0 at.% Cd (0.9 wt.% Cd) given for β at the peritectic temperature in the current assessment is based primarily on the work of Evans and Prince [5]. Other values determined previously for this β composition are 2.0 at.% Cd (1.9 wt.% Cd) [6] and 1.5 at.% Cd (1.4 wt.% Cd) [7]. To verify the β composition at the peritectic isotherm for this study, two quite different techniques were attempted: differential scanning calorimetry (DSC) and directional solidification combined with electron probe microanalysis. The DSC instrumentation and procedure utilized did not produce conclusive results for the Sn-Cd system. As an alternative method for gathering phase diagram information, an existing directional solidification apparatus was used to grow a sample which supplied the requisite phase composition through electron microprobe examination.

Directional solidification is based on unidirectional heat flow parallel to the sample axis in the vicinity of the solid-liquid interface, such that the isotherms are perpendicular to the sample axis and growth direction. This situation can be achieved by placing one end of the sample in a hot chamber and the other end in a cold chamber with an insulator located in an intermediate position at the solid-liquid interface to prevent radial heat flow. Prior to the start of directional solidification, the sample is assumed to be in thermal equilibrium with a planar solid-liquid interface, a uniform solid composition near the interface, and a homogeneous liquid composition. Movement of either the sample or the hot chamber and cold chamber relative to the sample initiates directional solidification. When directional solidification begins, solute (Cd in this case) is rejected into the liquid at the interface. This solute accumulation causes the solute concentration of the liquid near the interface to increase. The solute concentration of the solid at the interface increases as well, since the solid and liquid compositions are linked through the requirements for localized equilibrium. If a sample with a solute concentration slightly greater than that of the liquid at the peritectic isotherm is directionally solidified, the composition of the first β solid to form will be approximately that of β at the peritectic temperature. In practice, the determination of this composition requires measuring the solute accumulation in the solid that occurred during the first stage of directional growth and extrapolating back to the lowest solid composition at the onset of solidification (see Figure 2).

Material of the desired composition was prepared by melting 100 g batches of Sn and Cd of 99.99% purity in evacuated and Ar back-filled fused silica crucibles followed by agitation and quenching into water to promote homogeneity. These cast rods were then swaged to 5.1 mm in diameter. Transverse sections approximately 1 mm thick weighing 150 mg were cut for DSC and bulk compositional analysis. The actual sample compositions were determined by inductively coupled plasma-atomic emission spectrometry (ICP-AES) to 95% confidence limits

of better than 0.1 % Cd. It should be noted that compositions were determined in wt.% Cd and converted to at.% Cd with atomic mass values of 118.69 and 112.40 g/mole for Sn and Cd, respectively.

For DSC analyses, samples with compositions of 1.1, 1.5, and 1.8 at.% Cd (1.0, 1.4, and 1.7 wt.% Cd) were heated and cooled at a rate of 0.1°C/min through a temperature range of roughly 190 to 240°C. This procedure worked well for a previous investigation in the peritectic region of the In-Sn system [8], but yielded inconclusive results in the case of Sn-Cd. During the heating cycle, no peak was observed which could be matched with the β solidus. Since β decomposes through a eutectoid reaction at 133°C, this lack of a transition peak might be attributed to insufficient time for β to form once the material was heated above that temperature. During the cooling cycle, the undercooling apparently required for the formation of α was severe enough that in some cases even the peritectic reaction was masked. Rather than attempt to design a more complicated heating and cooling schedule for the DSC equipment available which would have increased analysis costs, directional solidification techniques were utilized instead.

The target composition for the directional solidification sample was slightly higher than the liquid composition of 4.0 at.% Cd (3.8 wt.% Cd) at the peritectic isotherm. The actual composition was determined to be 4.1 at.% Cd (3.9 wt.% Cd). A section of swaged rod with a mass of 28 g was solidified vertically upward in a 6 mm ID fused silica crucible as described in more detail in [9]. The microstructure which developed in the region of initial directional solidification is shown in Figure 3. The start of directional solidification was apparent from the microstructure and is indicated on the figure. Beta appeared to be the only solidification product. The "β" solid in the micrograph has a somewhat mottled appearance due to the fact that it decomposed through the eutectoid transformation during cooling. The transformed β is a two-phase mixture of (Sn) and (Cd), but for simplicity will be referred to as β.

The β composition profile in the vicinity of the initial directional solidification was developed by analyzing a series of points using an electron microprobe with wavelength dispersive spectrometers and pure elemental standards. The electron beam was defocused to a 10-15 μm diameter in order to increase sampling volume. At a given solidification distance in the region of interest, 54 points spaced 0.1 mm apart were analyzed along a line perpendicular to the growth direction. These values were averaged to obtain a β composition for that particular solidification distance. This procedure was repeated at 0.2 mm intervals parallel to the growth direction. The resulting composition profile, corresponding to the area near the start of directional solidification in Figure 3, is shown in Figure 4. The β composition at the onset of directional solidification is 1.1 at.% Cd (1.0 wt.% Cd) to a 95% confidence limit of 0.1 % Cd. As stated previously, this composition is also the β composition at the peritectic temperature. This value agrees with the currently accepted value given by Evans and Prince [5] within the error limits of the technique. Thus, directional solidification combined with electron microprobe analyses provided an alternative means for obtaining the peritectic phase composition without the need for multiple sample compositions and analyses as would be required for more conventional DSC techniques.

Acknowledgments

The authors would like to thank R. Trivedi of Ames Laboratory-U. S. Department of Energy and the Department of Materials Science and Engineering at Iowa State University for helpful discussions. A. Kracher of the Department of Geological and Atmospheric Sciences at Iowa State University conducted the electron microprobe analyses. This work was supported by the National Aeronautics and Space Administration under NASA Grant #NAG8-963 and was performed at Ames Laboratory. Ames Laboratory is operated for the U. S. Department of Energy by Iowa State University under contract No. W-7405-ENG-82.

References

1. W. J. Boettinger: *Metall. Trans.*, 1974, vol. 5, pp. 2023-2031 .
2. H. D. Brody and S. A. David: in *Solidification and Casting of Metals*, The Metals Society, London, 1979, pp. 144-151.
3. W. T. Pell-Walpole: in *Metals Handbook*, ASM, Cleveland, 1948, pp. 1189-1190.
4. J. Dutkiewicz, L. Zabdyr, Z. Moser, and J. Salawa: *Bull. Alloy Phase Diagrams*, 1989, vol. 10, pp. 223-229.
5. D. S. Evans and A. Prince: *Thermochim. Acta*, 1982, vol. 58, pp. 199-209.
6. D. Hanson and W. T. Pell-Walpole: *J. Inst. Met.*, 1936, vol. 59, pp. 281-300.
7. C. E. Homer and H. Plummer: *J. Inst. Met.*, 1939, vol. 64, pp. 169-200.
8. K. L. Zeisler-Mashl and T. A. Lograsso: *J. Phase Equilibria*, 1995, vol. 16, pp. 516-519.
9. K. L. Zeisler-Mashl and T. A. Lograsso: Accepted October 1996 for publication in *Metall. and Mater. Trans. A*.

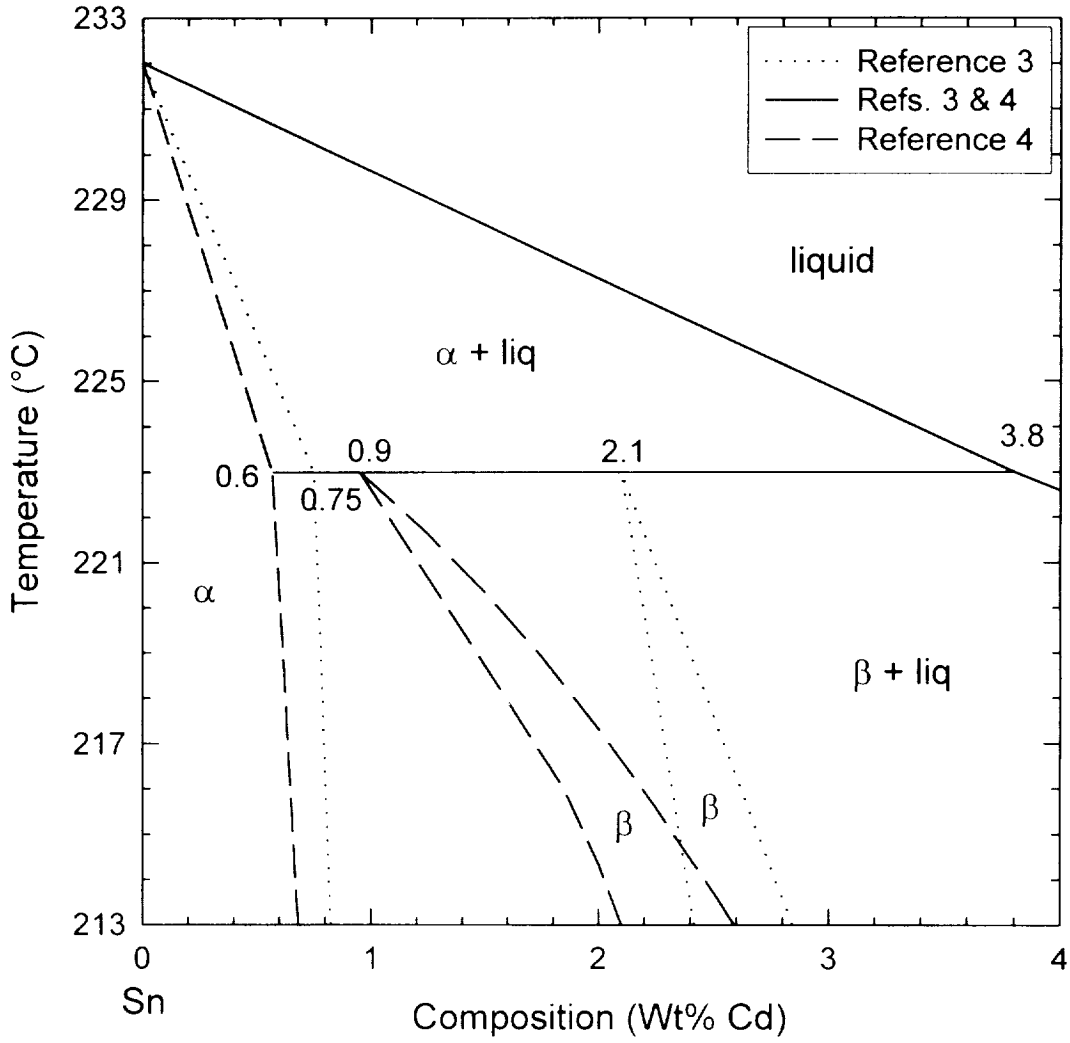

Figure 1. The peritectic region in the Sn-Cd phase diagram redrawn from the work of Pell-Walpole [3] and Dutkiewicz *et al.* [4].

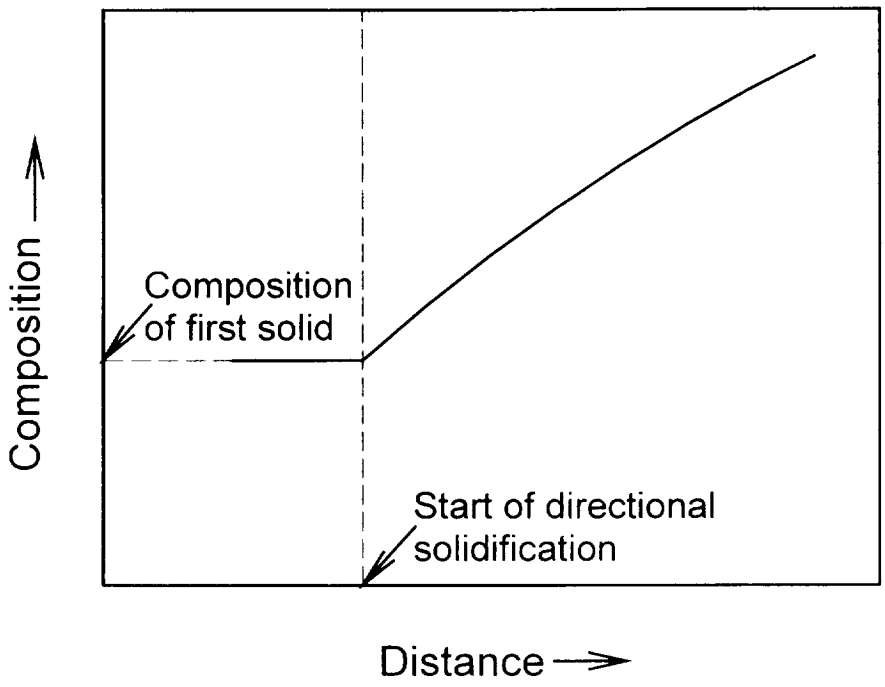

Figure 2. Schematic diagram showing the composition profile in the region corresponding to the start of directional solidification.

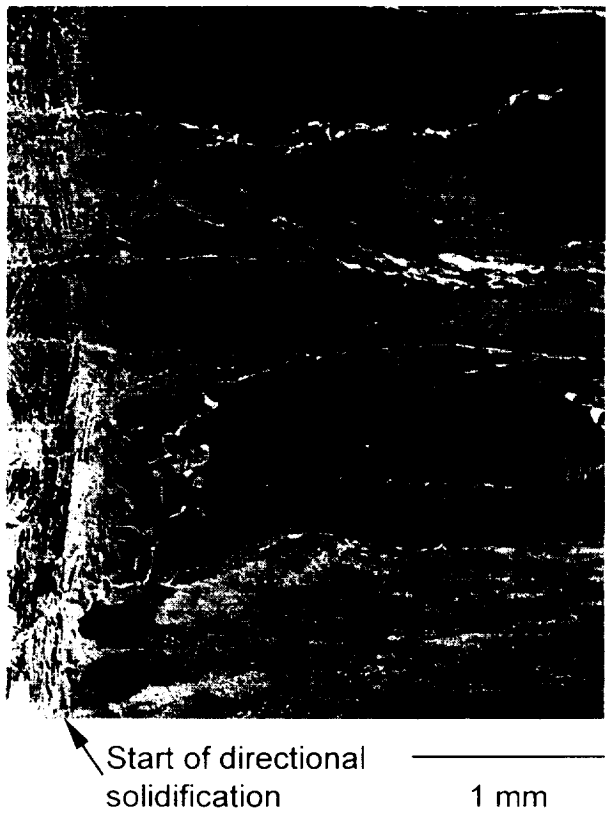

Figure 3. Optical micrograph of a longitudinal section through the center of the sample showing the initial directional solidification region. The starting point for directional solidification is indicated on the figure. While the sample was solidified vertically upward, the micrograph is oriented such that the growth direction is from left to right.

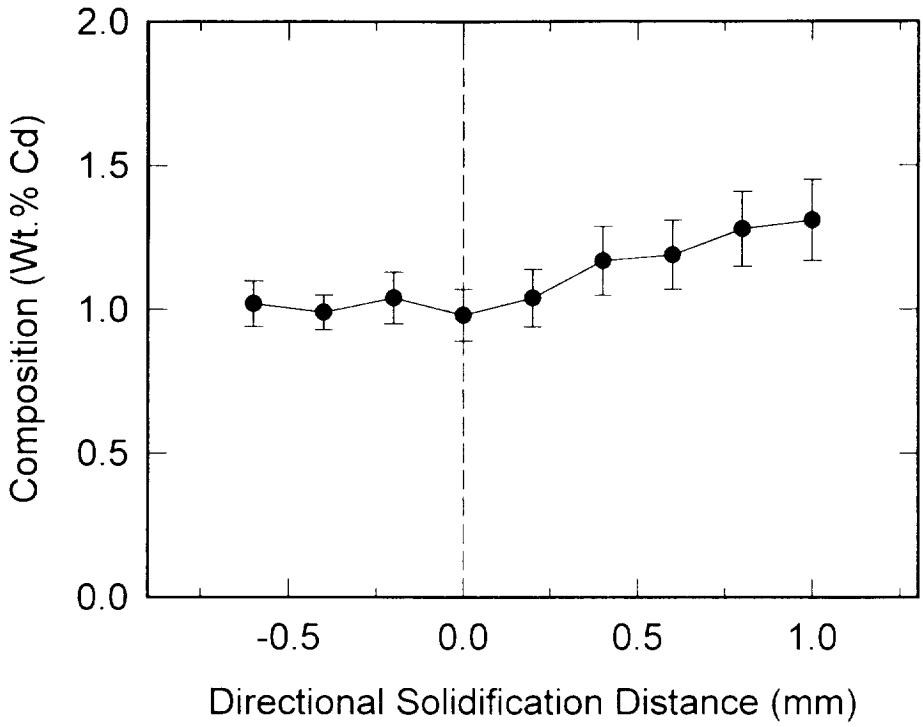

Figure 4. Composition profile in the β solid in the region of initial directional growth as measured with an electron microprobe. Error bars represent 95% confidence limits. The dashed line indicates the start of directional solidification.

Section III: The Occurrence and Periodicity of Oscillating Peritectic Microstructures Developed during Directional Solidification

Abstract

The layered microstructures that can form during plane-front directional solidification in peritectic systems were characterized quantitatively as a function of growth velocity using a Sn-Cd alloy. Layers were formed for an alloy composition outside of the two-phase peritectic region in the absence of longitudinal macrosegregation. The layers did not extend over the entire sample cross-sections, so that the layered regions had a different composition than the alloy. Each of the two solids was found to be interconnected and continuous in three dimensions. The layer lengths and individual layer compositions did not vary with solidification distance. The average layer compositions were not a function of growth velocity and were approximately those at the peritectic temperature. This research was compared to the current model by Trivedi, which is based upon cyclic accumulation and depletion of solute in the liquid ahead of the interface linked to repeated nucleation events. The dependence of layer length on growth velocity predicted by the model was not obtained experimentally. The differences between results and predictions are related to the continuity of the two solids and the non-uniform cross-sectional composition in the Sn-Cd samples, which contradict assumptions of the model. A formation mechanism involving competitive lateral growth between the two solids at the solid-liquid interface would be more consistent with the current research.

Introduction

One of the microstructural variants that can occur in binary peritectic alloys during directional solidification with a planar solid-liquid interface is alternating layers of primary solid and peritectic solid oriented perpendicular to the growth direction [1-10]. For an alloy system where the solute element is more dense in the liquid state than the solvent element, solidification upward tends to stabilize the liquid against convective mixing in a terrestrial environment. Under these conditions, the layers of primary and peritectic solid can form over large solidification distances (see example in Reference 5). Layer formation in this case has been reported for alloy compositions between the primary and peritectic phase compositions at the peritectic isotherm [2,3,5].

The majority of these directional solidification studies on peritectic systems were concerned with establishing the correlation between the morphology of the solid-liquid interface, the phases forming at this interface, the alloy composition, and the ratio of temperature gradient in the liquid to growth velocity (G/V). The development of the layered microstructures was explained only qualitatively; three types of mechanisms intrinsic to the peritectic alloys have been given. 1). Repetitive accumulation and depletion of solute in the liquid ahead of the interface results from and causes alternating nucleation and growth of the two solids [2,3]. 2). The primary solid nucleates in the peritectic solid behind the solid-liquid interface and grows

past the peritectic solid until sufficient solute accumulates in the liquid ahead of the interface to cause nucleation of the peritectic solid [5]. 3). Metastable peritectic solid with a planar solid-liquid interface can grow at a higher temperature than primary solid with a planar solid-liquid interface, which suggests that a layer of peritectic solid can form ahead of the planar primary front. However, the peritectic solid is not stable with respect to the primary solid above the peritectic temperature, so the primary solid may nucleate and grow at the interface at the expense of the peritectic solid [11].

A model has recently been developed by Trivedi [12] based on the first mechanism listed above, which was originally proposed by Boettinger [2]; it can be summarized as follows. The model assumes that solute transport in the liquid occurs only through diffusion (no convective mixing), solid state diffusion is insignificant, and solidification conditions are such that a planar solid-liquid interface is stable. This implies that a section perpendicular to the growth direction will be not only isothermal but also generally have a uniform composition. For an alloy composition between the primary α phase and peritectic β phase compositions at the peritectic temperature, directional solidification starts with the formation of primary α. Solute is rejected into the liquid ahead of the solid-liquid interface, so that the liquid composition rises. Since the compositions of α and the liquid are linked through the requirement for equilibrium at the interface, the composition of α likewise rises and the interface temperature decreases. Once the interface temperature drops below the peritectic temperature, the metastable α liquidus is lower than the equilibrium β liquidus. If this undercooling provides sufficient driving force, β can nucleate before steady state solidification conditions are achieved for α. As β nucleates and grows, less solute is distributed into the liquid ahead of the interface because β has a higher solute content than α. As a consequence, the liquid composition at the interface decreases, the β composition at the interface decreases, and the interface temperature increases. Once the interface temperature exceeds the peritectic temperature, a driving force exists for the nucleation of α. If α nucleates before steady state formation of β is achieved, the first α layer is formed and the cycle repeats.

A mathematical description of this process was derived for the model by Trivedi [12] using the evolution of the solute boundary layer described by Tiller *et al.* [13]. The equations so developed predict the composition profiles across the layers and the lengths of the layers as functions of growth velocity, alloy composition, and various system parameters such as the diffusion coefficient in the liquid, distribution coefficients, nucleation undercoolings, and liquidus slopes. The equations for the solid composition profiles in the initial α transient, a β layer, and an α layer are written as:

$$C_\alpha = C_0 - \left(C_0 - k_\alpha C_0\right)\exp\left[-k_\alpha VZ/D_L\right] \qquad [1]$$

$$C_\beta = C_0 - \left(C_0 - k_\beta C_L^{\alpha\to\beta}\right)\exp\left[-k_\beta V\left(Z - Z_{\alpha\to\beta}\right)/D_L\right] \qquad [2]$$

$$C_\alpha = C_0 - \left(C_0 - k_\alpha C_L^{\beta\to\alpha}\right)\exp\left[-k_\alpha V\left(Z - Z_{\beta\to\alpha}\right)/D_L\right] \qquad [3]$$

where C_α is the composition in the α phase at the solid-liquid interface, C_β is the composition in the β phase at the interface, C_0 is the overall alloy composition, $C_L^{\beta\to\alpha}$ and $C_L^{\alpha\to\beta}$ are the

liquid compositions at the interface for the layer transition points, k_α is the distribution coefficient for α ($= C_\alpha / C_L^\alpha$), k_β is the distribution coefficient for β ($= C_\beta / C_L^\beta$), V is the growth velocity, D_L is the diffusion coefficient for solute in the liquid, Z is the solidification distance measured from the start of the initial transient, and $Z_{\beta\to\alpha}$ and $Z_{\alpha\to\beta}$ are the solidification distances at the most current layer transitions. The values of $C_L^{\beta\to\alpha}$ and $C_L^{\alpha\to\beta}$ are fixed by the respective undercoolings required for nucleation and the liquidus lines. Expressions for the lengths of the layers, λ_α and λ_β, are produced by rearranging terms in equations 2 and 3 and substituting values for compositions and distances at the transition points.

$$\lambda_\alpha = \left(\frac{D_L}{k_a V}\right) \ln\left[\frac{C_0 - k_\alpha C_L^{\beta\to\alpha}}{C_0 - k_\alpha C_L^{\alpha\to\beta}}\right] \qquad [4]$$

$$\lambda_\beta = \left(\frac{D_L}{k_\beta V}\right) \ln\left[\frac{k_\beta C_L^{\alpha\to\beta} - C_0}{k_\beta C_L^{\beta\to\alpha} - C_0}\right] \qquad [5]$$

A direct comparison between layer compositions and lengths calculated through the model and those determined experimentally can be made only if values have been well established for the terms on the right hand side of equations 1-5. Even if these values are unavailable, certain comparisons are still possible between predicted and observed layer features. For a given alloy composition between the primary and peritectic phase compositions at the peritectic isotherm, the model predicts that the layer lengths and the compositions at the transitions between layers should not vary with solidification distance. The compositions at the transition points should also be independent of growth velocity, because these values are linked only to the nucleation undercoolings. Additionally, the lengths of individual layers should be inversely proportional to the growth velocity.

Although this type of layered growth has been noted as an alternative type of two phase growth for binary peritectic systems, the mechanism by which it forms and the precise conditions necessary for its formation have yet to be verified experimentally. In the current study, these oscillations in phase solidification have been characterized in terms of layer length and composition measured parallel to the growth direction as a function of growth velocity and alloy composition. These data along with other microstructural features were then compared to the model in order to refine the present understanding of layer development. This paper focuses on the experimental results for one alloy composition in the selected alloy system.

Materials and Experimental Procedure

The Sn-Cd system was chosen for study, since this low melting point system has already been observed to form layered structures in bulk directional solidification experiments [2,5]. In addition, the solute element Cd is more dense in the liquid state than Sn. A stabilizing density gradient is expected to develop during solidification upward, which should, in turn, minimize density-driven convective flows. The section of the Sn-Cd phase diagram containing the

peritectic reaction is shown in Figure 1. This figure is drawn from Reference 14, which is the currently published phase diagram evaluation. At the peritectic temperature of 223°C, three phases are in equilibrium: primary solid α with a composition of approximately 0.6 wt.% Cd, peritectic solid β with a composition of approximately 0.9 wt.% Cd, and liquid with a composition of 3.8 wt.% Cd. The reported location of the β phase field at the peritectic temperature has varied significantly, from 0.9 to 2.1 wt.% Cd, in different versions of the phase diagram; recent work has confirmed that the composition of β at the peritectic temperature is 1.0 ±0.1 wt.% Cd [15]. It should be noted that β exists as a two-phase mixture of α and (Cd) at room temperature as the result of a eutectoid transformation which occurs during cooling. For simplicity, this two-phase mixture will be referred to as β in the remainder of the paper.

Alloy rod stock for directional solidification was prepared as follows. In 100 g batches, Sn and Cd of 99.99% purity in the appropriate amounts to yield the desired composition were sealed in fused silica crucibles that had been evacuated and back-filled with Ar. This material was then melted in a furnace, mixed by agitating the crucible, and quenched in water to promote the degree of homogeneity. Each cast rod was swaged down to approximately 5 mm, so that pieces of the alloy rod totaling roughly 28 g could be placed in 6 mm ID fused silica crucibles for directional solidification.

In the directional solidification apparatus (described in detail in Reference 16), the sample crucible remains stationary while the furnace and cooling chamber assembly are moved upward at the desired growth velocity (see Table I), which produces solidification in the upward direction. Average growth velocities were verified by a dial indicator and through the measured sample directional solidification distance. The temperature gradient produced in a given material is determined by the furnace temperature, the temperature of the water in the cooling chamber, and, to a lesser degree, the growth velocity. For these experiments, the furnace was set at 750°C, which yielded a temperature gradient in the liquid ahead of the solid-liquid interface of approximately 17°C/mm (see Table I). The value of this temperature gradient was obtained by recording temperature as a function of time while solidifying the alloy past a stationary thermocouple placed inside the crucible.

For the directional solidification experiments, the sample was kept under vacuum during the initial heating stage to remove water vapor and deleterious gases until the furnace temperature approached to within 50°C of the onset of melting. At this point, the crucible was back-filled with Ar to minimize gas-sample reactions and material loss through vaporization. The molten alloy was stirred to eliminate gas bubbles and promote homogenization after the furnace reached 750°C. After time was allowed for thermal equilibration, the sample was rapidly solidified at 0.5 mm/sec for approximately 20 mm to facilitate heat transfer in the cold zone. The length of material remaining for directional solidification was approximately 100 mm. After thermal equilibration, a typical length of 40 to 50 mm of alloy was directionally solidified prior to quenching to preserve the solid-liquid interface. Sections of the sample were mounted, ground, and polished using conventional techniques and then etched with a solution of 5% nitric acid and 95% lactic acid.

Bulk compositions were determined using inductively coupled plasma-atomic emission spectrometry (ICP-AES). Sample disks were cut from alloy rod stock with a thickness of approximately 1 mm and weighing 150 mg. Following dissolution, Cd contents were measured

by analyzing each sample solution six times with a standard solution analyzed between each of the six sample determinations. This procedure yielded Cd compositions with 95% confidence limits of better than ±0.1 wt.% Cd. Initial alloy compositions were determined from the unmelted part of three directionally-solidified samples (see Table I).

The crystallographic orientations of adjacent α layers were determined through electron backscatter diffraction analysis [17,18] of longitudinal sections of an alloy rod. To ensure a minimally deformed sample surface, the mounted sample was repolished with 0.05 μm alumina and colloidal silica followed by a light etch. The orientation information was obtained in a scanning electron microscope (SEM) at low magnifications with the sample tilted 64° from horizontal. Two layered regions, between 25 and 40 mm on a side, were analyzed in a 101x101 grid of points. For each analysis region, the sample remained stationary while the electron beam was moved. At each beam location, the electron backscatter diffraction pattern was digitized and then indexed and converted to an orientation value using lattice parameters and crystal structures for pure Sn and Cd. The point-to-point sensitivity of the technique is on the order of 0.5°. The orientation was identified for at least 80% of the locations; each orientation was assigned a gray scale value. The analysis positions were corrected for the length distortion introduced by the sample tilt, so that the resulting orientation-location map could be compared to an optical micrograph of the same sample area.

The lengths of the layers were obtained from longitudinal sections located near the center of the sample. These lengths were measured along lines drawn parallel to the growth direction through regions containing a regular distribution of the primary α and peritectic β phases. The α and β lengths were plotted as a function of solidification distance, which was measured from the beginning of the initial transient to the midpoint of the respective layer. To account for potentially missing layers, *i.e.*, layers not observed in the particular longitudinal section, a procedure was developed to identify those long α and β layers which could include an extra set of oscillations. The average α layer length and average β layer length were determined for each sample. For the case of a missing α layer, β lengths were excluded if longer than twice the average β length plus the average α length. For the case of a missing β layer, α lengths were removed if longer than twice the average α length plus the average β length. The average layer lengths were then recalculated and the process iterated until no more lengths that could include missing layers were identified. The layer lengths reported in the results were adjusted in this manner.

Phase compositions were determined with an electron microprobe equipped with wavelength dispersive spectrometers. The electron microprobe was operated at 15 keV accelerating voltage and approximately 25 nA beam current. When analysis regions included the two-phase mixture that was formerly β, the electron beam was defocused to a diameter of 10-15 μm to increase the sampling volume. Pieces of the pure Sn and pure Cd that were used to make the alloys served as elemental standards. Areas of interest on the etched sample were marked with a microhardness indenter, so that the sample could be repolished and analyzed in an unetched condition to minimize any compositional bias. In order to check that the electron microprobe and the ICP-AES method produced equivalent results, the mounted longitudinal section of one of the samples grown at 3.8 μm/sec (Sample 21 in Table I) was cut transversely in the directionally-solidified region to yield three surfaces for microprobe analyses and three

corresponding half-disks for ICP-AES analyses. The average compositions of the transverse surfaces determined with the microprobe were quite similar to those determined for the corresponding slices with ICP-AES, although the microprobe values were consistently 0.1-0.2 wt.% Cd lower. Thus, compositions measured by the two methods can be directly compared with only a small potential error involved. If a higher level of Cd were present at the outer edge of the sample rod where analysis with the electron microprobe is not feasible, this would account for the slightly higher values determined by ICP-AES.

Results

Description of Microstructures

Layered microstructures in bulk Sn-Cd samples have been reported at alloy compositions of 1.0, 1.3, and 1.5 wt.% Cd [2,5]. Initial studies on alloys with nominal compositions of 1.0 and 1.7 wt.% Cd suggested that an intermediate composition would produce a more regular sequence of layers through more equal fractions of the primary α and peritectic β phases. Hence, alloys with a nominal composition of 1.4 wt.% Cd were solidified at various growth velocities and essentially the same temperature gradient in the liquid, quenched, and characterized in terms of interface morphology and microstructure (see Table I). The dividing line between a cellular and a planar solid-liquid interface occurred between growth velocities of 6.8 and 3.8 μm/sec. Layers of α and β were observed at growth velocities of 3.8, 2.8, 1.9, and 1.6 μm/sec. The lower bound on velocity for layered growth at this composition and temperature gradient in the liquid fell between 1.6 and 1.0 μm/sec. The α and β layers in the sample grown at 1.0 μm/sec consisted of a coarse, aligned structure with few grains of either phase present. Apparently the oscillations between α and β at the solid-liquid interface were either perturbed or suppressed at this low growth velocity.

A layered microstructure representative of the growth velocity of 3.8 μm/sec is shown in Figure 2 for Sample 15, which was cut into multiple pieces for ease of sample preparation. These longitudinal sections were located as close as possible to the center of the rod; the first 20 mm of directional solidification distance are included. After the initial transient of α (see Figure 2a), the formation of α and β fluctuated somewhat, with the α phase joined together toward the right side of the micrographs. With further solidification, the α layers became separated in the two-dimensional section, and the β phase appeared to be continuous (see Figure 2b). The formation of phases oscillated between α and β for a significant distance, although the α layers did not extend across the entire section. Examination of a number of samples, both the longitudinal sections and a few transverse sections, indicated that the α layers appeared at or near the edges of the sample in some regions and near the rod center in other regions. This changing location suggested that layer formation was not linked to a particular site in the sample rod. An example of a quench interface in the layered region is shown in Figure 3 from a longitudinal section through the center of the rod in Sample 21. Both α and β are present at a reasonably planar, isothermal interface.

The linked formation of α layers was not observed as often in the samples grown at 3.8 μm/sec as the continuous nature of β formation, but the perceived distribution of the phases depends on the location of the particular section in the three-dimensional sample. In order to

determine if the α layers could be interconnected frequently in other sections, the crystallographic orientations of the solid phases were measured in two layered regions of Sample 29 (see example in Figure 4). The α layers in Figure 4a exhibit obvious grain boundaries. The corresponding orientation map in Figure 4b identifies the two larger grains in three of the α layers as having distinct orientations. These two different grain orientations are aligned in adjacent layers along the growth direction, which proves that the orientation of the α phase is repeated in this series of layers. This repetition, combined with instances of ligaments between layers in the two-dimensional sections, implies that the α layers are indeed linked in three dimensions.

The layered microstructure that formed at a velocity of 1.6 μm/sec (Sample 18) is shown in Figure 5. The region after the initial transient shows a high degree of α connectivity in this particular longitudinal section (see Figure 5a). The following region exhibits both α layers that extend across the entire sample width and α layers that are a small fraction of the sample width (see Figure 5b). Compared to the microstructure in Figure 2, these layers have a much less regular distribution.

The apparent progression to less α and more β as the fraction solidified increased as shown in Figures 2 and 5 suggests that convective mixing in the liquid led to enrichment of Cd in the bulk liquid as solidification occurred. However, a comparison of the composition from the unmelted part of the sample rod to the composition of the quenched liquid far from the solid-liquid interface for several of the samples grown at 3.8 μm/sec indicated that solute was not accumulating in the bulk liquid during solidification. Thus, long-range mixing in the liquid was not a factor in layer formation for this system. Some of these apparent differences in phase fractions could be accounted for by sectioning effects. Another possible explanation for the higher proportion of α observed at small solidification distances in some of the samples is that the initial solidification transient extended into the layered microstructure.

Lengths of Layers

The lengths of the α and β layers were determined as a function of solidification distance for all of the samples which exhibited oscillating phase formation; examples for the fastest and slowest growth velocities, 3.8 and 1.6 μm/sec, are shown in Figures 6 and 7, respectively. The length of the α layers for all four growth velocities was essentially unchanged during directional solidification, as shown by a linear regression fit to the data. The β layer length at growth velocities of 3.8 and 2.8 μm/sec was approximately constant during solidification, while the β length at velocities of 1.9 and 1.6 μm/sec increased somewhat with solidification distance.

In order to evaluate the effect of growth velocity on α and β layer lengths, average lengths were determined for the various velocities. This calculation is valid for α, since the lengths of the α layers did not vary with solidification distance. In the case of β, the length of the β layers appeared to vary somewhat with solidification distance, so that an average value may be less descriptive of the oscillating microstructural formation. The average layer lengths as a function of growth velocity are plotted on a log-log scale in Figure 8 with a linear fit to the data. The layer lengths for both phases decrease as growth velocity increases, although the data for β have more scatter. From the log-log plots, the value of the slope for α is -0.5, and the value of the slope for β is -0.3.

Compositions of Layers

Compositional analyses were conducted across three layered regions in one of the samples solidified at 3.8 μm/sec (Sample 11) and in the sample solidified at 1.6 μm/sec (Sample 18). Five analysis points spaced 20 μm apart perpendicular to the growth direction were averaged to produce a representative layer composition at that particular distance along the sample. These five analysis points were repeated every 20 μm parallel to the growth direction to develop a composition profile in each layer.

One of the layered regions that was analyzed in the sample solidified at 3.8 μm/sec (Sample 11) is shown in Figure 9, and the corresponding solid composition profile is given in Figure 10 with error bars at 95% confidence limits. The boundaries between the layers are for the most part well defined in the plot. The α layers have the lower Cd content. The β layers show more compositional scatter than the α layers because they are a two-phase mixture at room temperature. No consistent compositional trends are apparent within the individual α layers or β layers. The average composition of each complete, well-defined layer in Figure 10 and in the other two regions analyzed is plotted against solidification distance in Figure 11 with error bars at 95% confidence limits. It should be noted that the actual error range should be larger than that indicated in Figure 11, since only a small section of each layer was analyzed. A linear fit of these points for the α layers shows no composition change with solidification distance. The compositional trend for the β layers is slightly upward, but this shift is most likely not significant. The α layers have a composition of approximately 0.4 wt.% Cd and the β layers are close to 0.9 wt.% Cd.

The composition profiles for the three layered regions analyzed in the sample grown at 1.6 μm/sec (Sample 18) likewise showed distinct layers with no consistent composition gradients within individual layers. The average compositions for well-defined α and β layers also exhibited no significant changes as a function of solidification distance. The composition of the α layers was approximately 0.4 wt.% Cd, and the composition of the β layers was 1.0 wt.% Cd within ±0.1 wt.% Cd at 95% confidence limits. These layer compositions are essentially the same as those determined at a growth velocity of 3.8 μm/sec, which indicates that the layer compositions do not vary with growth velocity.

A comparison of the phase compositions in the layers determined with the electron microprobe and the alloy compositions determined by ICP-AES reveals that there is a discrepancy in the measured Cd content. The apparent composition in the layered region is less than the alloy Cd level. Since the two compositional analysis methods provided essentially the same numbers when neighboring transverse sections were examined, this difference must be caused by the regions being sampled. From several transverse sections of a sample grown at 3.8 μm/sec (Sample 21), measurements along radial directions with the microprobe revealed no clear and consistent segregation patterns. However, the composition of the β phase was found to be higher in the β regions adjacent in a radial sense to the layered regions (see Figure 12) than it was within the layers. The composition of the β in the regions adjacent to the layers was high enough that the average composition on each transverse section from the microprobe data was the same as the composition determined by ICP-AES within ±0.2 wt.% Cd. In other words, the expected level of Cd was shown to be present on a given rod cross section in agreement with the absence of measurable longitudinal macrosegregation. This Cd was not distributed uniformly on

transverse sections, since α and β were present in adjoining regions and the β composition varied.

A representative value for the composition of the layered regions can be obtained through the average layer compositions and the volume fractions of the two phases estimated from the average layer lengths. The average α and β layer lengths are 0.32 and 0.44 mm for a velocity of 3.8 μm/sec and 0.46 and 0.70 mm for a velocity of 1.6 μm/sec. The approximate compositions of the layered regions are 0.7 and 0.8 wt.% Cd for growth velocities of 3.8 and 1.6 μm/sec, respectively. Thus, the apparent composition of the layered regions falls between the compositions of the primary and peritectic phases at the peritectic isotherm, namely 0.6 and 0.9 wt.% Cd, respectively.

Discussion

The layer formation in the current study occurred without measurable longitudinal macrosegregation, although the composition on transverse sections was found to be inhomogeneous. The measured layer lengths and average compositions for individual layers did not vary with solidification distance, at least on the scale of 50 mm (see Figures 6, 7, and 11). This uniform repetition indicates that the layers were not damping out or approaching some other solidification condition, as might be expected since the alloy composition was outside of the composition range between α and β at the peritectic temperature. This type of two-phase growth appears to be an oscillatory but stable solidification mode for peritectic systems.

The layers observed for Sn-Cd did not usually fill the rod cross sections (see Figures 2-5 and 9), which allowed the β phase to be continuous. The α phase also appeared to be highly interconnected in the three-dimensional sample. This indicates that nucleation was not required for each successive layer. The fact that the layers did not cover the entire cross section also enabled a different composition locally in the layered regions than the overall alloy composition. In addition, the β composition differed between the layered regions and the regions laterally adjacent to the layers (see Figures 10-12), which suggests that localized composition variations were occurring in the liquid during solidification. These composition variations might be attributable to a combination of three factors. 1) The liquid near the crucible wall may have a different composition than the liquid away from the crucible, since this location represents a surface in contact with a foreign material and should also experience reduced fluid flow relative to the more centralized bulk liquid. 2) During layer development, two different solids form at a common interface with the liquid, which will result in different solute profiles in the liquid near the interface. If diffusive and/or convective solute transport are not sufficient to redistribute the solute as the interface travels, these differences will persist. 3) Variations in liquid composition in the vicinity of the solid-liquid interface will cause density gradients, which may induce lateral convective flows. These convective flows, depending on their direction and scale, could act to homogenize or to segregate the solute distribution. Whatever the magnitudes of these three factors are, the net effect is a sustained compositional inhomogeneity at the interface.

Consistent composition gradients parallel to the growth direction were not apparent experimentally within individual layers. However, the levels of solute present in the two phases are low enough that small changes would be difficult to detect. The average α layer

compositions and β layer compositions did not vary with growth velocity and were close to the phase compositions at the peritectic temperature (see Figure 1). The average α layer composition, 0.4 wt.% Cd, is slightly lower than the reported α composition at the peritectic temperature, 0.6 wt.% Cd, which suggests either that α forms above the peritectic temperature or that the reported composition is high by a small amount. The average β layer composition matches that reported at the peritectic temperature, 0.9 wt.% Cd, within the experimental error range. These compositional data are in agreement with phase formation in the layered regions near the peritectic temperature.

The model by Trivedi [12] assumes explicitly that nucleation is mandatory for each new layer and implicitly that the cross-sectional composition remains generally uniform. Both of these assumptions were found to be invalid for the observed layer formation in the Sn-Cd system. The α phase and β phase were both determined to be interconnected and contiguous, which removes the necessity for nucleation at the start of each new layer. In the absence of nucleation barriers for both solid phases, the predicted compositions at the solid-liquid interface would remain at the values on the peritectic isotherm, and the predicted layer lengths from equations 4 and 5 would approach zero. The compositions in transverse directions were not uniform, because the layers did not extend across the entire sample and the β phase radially adjacent to the layers exhibited composition variations. Additionally, the model predicts that the layer lengths will vary with the inverse of growth velocity. The relationship determined experimentally was that layer lengths varied with the inverse square root of velocity. Based on these differences, some other formation mechanism must be operative.

The most probable formation mechanism is competitive lateral growth of the primary and peritectic solids at a mutual solid-liquid interface. Unlike the eutectic case where the two solids cooperate through solute exchange in the liquid, the two solids in the peritectic reaction both reject solute into the liquid. The solid phase which can most effectively disperse solute into the liquid will gradually cover more of the solid-liquid interface. Since the liquid composition is not uniform on the rod cross section, the solid phase which temporarily has the growth advantage will extend into regions where solute conditions are no longer favorable. At this point, the other solid phase will begin to encroach at the interface, and the oscillatory sequence continues. Described from another viewpoint, the three-phase junction between the two solids and the liquid does not experience a net balance of forces, so that its position is not fixed in space but can wander as observed by Lee and Verhoeven in the Ni-Al system [9]. A model for the development of layered microstructures in peritectic systems must account for competitive lateral growth of the primary and peritectic phases at the solid-liquid interface in the context of sustained composition variations across the solid-liquid interface.

Summary and Conclusions

1). This research is the first attempt to characterize on a quantitative basis the layered microstructures that can develop during directional solidification in peritectic systems. Layer formation occurred over long distances in the Sn-Cd system under the condition of no solute accumulation in the bulk liquid. Layers were observed for an alloy composition of Sn-1.4 wt.% Cd, which is outside of the expected composition range for layer formation. However, the

estimated composition within the layered regions, Sn-0.8 wt.% Cd, is in the composition range where both primary and peritectic phases are stable at or below the peritectic temperature.

2). Layer lengths and average compositions of individual layers did not vary with solidification distance. Compositional gradients parallel to the growth direction were not observed within individual layers, but small changes in the already low solute levels would be below the resolution limit of the technique. Average layer compositions were independent of growth velocity and close to the values at the peritectic isotherm. Average layer lengths were proportional to the inverse square root of growth velocity.

3). The layers which formed did not usually extend across the entire transverse section, which allowed the peritectic phase to be continuous. The primary phase was also interconnected in three dimensions, which negated the requirement for nucleation associated with each successive layer. In addition, solid compositions were not uniform through the sample cross section, which permitted the formation of layers in the Sn-1.4 wt.% Cd material. The liquid composition must likewise have been inhomogeneous in the cross section near the solid-liquid interface.

4). The observed continuity of the solid phases and the non-uniform cross-sectional compositions invalidate two assumptions of the Trivedi model for oscillating solidification microstructures in peritectic systems. The layering model should incorporate competitive lateral growth of the primary and peritectic phases at the solid-liquid interface and varying composition gradients in its vicinity.

Acknowledgments

The authors would like to thank R. K. Trivedi of Ames Laboratory-U. S. Department of Energy and the Department of Materials Science and Engineering at Iowa State University for the use of equipment and helpful discussions. J. T. Wheelock of the Materials Preparation Center at Ames Laboratory prepared the initial material; other MPC personnel performed the compositional analyses. H. E. Sailsbury (MPC) was responsible for metallographic preparation of the samples and micrographs. A. Kracher of the Department of Geological and Atmospheric Sciences at Iowa State University conducted the electron microprobe analyses. J. L. Hurd of IBM Analytical Services Group conducted the electron backscatter diffraction analyses. This work was supported by the National Aeronautics and Space Administration under NASA Grant #NAG8-963 and was performed at Ames Laboratory. Ames Laboratory is operated for the U. S. Department of Energy by Iowa State University under contract No. W-7405-ENG-82.

References

1. N. J. W. Barker and A.Hellawell: *Met. Sci.*, 1974, vol. 8, pp. 353-356.

2. W. J. Boettinger: *Metall. Trans.*, 1974, vol. 5, pp. 2023-2031 .

3. A. P. Titchener and J. A. Spittle: *Acta Metall.*, 1975, vol. 23, pp. 497-502.

4. A. Ostrowski and E. W. Langer: in *Solidification and Casting of Metals*, The Metals Society, London, 1979, pp. 139-143.

5. H. D. Brody and S. A. David: in *Solidification and Casting of Metals*, The Metals Society, London, 1979, pp. 144-151.

6. D. J. Larson, R. G. Pirich, and W. R. Wilcox, Annual Report on Contract NAS8-32998, Marshall Space Flight Center, 1981.

7. B. C. Fuh: Ph.D. Dissertation, Iowa State University, Ames, IA, 1984.

8. B. F. Oliver and B. Kad: *J. Less-Common Met.*, 1991, vol. 168, pp. 81-90.

9. J. H. Lee and J. D. Verhoeven: *J. Cryst. Growth*, 1994, vol. 144, pp. 353-366.

10. J. W. Rutter, M. G. Julien, and G. R. Purdy: *Mater. Sci. and Technol.*, 1995, vol. 11, pp. 1233-1240.

11. M. Hillert: in *Solidification and Casting of Metals*, The Metals Society, London, 1979, pp. 81-87.

12. R. Trivedi: *Metall. and Mater. Trans. A*, 1995, vol. 26A, pp. 1583-1589.

13. W. A. Tiller, K. A. Jackson, J. W. Ritter, and B. Chalmers: *Acta Metall.*, 1953, vol. 1, pp. 428-437.

14. J. Dutkiewicz, L. Zabdyr, Z. Moser, and J. Salawa: *Bull. Alloy Phase Diagrams*, 1989, vol. 10, pp. 223-229.

15. K. L. Zeisler-Mashl and T. A. Lograsso: *J. Phase Equilibria*, 1996, vol. 17, pp. 7-9.

16. J. T. Mason: *An Apparatus for Directional Solidification*, IS-4817, UC-37, 1982.

17. J. A. Venables and C. J. Harland: *Phil. Mag.*, 1973, vol. 27, pp. 1193-1200.

18. J. L. Hurd, K. P. Rodbell, D. B. Knorr, and N. L. Koligman: *Polycrystalline Thin Films: Structure, Texture, Properties and Applications*, Mat. Res. Soc. Proc. vol. 343, Materials Research Society, Pittsburgh, PA, 1994, pp. 653-658.

Table I. Description of Directionally Solidified Sn-1.4 Wt.% Cd Samples

Sample Number (Meas. C_O)	Average Velocity μm/sec	G_L °C/mm	G_L/V °Cs/mm^2	Fraction Solid	Interface Morph.	Phase Description
13	9.9	17.2	1700	0.4	Cellular	Cellular α, intercellular β
17	6.8	17.1	2500	0.5	Cellular	Cellular α, intercellular β
11 (1.6 wt% Cd)	3.8	17.0	4500	0.5	Planar	α and β layers
14 (1.3 wt% Cd)	3.8	17.0	4500	0.4	Planar	α and β layers
15	3.8	17.0	4500	1.0	No quench interface	α and β layers for first ≈50 mm
21 (1.4 wt% Cd)	3.8	17.0	4500	0.4	Planar	α and β layers
29	3.8	17.0	4500	0.5	Planar	α and β layers
16	2.8	17.0	6200	0.5	Planar	α and β layers
19	1.9	16.9	8900	0.5	Planar	α and β layers
18	1.6	16.9	11000	0.4	Planar	α and β layers
28	1.0	16.9	17000	0.5	Planar	α and β, not layers

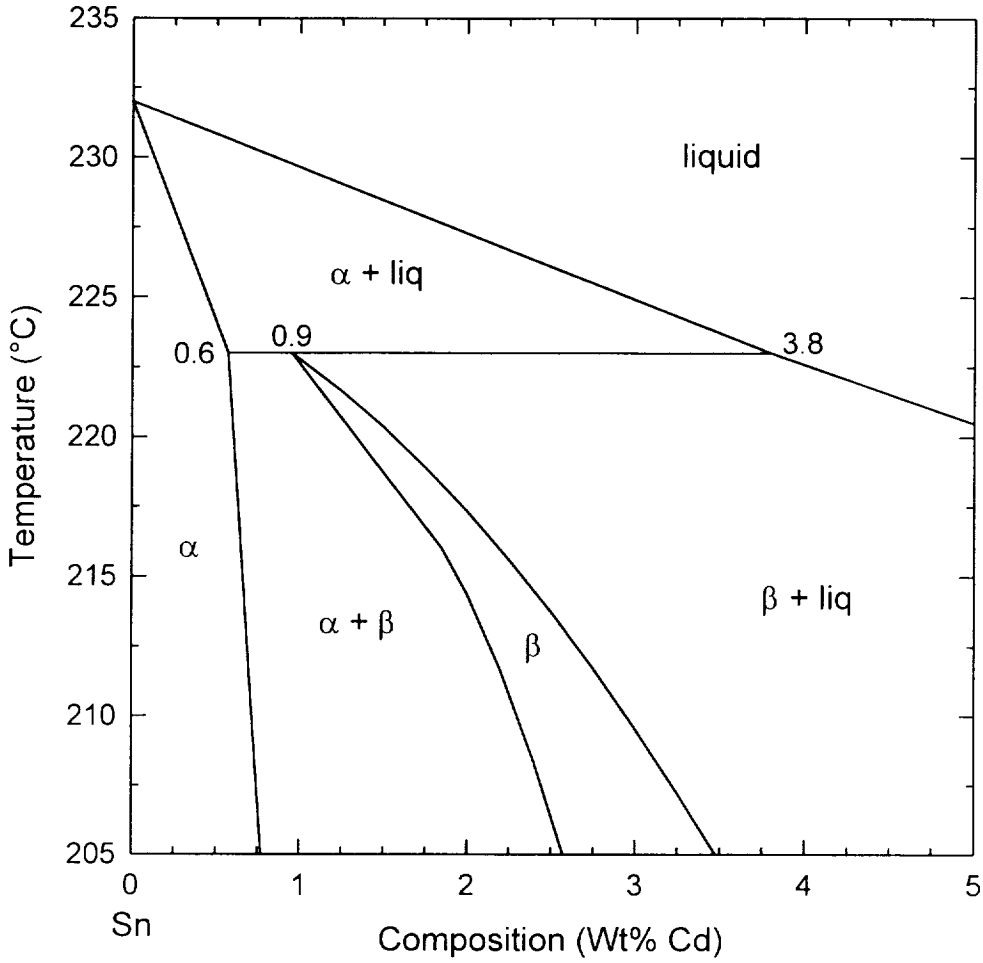

Figure 1. Section of the Sn-Cd phase diagram containing the peritectic reaction drawn from Reference 14.

a)

Figure 2. Optical micrographs of longitudinal sections near the center of a Sn-1.4 wt.% Cd rod directionally solidified at 3.8 μm/sec (Sample 15) showing a) the region near the initial transient of α and b) the adjoining section of the sample, minus approximately 1.5 mm lost to cutting between the two sections. The light phase is α, and the mottled microconstituent that appears after the initial transient is β which has transformed into a two-phase mixture during cooling. The micrographs are oriented so that the growth direction is upward.

b)

Figure 2. (continued)

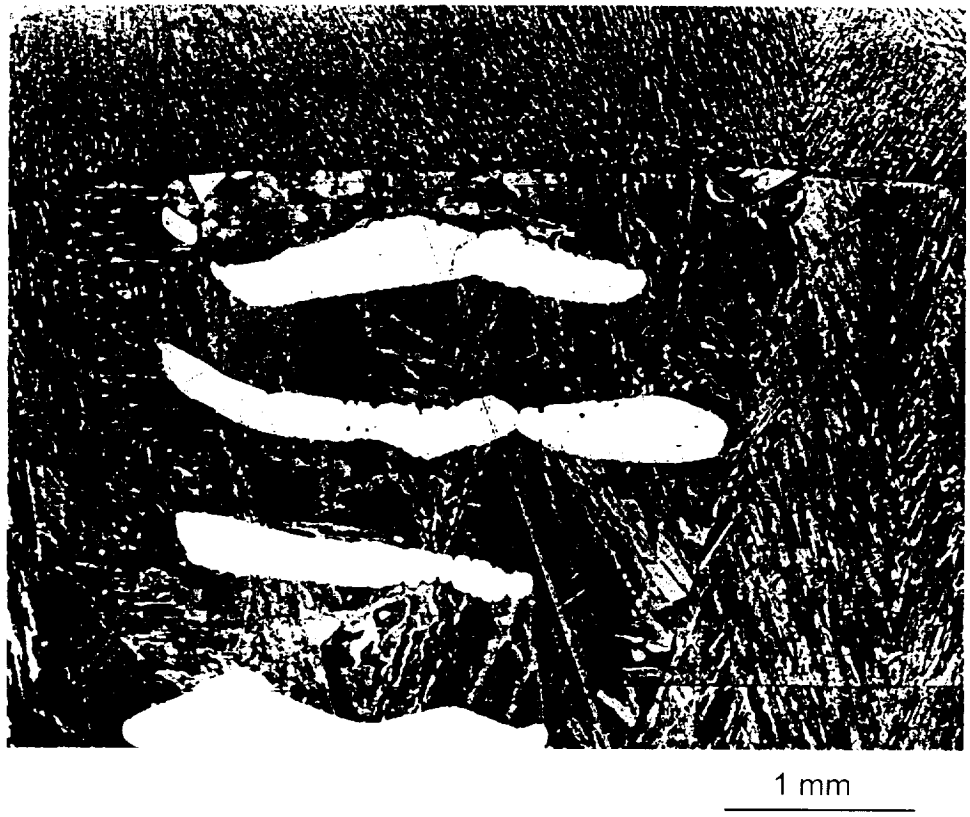

Figure 3. Optical micrographs of a longitudinal section near the center of a Sn-1.4 wt.% Cd rod directionally solidified at 3.8 μm/sec (Sample 21) showing the quench interface in the layered region. The growth direction is upward.

a)

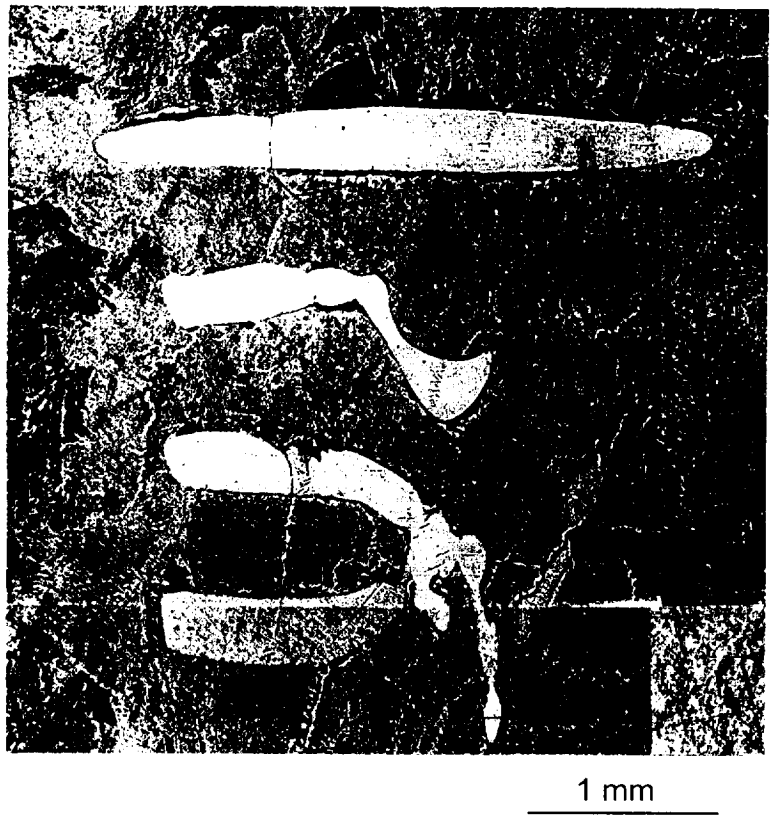

Figure 4. A longitudinal section near the center of a Sn-1.4 wt.% Cd rod directionally solidified at 3.8 μm/sec (Sample 29) showing a layered region by a) optical micrographs and b) an orientation map. In part b, regions with the same gray level have the same crystallographic orientation; a black region signifies that the orientation could not be determined. The growth direction is upward.

b)

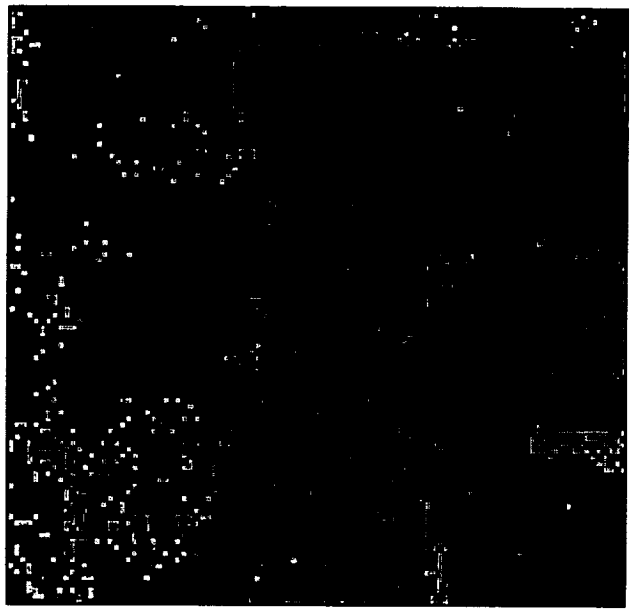

Figure 4. (continued)

a)

Figure 5. Optical micrographs of longitudinal sections near the center of a Sn-1.4 wt.% Cd rod directionally solidified at 1.6 μm/sec (Sample 18) showing a) the region near the initial transient of α and b) the adjoining section of the sample, minus approximately 1.5 mm lost to cutting between the two sections. The micrographs are oriented so that the growth direction is upward.

b)

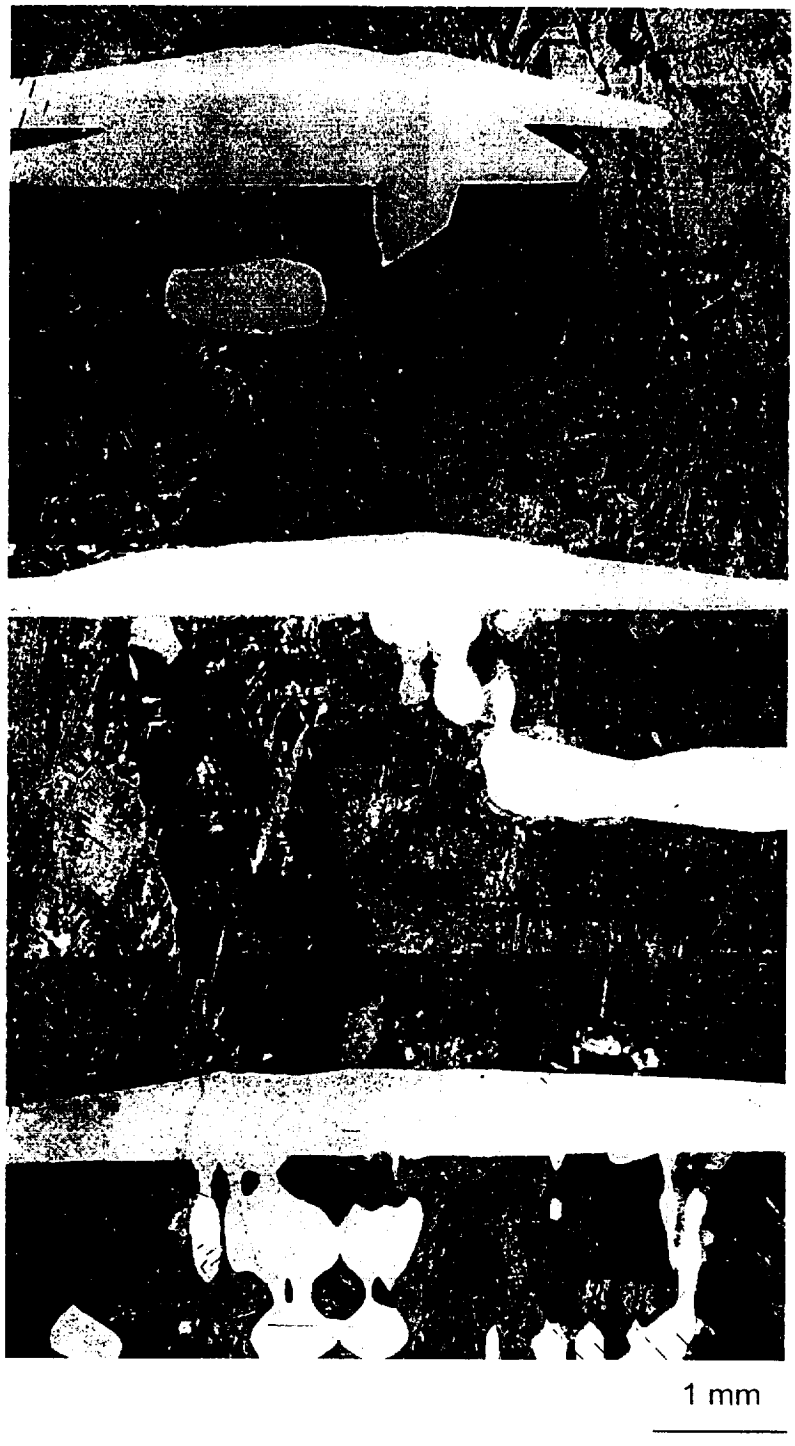

Figure 5. (continued)

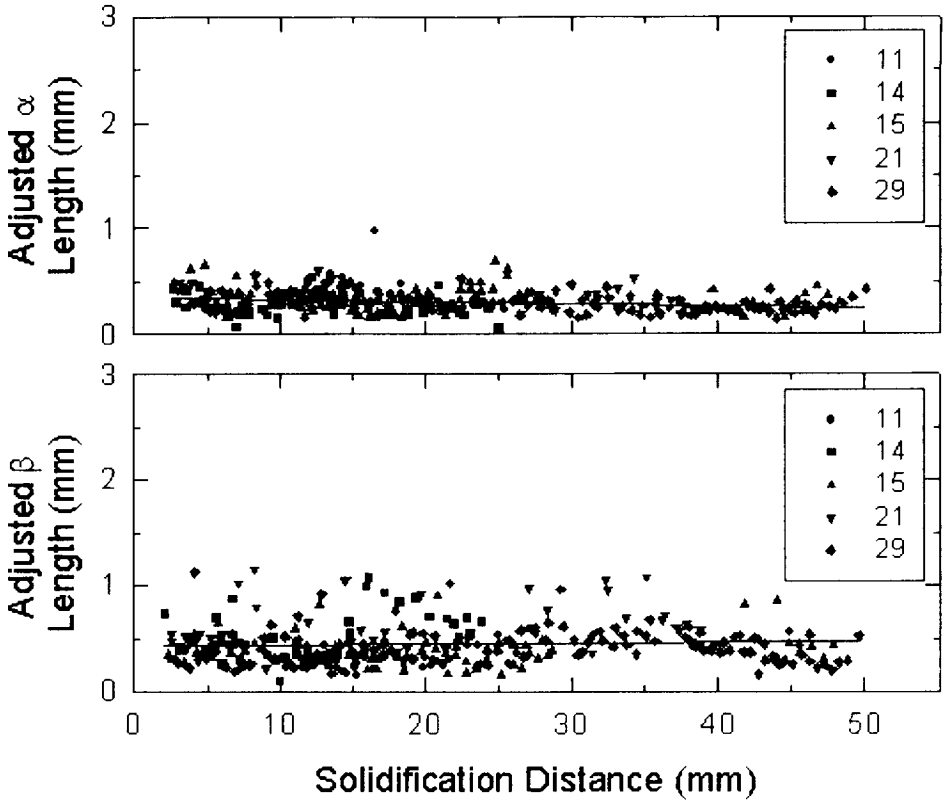

Figure 6. Adjusted lengths of the α and β layers measured parallel to the growth direction for samples directionally solidified at 3.8 μm/sec (Samples 11, 14, 15, 21, and 29) with a linear regression fit to the data.

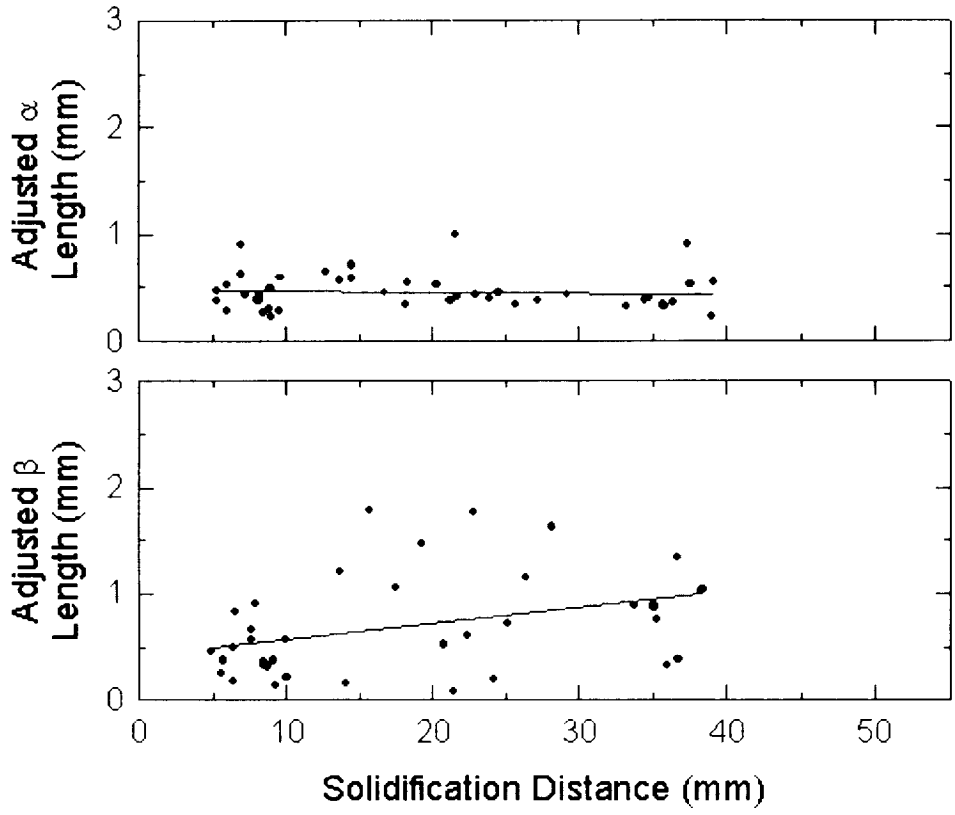

Figure 7. Adjusted lengths of the α and β layers measured parallel to the growth direction for a sample directionally solidified at 1.6 μm/sec (Sample 18) with a linear regression fit to the data.

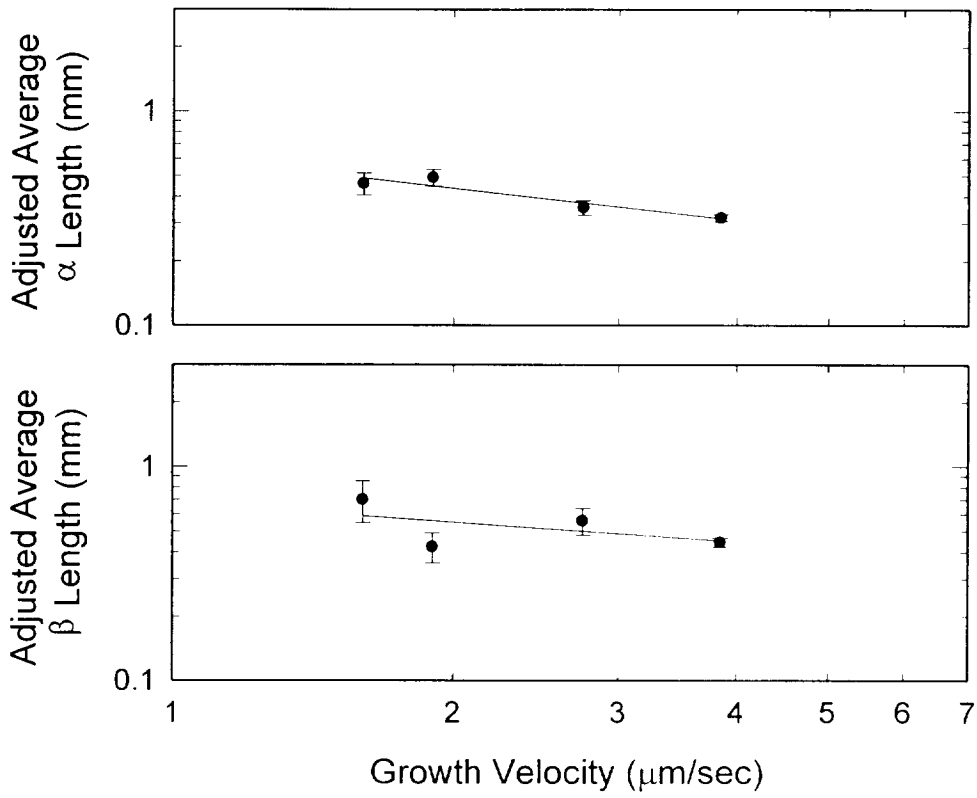

Figure 8. Average adjusted lengths of the α and β layers as a function of growth velocity with a linear regression fit to the data. Error bars represent 95% confidence limits.

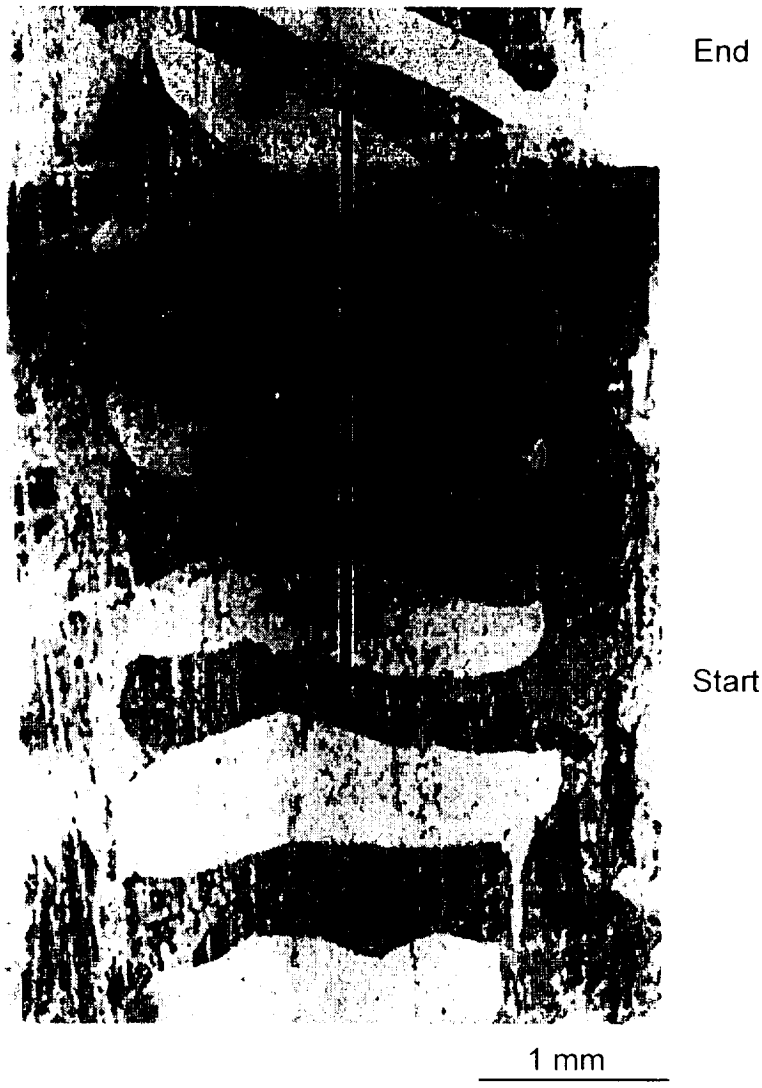

Figure 9. Optical micrographs of a longitudinal section near the center of a Sn-1.4 wt.% Cd rod directionally solidified at 3.8 μm/sec (Sample 11) showing one of the layered regions in which phase compositions were measured. The starting point and ending point for the analyses are indicated on the micrographs. The growth direction is upward.

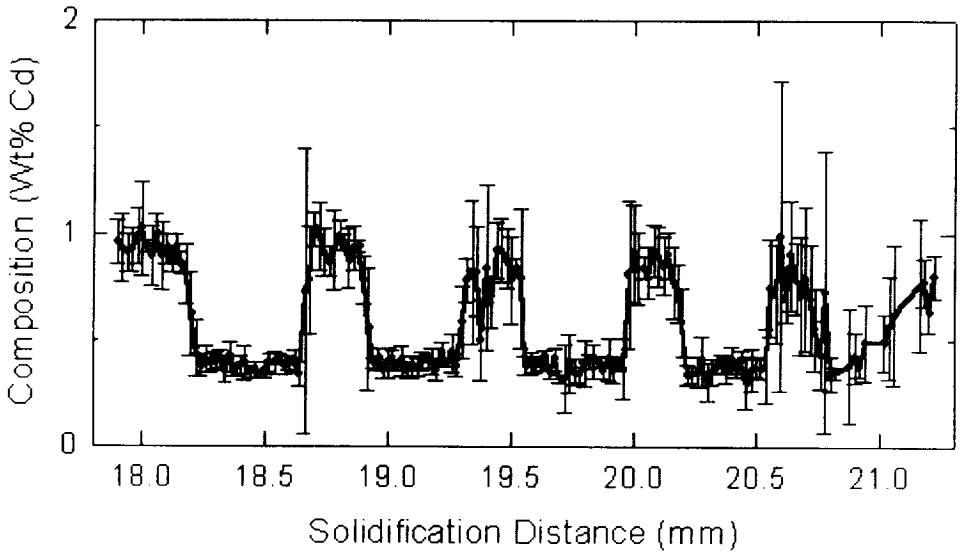

Figure 10. Solid compositional profile obtained with an electron microprobe from a sample directionally solidified at 3.8 μm/sec (see Sample 11 in Figure 9) with error bars at 95% confidence limits.

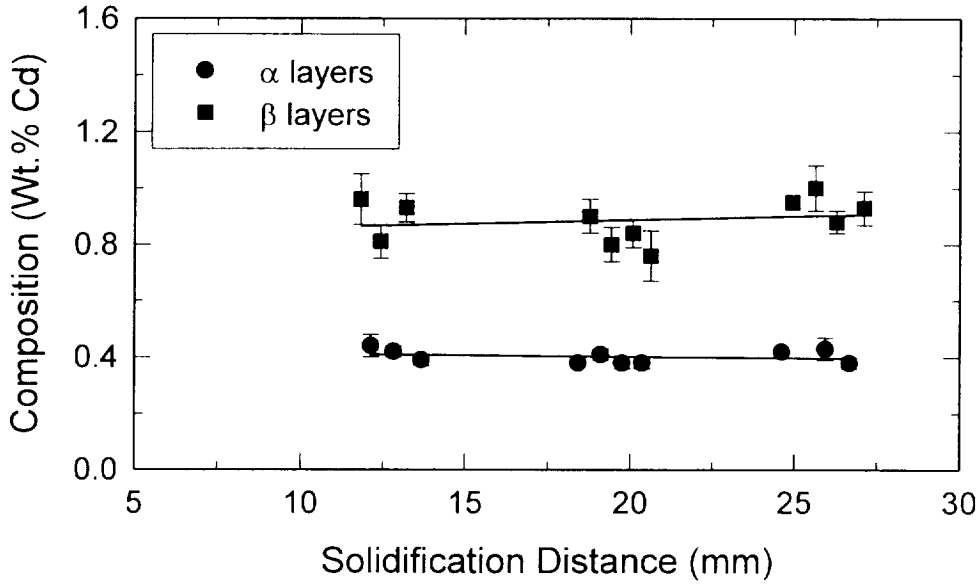

Figure 11. Average compositions of complete and well-defined layers for a sample directionally solidified at 3.8 μm/sec (Sample 11) as a function of solidification distance with 95% confidence limits and linear fit of the data. The compositions for the layered microstructure shown in Figure 9 are plotted as the middle set of data.

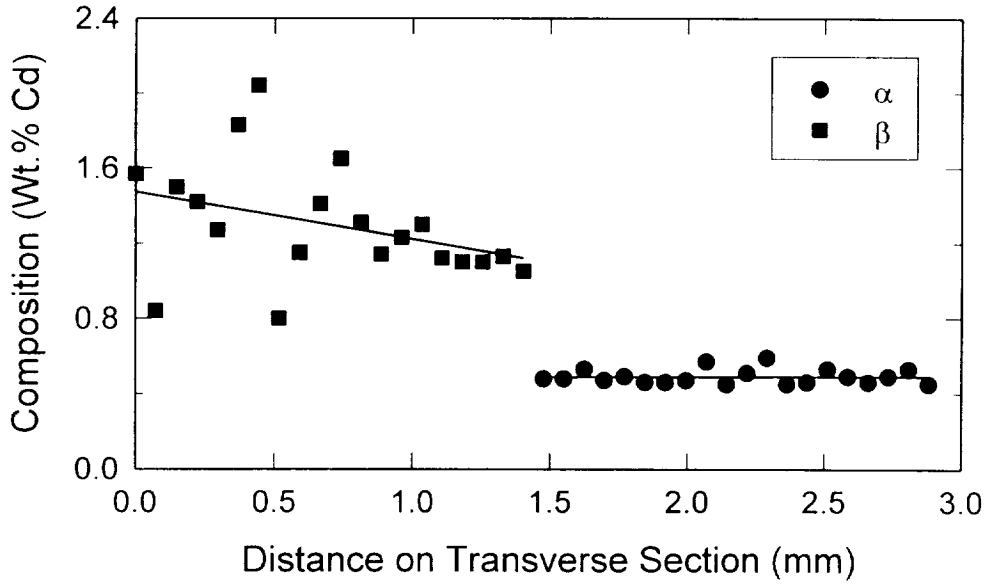

Figure 12. Compositions measured with an electron microprobe along a line from the outside edge to the rod center on a transverse section of a sample directionally solidified at 3.8 μm/sec (Sample 21). The data points and corresponding linear regressions were obtained from β adjacent to a layered region in the radial sense and from α within the layered region, as indicated on the plot.

Section IV: The Effect of Alloy Composition on Oscillating Peritectic Microstructures Developed during Directional Solidification

Introduction

Directional solidification in binary peritectic systems with a planar solid-liquid interface has been shown in some cases to produce a two phase arrangement referred to as layering [1-11]. In these microstructures, the primary solid and the peritectic solid form as alternating layers perpendicular to the growth direction. For alloy systems and growth conditions which minimize convectively driven flows in the liquid that could lead to longitudinal macrosegregation, layers have been observed to grow repetitively over significant solidification distances [2,3,5,11]; this layer formation has often been related to alloy compositions between the primary and peritectic phase compositions at the peritectic temperature. A number of layer formation mechanisms have been proposed [1-4,10,12], ranging from externally induced growth perturbations [1,4,10] to alternating nucleation and growth of the two solids at the solid-liquid interface linked to composition oscillations in the liquid ahead of the interface [2,3]. The current model for layered microstructures in minimally convecting peritectic systems, developed by Trivedi [13], is based upon the latter mechanism. However, the particular formation mechanism operating for specific alloy compositions and growth conditions has not yet been confirmed experimentally.

Recent research using a Sn-Cd alloy over a range of growth velocities, in which external influences were minimized as much as possible, has shown that repetitive nucleation and growth events are not a requirement for layer development in this system [11]. Moreover, layers formed in this alloy even though the content of the solute element Cd was greater than the predicted composition limit and macrosegregation did not occur longitudinally. As an extension of this work, four additional Sn-Cd alloys were examined. The arrangement of phases, layer repeat distances, and phase compositions were characterized along the growth axis as a function of alloy composition and growth velocity in order to elucidate a formation mechanism.

Materials and Experimental Procedure

Directional solidification experiments were conducted using Sn-Cd alloys in the composition range from 0.8 to 1.7 wt.% Cd (see Tables I and II). In terms of the peritectic isotherm at 223°C (see Figure 1), an alloy composition of 0.8 wt.% Cd falls between primary α and peritectic β, 1.0 wt.% Cd is the composition of peritectic β with the limits of measurement techniques [15], and 1.4 and 1.7 wt.% Cd are between the composition of peritectic β and the liquid. One of the advantages of this system is that the solute element Cd is more dense in the liquid state than Sn, which should minimize density-driven convective flows during solidification upward. Macrosegregation along the length of the rod was not apparent at a growth velocity of 3.8 μm/sec [11].

Alloy rods were prepared from 99.99% pure Sn and Cd in 100 g batches (see Section III and Reference 11 for more procedural details). The pure metals were sealed in fused silica crucibles under an Ar atmosphere, melted, mixed, and rapidly quenched in water. Each casting

was swaged to 5 mm to fit in the 6 mm ID fused silica crucibles used for directional solidification. In the directional solidification unit (described in detail in Reference 16), solidification upward is produced by moving a furnace and cooling chamber assembly upward relative to a stationary sample at the desired velocity. Average growth velocities were checked by a dial indicator. The temperature gradient in the liquid ahead of the solid-liquid interface was approximately 17 °C/mm, which was determined by solidifying a Sn-Cd sample past a stationary thermocouple in the crucible. An Ar atmosphere was used during solidification. After rapidly solidifying for 20 mm to enhance heat transfer in the cold zone, samples were typically directionally solidified for 40 to 50 mm out of a total rod length of approximately 100 mm before quenching to preserve the shape of the solid-liquid interface. Each sample was sectioned, mounted, ground, and polished following standard techniques and etched in a solution of 5% nitric acid in lactic acid. Initial work had shown that an average growth velocity of 3.8 μm/sec produced reasonably regular layered microstructures [11]; a majority of the samples were grown at this velocity (see Table I). Samples of two of the alloys were directionally solidified at higher and lower velocities to determine the stability range for layered growth (see Table II).

Bulk compositions were measured using inductively coupled plasma-atomic emission spectrometry (ICP-AES) techniques, which yielded Cd compositions with 95% confidence limits of better than ±0.1 wt.% Cd. The composition of the 1.7 wt.% Cd alloy was determined from pieces from the top and bottom of the as-cast rod prior to swaging; the compositions of the other alloys were determined from slices of the unmelted section of the directionally solidified rods (see Tables I and II). Phase compositions were measured from polished, unetched sample surfaces using an electron microprobe with wavelength dispersive spectrometers and pure elemental standards . For layer compositions as a function of solidification distance, five analysis points at the same solidification distance and separated by 20 μm laterally were averaged to decrease the scatter in the profile. The ICP-AES results and microprobe results were the same within 0.1-0.2 wt.% Cd [11].

Wavelengths were measured along lines drawn parallel to the growth direction through layered regions on longitudinal sections near the rod centers. To account for sets of layers not included in a particular longitudinal view, those wavelengths which were greater than twice the average wavelength were removed from the data set. The average was calculated again and the process repeated until the average remained unchanged. Usually no more than one iteration was required; all reported wavelengths were treated in this manner.

Results

Description of Microstructures

Directional solidification experiments in the Sn-Cd system using an alloy composition of 1.4 wt.% Cd were reported previously [11]; these results will be summarized and included as necessary. Layered microstructures consisting of the primary α phase and the peritectic β phase were observed in the 1.4 wt.% Cd samples directionally solidified at 3.8 μm/sec (see example in Figure 2). It should be noted that β undergoes a eutectoid transformation into α and (Cd) during cooling to ambient temperatures; however, this two-phase mixture will be referred to as β for the sake of clarity. The α and β layers did not extend across the entire width of the longitudinal

section; β was present radially adjacent to the layered regions. This arrangement of phases allowed β to be continuous. The determination that the crystallographic orientation in a series of α layers was the same, combined with occasional ligaments joining these layers, suggested strongly that the α phase was also interconnected in three dimensions. In longitudinal sections after the initial transient region, the location of the layers was observed to shift between the center and the periphery of the rods with no apparent preference.

Samples with compositions of 1.0 and 1.2 wt.% Cd showed a similar arrangement of the α and β phases after directional solidification at 3.8 μm/sec; a representative layered microstructure from Sample 32 is given in Figure 3. After an initial transient of α, the β phase formed at the periphery of the sample rod, which was evident on a longitudinal section at one or both of the edges parallel to the growth direction. The α phase was also continuous, occurring at the rod center and also at an edge if the β phase was not located there. Transverse sections from Sample 33 (see example in Figure 4) indicated that the β phase was distributed in a crescent shape around part of the rod circumference. The layering for these two alloy compositions could be described as a narrow region of phase boundary oscillation between the two continuous zones of α and β. As shown by the quenched interface from Sample 33 in Figure 5, α and β formed at a common interface, which was slightly curved but still a planar growth front. Assuming that the isotherms in the liquid were perpendicular to the growth axis, the difference in temperature between the lowest point on the β-liquid interface and the highest point on the α-liquid interface is on the order of 5°C.

Samples of the 0.8 and 1.7 wt.% Cd alloys, the extremes of the composition range studied, did not exhibit regularly layered microstructures at a growth velocity of 3.8 μm/sec in the longitudinal sections examined (see Table I). For the case of the 0.8 wt.% Cd rod (Sample 27), α was present from the onset of directional solidification. Occasional β layers were apparent at the rod perimeter, but not with any consistent frequency. For a composition of 1.7 wt.% Cd (Sample 5), an initial transient of α was followed by β containing a few α layers. Apparently the phase fractions were different enough that either 1) the minor phase was not continuous or 2) the regularly layered region was limited in extent and not sectioned in the particular longitudinal view.

Layer Wavelengths

Due to the limited width of the layered regions, a layer repeat distance in the growth direction, *i.e.*, wavelength, was measured rather than lengths of individual layers as was done previously [11]. Layer wavelengths as a function of solidification distance at a growth velocity of 3.8 μm/sec are shown for alloy compositions of 1.4 and 1.0 wt.% Cd in Figures 6 and 7, respectively. The wavelengths measured for the 1.4 wt.% Cd samples did not vary significantly with solidification distance, as indicated by the linear regression fit to the data. The two other alloys which exhibited regular layer formation, 1.0 and 1.2 wt.% Cd, behaved in a similar manner. The wavelengths were basically constant in the range of 50 mm of directional growth, which means that a representative value for each alloy composition could be determined by averaging the data. The average wavelengths are plotted in Figure 8. The wavelengths for alloy compositions of 1.0 and 1.2 wt.% Cd are essentially the same, since the confidence intervals overlap. The average wavelength determined for the 1.4 wt.% Cd samples is somewhat higher. This difference may in part be a sectioning effect, since the more varied arrangement of phases in

the layered regions of the 1.4 wt.% Cd alloys compared to the two lower Cd alloys added to the probability that layers would be missing from a given field of view, thus possibly increasing some of the measured wavelengths.

Compositions of Layers and Phases

Compositional data measured parallel to the growth direction in layered regions of the 1.4 wt.% Cd samples [11] indicted that compositions showed no consistent trends within individual layers. Also, average α and β layer compositions did not vary with solidification distance. The average α layer composition was determined to be approximately 0.4 wt.% Cd, and the average β layer composition was approximately 1.0 wt.% Cd in the velocity range from 3.8 to 1.6 μm/sec. Using these compositions and estimating the phase fractions in the layered regions from the average layer lengths, a representative composition for the layered regions was calculated to be roughly 0.8 wt.% Cd.

Phase compositions were measured parallel to the growth direction in the layered region of a 1.0 wt.% Cd alloy directionally solidified at 3.8 μm/sec (Sample 31); the microstructure is shown in Figure 9, and the corresponding compositional profile is given in Figure 10. The boundaries between the layers are clearly defined for the first 3 mm plotted in Figure 10. The β layers have the higher Cd content. As was found for the 1.4 wt.% Cd alloys, the compositions in individual layers did not exhibit consistent trends in the growth direction. The average layer compositions could not be determined as a function of solidification distance in the 1.0 wt.% Cd alloys, because the limited width of the layered regions made it difficult to center the analysis points in the layers. Average compositions for the α layers and for the β layers were calculated from the data in Figure 10 from 0 to 2.6 mm, excluding those few points at layer boundaries which contained information from both phases. The composition for the α layers was approximately 0.5 wt.% Cd and for the β layers was approximately 0.9 wt.% Cd. These values are essentially the same as those obtained for the 1.4 wt.% Cd alloys, which indicates that average layer compositions do not vary significantly with alloy composition. These values are also close to the α and β phase compositions reported at the peritectic temperature (see Figure 1).

Phase compositions were also measured on transverse sections of samples directionally solidified at 3.8 μm/sec. In the 1.4 wt.% Cd alloys, the β phase was found to have a higher Cd content in the regions adjacent in a radial sense to the layered regions than in the layers [11]. A compositional profile along a diameter is given in Figure 11 for a 1.0 wt.% Cd alloy (see the transverse section of Sample 33 in Figure 4). The analysis points in the first 1.4 mm of the plot appear to be from the β phase alone, while the points from 1.4 to 2.5 mm represent primarily the α phase with a few instances of β particles. The remaining compositional information is due to the α phase alone. The composition of the α phase appears to decrease from roughly 0.4 wt.% Cd next to the β phase to approximately 0.2 wt.% Cd at its lowest level a significant distance away from the β phase and therefore not in the layered region. Thus, the higher volume fraction phase in both the 1.4 and 1.0 wt.% Cd alloys exhibits compositional variations between the layered regions and the regions radially adjacent to them. The Cd content of the β phase in the 1.4 wt.% alloys increases from the layers to the regions adjacent to them, while the Cd content of the α phase in the 1.0 wt.% Cd alloys appears to decrease from the layers to the regions adjacent to them. Given that the temperature at the solid-liquid interface tends to increase for both α and

β as their Cd content decreases (see Figure 1), this description is consistent with the phase and presumed temperature distribution at the quenched interface of Sample 33 in Figure 5.

Effect of Growth Velocity

Samples with compositions of 1.4 and 1.0 wt.% Cd were directionally solidified over a range of growth velocities, which produced a variety of microstructures (see Table II). For the 1.4 wt.% Cd samples, the transition between a planar and a cellular interface morphology occurred between growth velocities of 3.8 and 6.8 μm/sec. Regularly layered microstructures formed at velocities from 3.8 to 1.6 μm/sec but changed to coarse, aligned grains of α and β at 1.0 μm/sec. For the 1.0 wt.% Cd alloy, the planar growth front became unstable between the same velocity values. However, regularly layered microstructures were observed over a more limited range of growth rates from 3.8 to 2.8 μm/sec and degenerated into irregular, apparently isolated instances of β at 1.6 μm/sec. The apparent isolation of β might be due to the lower fraction of β in the 1.0 wt.% Cd alloy and could partly be a sectioning effect.

Average wavelengths for the layered microstructures in the 1.4 and 1.0 wt.% Cd alloys are plotted in Figure 12 on a log-log scale. For the 1.4 wt.% Cd samples, the layer wavelengths decreased as the growth velocity increased; the slope was -0.4. For the 1.0 wt.% Cd samples, the data are insufficient to develop a relationship between wavelength and velocity. The wavelengths determined for the 1.0 wt. % Cd samples are below those determined for the 1.4 wt.% Cd samples.

Discussion

Comparison of Layered Microstructures

The first issue which must be addressed is whether the layers in the alloys studied formed in fundamentally the same way regardless of microstructural appearances in two dimensional views. Regular, repetitive layers were observed for three alloy compositions, 1.0, 1.2, and 1.4 wt.% Cd, at a growth velocity of 3.8 μm/sec. From longitudinal sections, the arrangement of phases was similar in the 1.0 and 1.2 wt.% Cd samples, whereas the arrangement of phases appeared different in the 1.4 wt.% Cd samples (compare Figure 3 with Figure 2). In the 1.4 wt.% Cd samples, the α phase and β phase formed at a common interface with the liquid, as shown by the quenched interfaces. The average compositions of the α and β in the layers were close to those reported for the peritectic reaction, suggesting that the phases in the layers were solidifying at or near the peritectic temperature. A representative composition for the layered regions was determined to be approximately 0.8 wt.% Cd. Layers occurred over only part of the rod cross sections, so that the β phase was continuous. The α phase also appeared to be interconnected in three dimensions. Compositional measurements on transverse sections verified that sustained compositional variations were present in the β phase, which in a sense allowed or accommodated the formation of layers in regions with a lower Cd content than the overall alloy. In the 1.0 and 1.2 wt.% Cd samples, the α phase and β phase also formed at a common interface with the liquid. The compositions of the phases in the layers of the 1.0 wt.% Cd alloy were essentially the same as those in the 1.4 wt.% Cd samples. Both α and β were obviously continuous in the growth direction, with layers occurring over a fraction of the rod cross section. Compositional

variations were also found for the 1.0 wt.% Cd alloy in the higher volume fraction phase, α in this case, on a transverse section. This comparison of layer characteristics strongly suggests that regular layers develop through a similar mechanism in these three alloys. The microstructure observed in the 0.8 wt.% Cd sample for the same growth conditions exhibits some of these characteristics. This alloy had the nominal composition determined for the layered regions in the 1.4 wt.% Cd samples. However, β was found only in isolated layers, so sustained compositional variations through the cross section were apparently present in this alloy as well. Three dimensional sectioning and imaging of the layered regions in these samples would allow the arrangement of phases to be described more completely and accurately.

The different appearance of the layers in the 1.4 wt.% Cd samples relative to the 1.0 and 1.2 wt.% Cd samples might be linked to the location of these regions in the sample rod. The layered regions in the 1.4 wt.% Cd samples wandered through the rod cross section with no obviously preferred site [11], while the layers in the 1.0 and 1.2 wt.% Cd samples were more likely to form in well defined zones closer to the crucible wall. As shown by the 1.2 wt.% Cd sample in Figure 13 (Sample 32), layers near the crucible wall were much more regular than those closer to the center of the rod. This implies that the appearance of the layers in the 1.4 wt.% Cd samples could change depending upon where in the sample rod they grew. This variation from the periphery to the center might be related to localized fluid flow near the solid-liquid interface; the liquid near the center could move or perturb more easily than that near the crucible. If this is the case, changing the crucible diameter should affect the appearance of the layers, especially in the 1.4 wt.% Cd alloys.

Effects of Alloy Composition and Growth Velocity

Alloy composition and growth velocity were both found to influence layers in the Sn-Cd system in terms of whether or not regular layers formed and the wavelengths representative of such layers. Conversely, alloy composition and growth velocity did not appear to affect the compositions of the solid phases in the layers, which indicates that layer formation is linked to a certain value or range of composition in the liquid. In other words, layers will occur in a given sample if the necessary liquid composition occurs over an adequate solidification distance in conjunction with the appropriate combination of growth velocity and temperature gradient in the liquid. Directional solidification for the system and the majority of conditions reported in this study appears to be accompanied by compositional variations in the sample rod cross section. Regular layers grew in those alloys where the compositional variations in the cross section included the range required for layer development, namely for alloy compositions of 1.0, 1.2, and 1.4 wt.% Cd. The compositional variations in the 0.8 and the 1.7 wt.% Cd samples impinged on the favorable range for layers, since isolated layers were observed, but were not sufficient to maintain significant fractions of layers as observed on longitudinal sections. The compositional variations in all of these Sn-Cd alloys occur in the context of solute transport from some combination of fluid flow and diffusion in the liquid near the interface. Changing the solute transport, such as by utilizing a different crucible diameter, should consequently alter layer development. Shifts in the type or magnitude of solute transport might also explain why regular layered microstructures were not observed at low growth velocities (see Table II). Slower growth velocities allow more time for diffusive transport, which should reduce compositional

variations and gradients in the liquid near the interface. On the other hand, more rapid growth velocities preclude layer formation as the planar solid-liquid interface becomes unstable.

For the measured layer wavelengths, increasing the Cd content from 1.0 to 1.4 wt.% Cd increased the wavelength (see Figure 8); this effect, although small, was apparent at growth velocities of 3.8 and 2.8 μm/sec (see Figure 12). Layer wavelengths varied with the approximate inverse square root of velocity in the 1.4 wt.% Cd alloys, while the results were not conclusive for the 1.0 wt.% Cd alloys. Explaining these wavelength data requires a more quantitative description of the layer formation mechanism.

Formation Mechanisms for Layered Microstructures

If compositions on the cross sections were uniform in the Sn-Cd samples, then the model by Trivedi [13] might apply to layer formation in this system. This model assumes that layers completely cover the cross section, so that renucleation is required for each successive layer. Nucleation events are triggered when solute accumulation or depletion in the liquid at the solid-liquid interface produces a sufficient undercooling. Layer formation in this case should only be observed for alloy compositions between α and β at the peritectic temperature. Solute transport in the liquid is strictly diffusive, resulting in a layer repeat distance that is inversely proportional to growth velocity. Since this situation does not describe the regularly layered microstructures observed in the Sn-Cd alloys, a different formation mechanism must be developed.

A schematic representation of the solid-liquid interface in the layered region was developed from the quenched interfaces and is shown in Figure 14. As mentioned previously, α and β form at a common interface with the liquid. At this three phase junction, α and β are in contact with a liquid of composition C_L at a temperature T_3. This temperature may be the peritectic temperature or some other value, depending upon the relative curvature of the two solids at the three phase junction. Certain parameters are controlled externally, namely the imposed growth velocity in the z direction, V_{imp}, and the temperature gradient in the liquid ahead of the interface, G_L. The velocity of the three phase junction may have two components: V_X for lateral motion in the x direction and V_Z for motion parallel to the rod axis in the z direction. If V_Z is not equal to V_{imp}, then T_3 must change as solidification occurs. In order for layers to form, the three phase junction must oscillate in the x direction in addition to traveling in the z direction; V_X will vary between negative and positive values. The reasons for this lateral movement are inherent to the peritectic reaction and the compositional relationships between the three phases at their junction. Both α and β reject solute at the solid-liquid interface. In this sense, growth in peritectic systems is competitive rather than cooperative like in eutectic systems, where the two solid phases exchange solute and solvent atoms through the liquid near the interface. For α and β in the peritectic system, the solute fluxes into the liquid in front of the two phases are not equal. This inequality provides a driving force for lateral solute diffusion and thus provides a net force on the three phase junction so that it shifts along the x axis with time.

Some of the layers in Figures 3, 9, and 13 exhibit a sawtooth shape, where one boundary is angled relative to the growth axis and the other boundary is perpendicular to the growth axis. This horizontal boundary can be achieved by two different solidification routes. In the first route, T_3 remains constant, and one solid phase grows very rapidly over the other ($|V_X| >> V_{imp}$). This occurrence would imply that the liquid in front of one solid phase somehow became

undercooled relative to the other solid phase, so that sufficient driving force existed for rapid overgrowth. In the second route, V_X is in the same order of magnitude as V_{imp}, and T_3 drops to produce the flat boundary. If T_3 decreases, then V_Z becomes less than V_{imp}. The drop in V_Z will affect the solute profile in the liquid ahead of the interface. Following the reasoning of Smith *et al.* for single phase systems [17], a decrease in interface velocity means that the system has to adjust to a temporary depletion of solute. For α and β solidifying next to each other, this solute depletion can be accommodated by preferential growth of the phase which generates more solute in the liquid. In other words, α will tend to grow over β. Examination of the layered regions containing sawtooth shapes in Figures 3, 9, and 13 indicates that flat boundaries are indeed associated with α growing over β, so that this sequence of events matches some of the features in the observed microstructures.

Layer boundaries that form at an angle to the growth axis can also be produced through the two routes mentioned above. If T_3 remains constant, an angled boundary results when V_X is in the same order of magnitude as V_{imp}. This situation implies that the liquid composition provides enough driving force for one phase to solidify in preference to the other, but not at a rapid rate. If T_3 drops somewhat, an angled boundary will result with α growing over β. If T_3 increases, V_Z will also increase. By similar reasoning as used previously, this increase in interface velocity will cause a temporary excess of solute [17], which can be accommodated by preferential growth of β over α.

For either solidification route, growth of one solid phase in preference to the other will slow and/or cease if the liquid composition near the three phase junction changes sufficiently. These changes in liquid composition could be related to perturbations or flows in the liquid near the interface, movement of the three phase junction through a lateral composition gradient in the liquid, or shifts in the solute redistribution ahead of the two solids. The compositional variations present on transverse sections of the 1.0, 1.2, and most likely the 1.4 wt.% Cd samples were apparently adequate at certain growth velocities to prevent complete domination of one solid phase over the other, which resulted in continuity for both solids in the growth direction. If one layer had completely covered the previous layer, then further layered growth would have been possible only by nucleation of the previous solid phase. This situation may have occurred in the 0.8 and 1.7 wt.% Cd samples for the minor phase, which appeared to be isolated. In the case where T_3 varies, the relative curvature of the two solids at the three phase junction should also change. For example, if T_3 is above the peritectic temperature, then α should be more curved than β, so that both solids are in equilibrium with liquid of the same composition. A decrease in T_3 would be accompanied by α growth over β and an increase in the curvature of β relative to α. Greater curvature could increase the effectiveness of solute dispersion, so that growth of β would be more competitive with α. This type of change would lead to slowing or stopping the solidification of α in preference to β. Another factor when T_3 varies is that the compositions of the phases at the three phase junction should also shift, which would alter the respective solute fluxes and redistribution. Finally, very low growth velocities seem to disrupt the competitive growth of α and β which produces oscillations in the position of the three phase junction. A 1.4 wt.% Cd sample directionally solidified at 1.0 μm/sec contained large aligned grains of α and β growing next to each other (see Table II). Apparently, solute was very effectively redistributed in the liquid ahead of the three phase junction at this growth velocity, so that the force acting on the junction was not sufficient to produce oscillations.

The results of this study do not prove conclusively whether the temperature at the three phase junction during layer formation remained constant, varied or showed each type of behavior in different regions. If the temperature varied, then the relative curvature of the solid phases should also change. The curvatures of α and β were not clear from the quenched interfaces; a more rapid quenching procedure might provide definitive information. Interface temperature, interface velocity, and liquid composition near the interface all clearly play a role in layer development. Any externally induced changes in these parameters should also affect the layers. Systematic variations in the growth conditions may be one way to gain a better understanding of the operative layer formation mechanisms.

Summary and Conclusions

1). For the Sn-Cd system under solidification conditions which produced no measurable longitudinal macrosegregation, the occurrence of oscillating peritectic microstructures and whether these oscillations were regular and repetitive depended upon both the alloy composition and the growth velocity . For a growth velocity of 3.8 μm/sec, regular layers were observed for alloy compositions of 1.0, 1.2, and 1.4 wt.% Cd, while some isolated layers formed for alloy compositions of 0.8 and 1.7 wt.% Cd. Layer formation became unfavorable between growth velocities of 3.8 and 6.8 μm/sec in 1.0 and 1.4 wt.% Cd samples as the solid-liquid interface changed from planar to cellular. Regular layer formation also ceased below growth velocities of 2.8 μm/sec for a 1.0 wt.% Cd alloy and 1.6 μm/sec for a 1.4 wt.% Cd alloy.

2). The regularly layered microstructures had certain features in common independent of alloy composition and growth velocity. The primary α phase and the peritectic β phase formed at a mutual interface with the liquid. Layers occurred on only a fraction of the rod cross sections, so that both solid phases were apparently continuous along the solidification axis. The compositions of the solids in the layers were approximately those of the respective phases at the peritectic temperature. Compositional variations were present on transverse sections, as demonstrated by the decreasing Cd content in the α phase going from the layered region to the radially adjacent single phase α region in a 1.0 wt.% Cd sample and by the increasing Cd content in the β phase going from the layered region to the radially adjacent single phase β region in a 1.4 wt.% Cd sample. These characteristics suggested that the same formation mechanism was producing the regular oscillations.

3). The layer wavelengths measured in the regular microstructures varied somewhat with alloy composition and growth velocity. Wavelengths decreased for growth velocities of 2.8 and 3.8 μm/sec as Cd content decreased from 1.4 to 1.0 wt.% Cd. For the 1.4 wt.% Cd samples, wavelengths varied approximately with the inverse square root of growth velocity.

4). The characteristics of the regularly oscillating microstructures are consistent with a formation mechanism based on competitive growth of the solid phases at a common interface with the liquid in the presence of sustained compositional variations on the sample cross sections. In this case, nucleation is not required for each successive layer. The layered regions are produced when the three phase junction between α, β, and liquid oscillates laterally during solidification due to imbalances between the solute fluxes in the liquid ahead of the two solids or due to other variations in the composition of the liquid near the interface. The shape of these

oscillations will be a function of the lateral velocity of the three phase junction and the vertical velocity of the junction relative to the imposed growth velocity, which will be linked to the temperature at the junction and the liquid composition in the vicinity of the solid-liquid interface. The relative values of these parameters and their relationship to the consequent layered microstructures were not clear from the experiments to date. For the microstructures with more isolated layers, nucleation would be necessary for oscillating peritectic growth if the minor phase was not continuous in three dimensions.

Acknowledgments

The authors would like to thank R. K. Trivedi of Ames Laboratory-U. S. Department of Energy and the Department of Materials Science and Engineering at Iowa State University for the use of equipment. J. T. Wheelock of the Materials Preparation Center at Ames Laboratory prepared the initial material. R. J. Hofer and C. A. Kamman (MPC) performed the compositional analyses. H. E. Sailsbury (MPC) was responsible for metallographic preparation of the samples and micrographs. A. Kracher of the Department of Geological and Atmospheric Sciences at Iowa State University conducted the electron microprobe analyses. This work was supported by the National Aeronautics and Space Administration under NASA Grant #NAG8-963 and was performed at Ames Laboratory. Ames Laboratory is operated for the U. S. Department of Energy by Iowa State University under contract No. W-7405-ENG-82.

References

1. N. J. W. Barker and A.Hellawell: *Met. Sci.*, 1974, vol. 8, pp. 353-356.
2. W. J. Boettinger: *Metall. Trans.*, 1974, vol. 5, pp. 2023-2031 .
3. A. P. Titchener and J. A. Spittle: *Acta Metall.*, 1975, vol. 23, pp. 497-502.
4. A. Ostrowski and E. W. Langer: in *Solidification and Casting of Metals*, The Metals Society, London, 1979, pp. 139-143.
5. H. D. Brody and S. A. David: in *Solidification and Casting of Metals*, The Metals Society, London, 1979, pp. 144-151.
6. D. J. Larson, R. G. Pirich, and W. R. Wilcox, Annual Report on Contract NAS8-32998, Marshall Space Flight Center, 1981.
7. B. C. Fuh: Ph.D. Dissertation, Iowa State University, Ames, IA, 1984.
8. B. F. Oliver and B. Kad: *J. Less-Common Met.*, 1991, vol. 168, pp. 81-90.
9. J. H. Lee and J. D. Verhoeven: *J. Cryst. Growth*, 1994, vol. 144, pp. 353-366.
10. J. W. Rutter, M. G. Julien, and G. R. Purdy: *Mater. Sci. and Technol.*, 1995, vol. 11, pp. 1233-1240.
11. K. L. Zeisler-Mashl and T. A. Lograsso: Accepted October 1996 for publication in *Metall. and Mater. Trans. A*.

12. M. Hillert: in *Solidification and Casting of Metals*, The Metals Society, London, 1979, pp. 81-87.

13. R. Trivedi: *Metall. and Mater. Trans. A*, 1995, vol. 26A, pp. 1583-1589.

14. J. Dutkiewicz, L. Zabdyr, Z. Moser, and J. Salawa: *Bull. Alloy Phase Diagrams*, 1989, vol. 10, pp. 223-229.

15. K. L. Zeisler-Mashl and T. A. Lograsso: *J. Phase Equilibria*, 1996, vol. 17, pp. 7-9.

16. J. T. Mason: *An Apparatus for Directional Solidification*, IS-4817, UC-37, 1982.

17. V. G. Smith, W. A. Tiller, and J. W. Rutter: *Can. J. Phys.*, vol. 33, pp. 723-745.

Table I. Description of Sn-Cd Samples Directionally Solidified at 3.8 μm/sec

Sample Number	Nominal Comp in Wt.% Cd (Meas. Comp.)	Fraction Solid	Interface Morphology	Phase Description from Longitudinal Section
27	0.8	0.6	Planar	α with some isolated β layers at edges
Test-2	1.0	0.3	No quench interface	Layers of α and β between α and β
31	1.0 (1.0)	0.5	Planar	Layers of α and β between α and β
33	1.0 (1.0)	0.5	Planar	Layers of α and β between α and β
32	1.2 (1.2)	0.5	Planar	Layers of α and β between α and β
11	1.4 (1.6)	0.5	Planar	α and β layers adjacent to β
14	1.4 (1.3)	0.4	Planar	α and β layers adjacent to β
15	1.4	1.0	No quench interface	α and β layers adjacent to β for first ≈50 mm
21	1.4 (1.4)	0.4	Planar	α and β layers adjacent to β
29	1.4	0.5	Planar	α and β layers adjacent to β
5	1.7 (Rod: 1.7)	0.6	Planar	β with some isolated α layers

Table II. Description of Sn-Cd Samples Directionally Solidified at Velocities Other Than 3.8 μm/sec

Sample Number	Nominal Comp in Wt.% Cd (Meas. Comp.)	Average Velocity (μm/sec)	G_L (°C/mm)	Fraction Solid	Interface Morph.	Phase Description from Long. Section
36	1.0 (1.0)	6.8	17.1	0.5	Cellular	Cellular α, intercellular β
34	1.0	2.8	17.0	0.5	Planar	Layers of α and β between α and β
35	1.0	1.6	16.9	0.7	Planar	α with some isolated β layers
17	1.4	6.8	17.1	0.5	Cellular	Cellular α, intercellular β
16	1.4	2.8	17.0	0.5	Planar	α and β layers adjacent to β
19	1.4	1.9	16.9	0.5	Planar	α and β layers adjacent to β
18	1.4	1.6	16.9	0.4	Planar	α and β layers adjacent to β
28	1.4	1.0	16.9	0.5	Planar	α and β, not layers

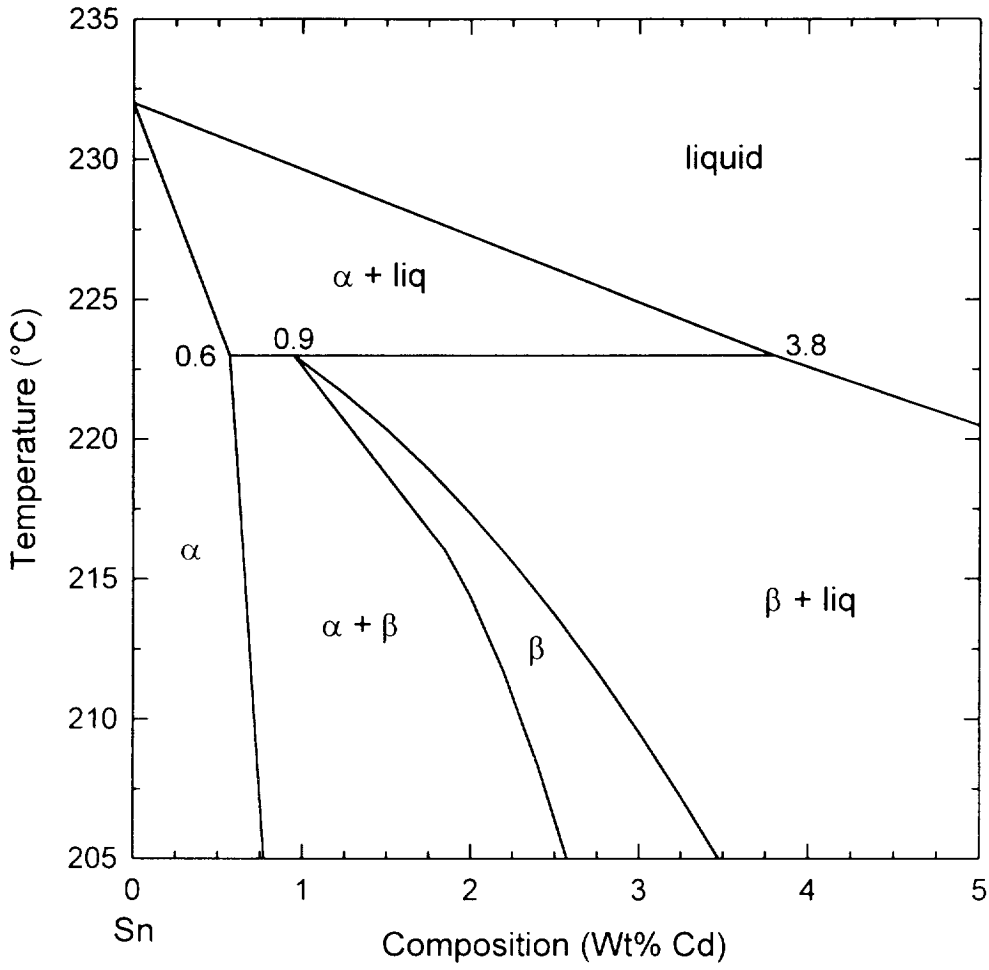

Figure 1. Section of the Sn-Cd phase diagram containing the peritectic reaction drawn from Reference 14.

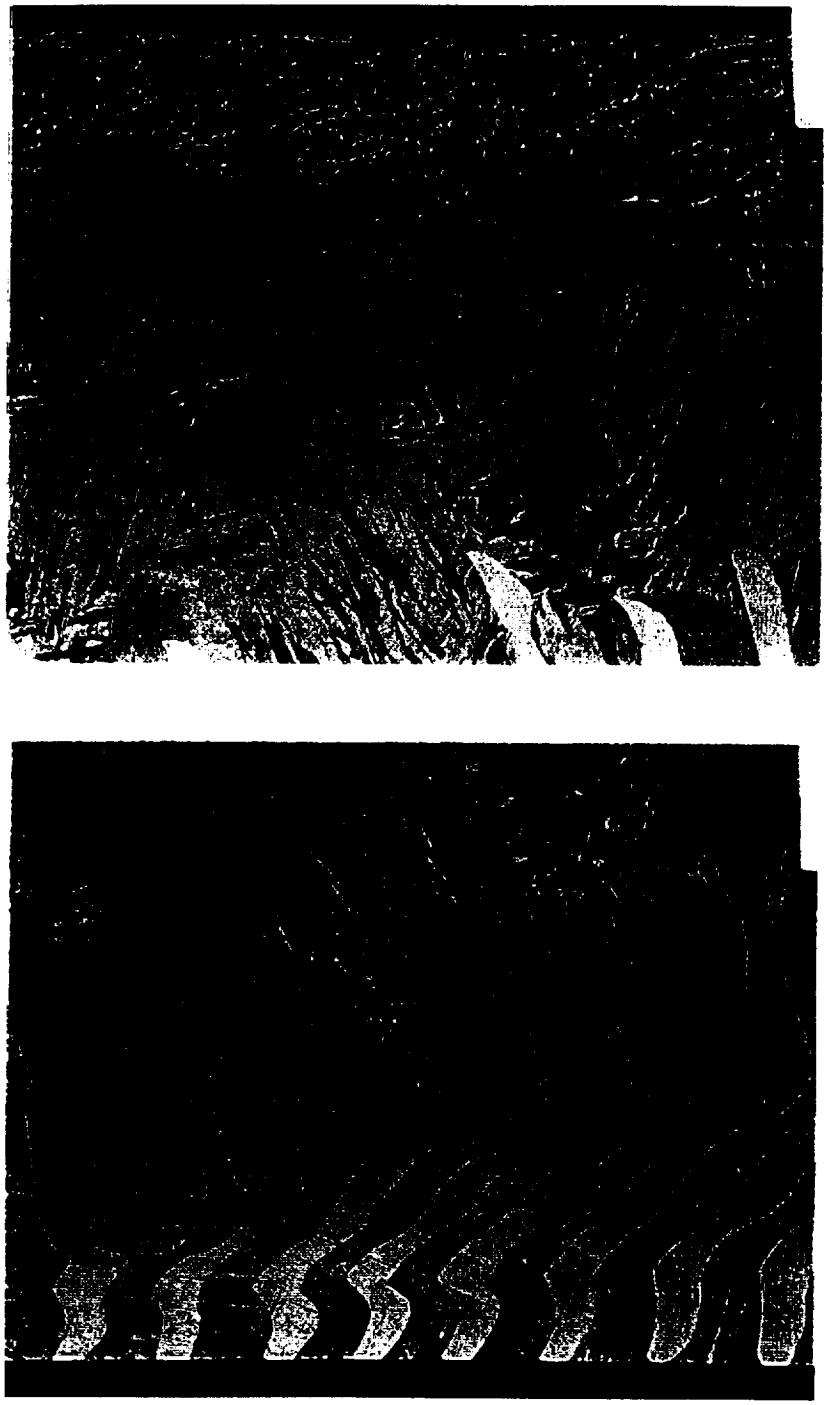

Figure 2. Optical micrographs of a longitudinal section near the center of a Sn-1.4 wt.% Cd rod directionally solidified at 3.8 μm/sec (Sample 29) showing the layered region. The light phase is α, and the mottled microconstituent is β which has transformed into a two-phase mixture during cooling. The micrographs are oriented so that the growth direction is left to right.

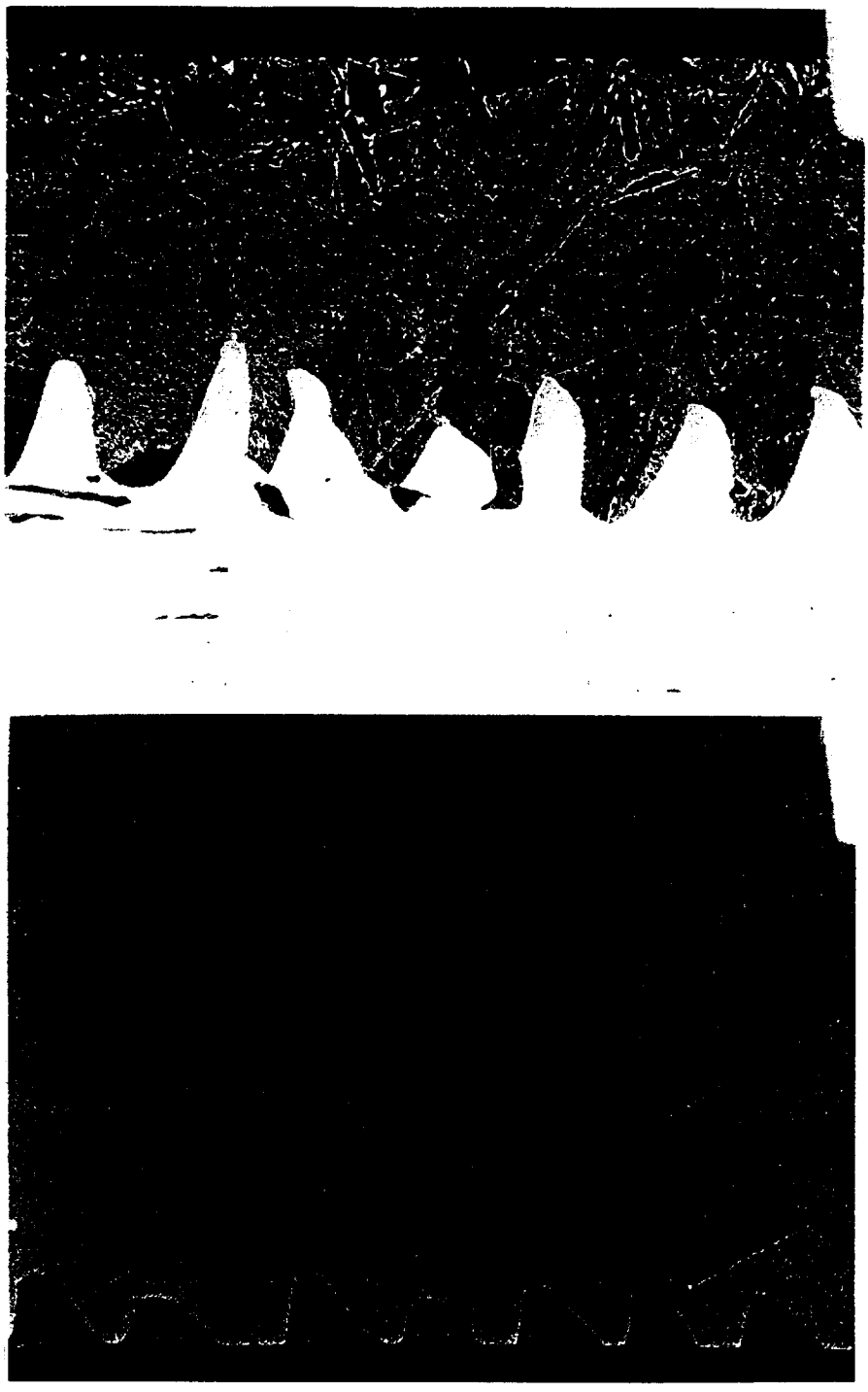

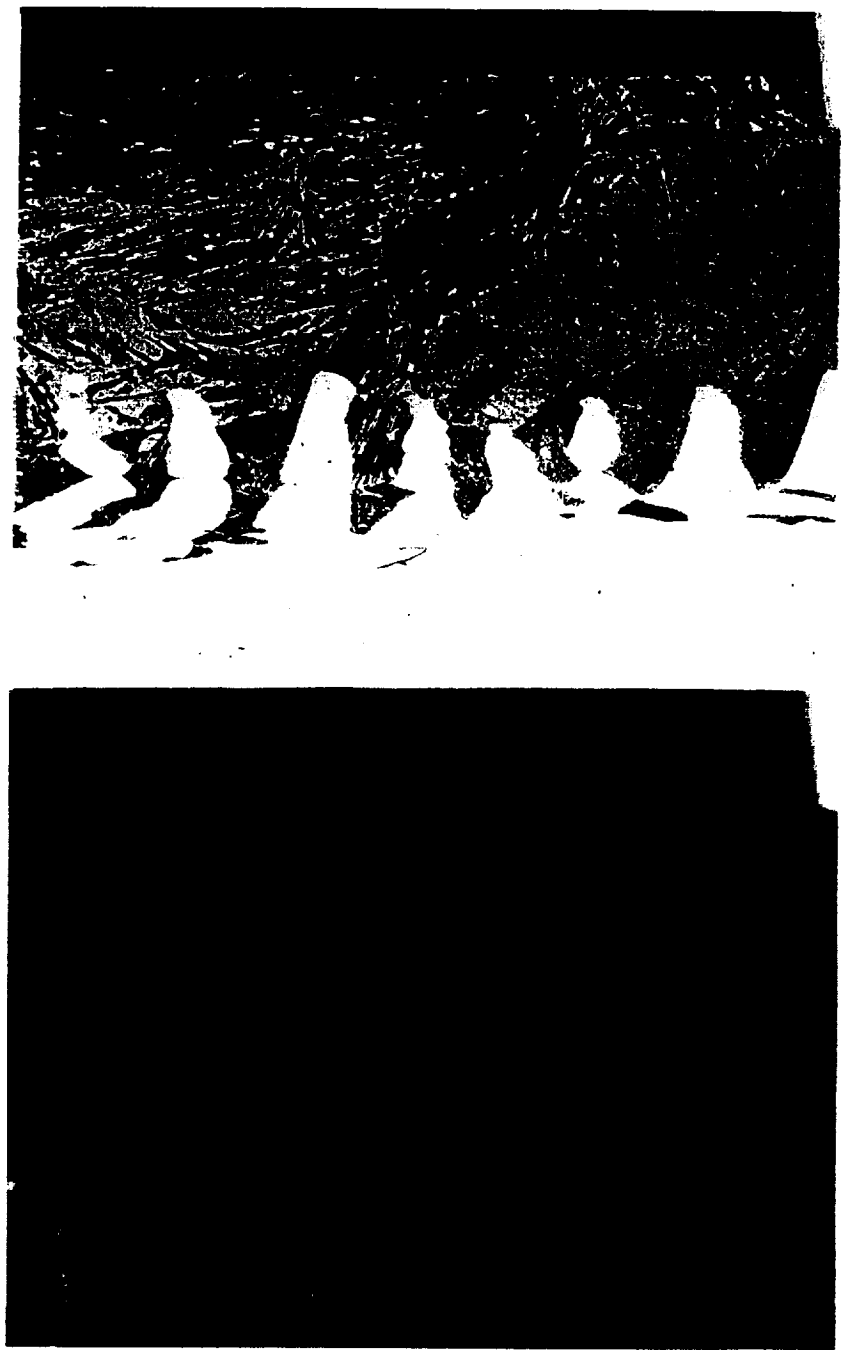

Figure 3. Optical micrographs of a longitudinal section near the center of a Sn-1.2 wt.% Cd rod directionally solidified at 3.8 μm/sec (Sample 32) showing the arrangement of phases in the layered regions. The growth direction is left to right.

Figure 4. Optical micrographs of a transverse section of a Sn-1.0 wt.% Cd rod directionally solidified at 3.8 μm/sec (Sample 33). The section is located approximately 35 mm from the start of directional solidification and 15 mm from the quenched interface.

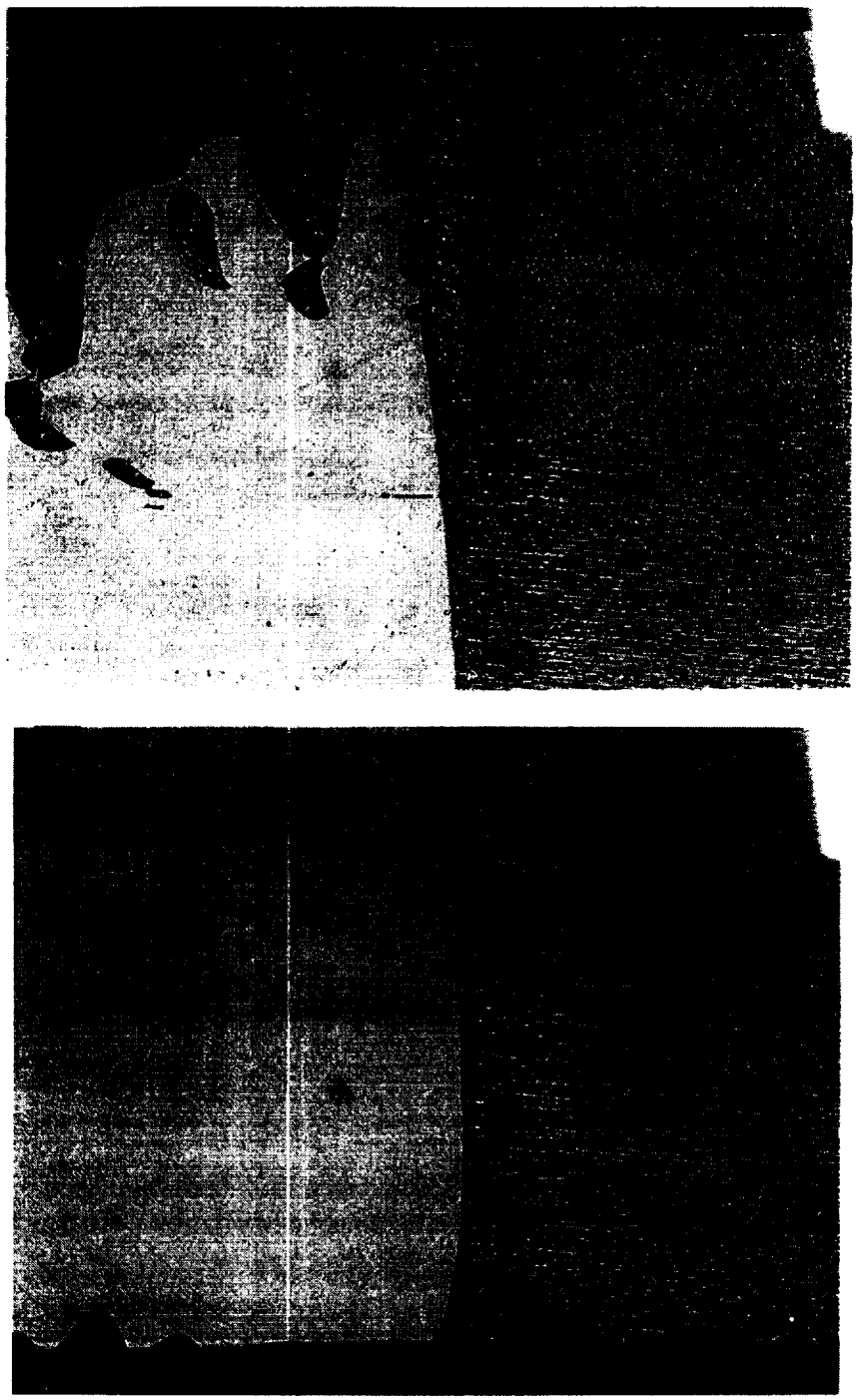

Figure 5. Optical micrographs of a longitudinal section near the center of a Sn-1.0 wt.% Cd rod directionally solidified at 3.8 μm/sec (Sample 33) showing the quenched interface in the layered region. The growth direction is left to right.

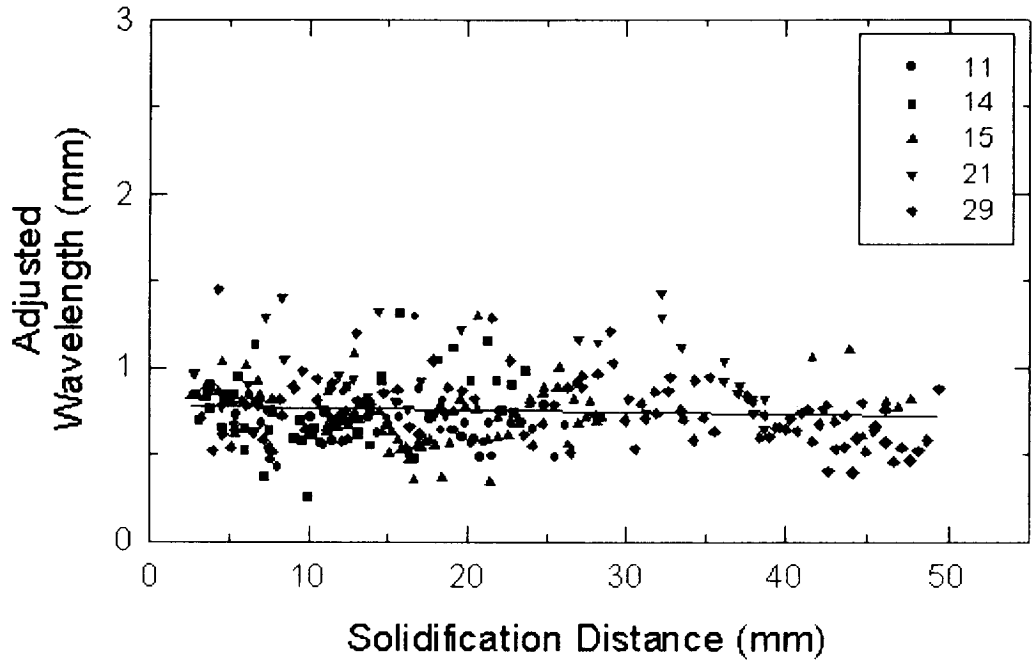

Figure 6. Adjusted layer wavelengths measured parallel to the growth direction for Sn-1.4 wt.% Cd samples directionally solidified at 3.8 μm/sec (Samples 11, 14, 15, 21, and 29) with a linear regression fit to the data.

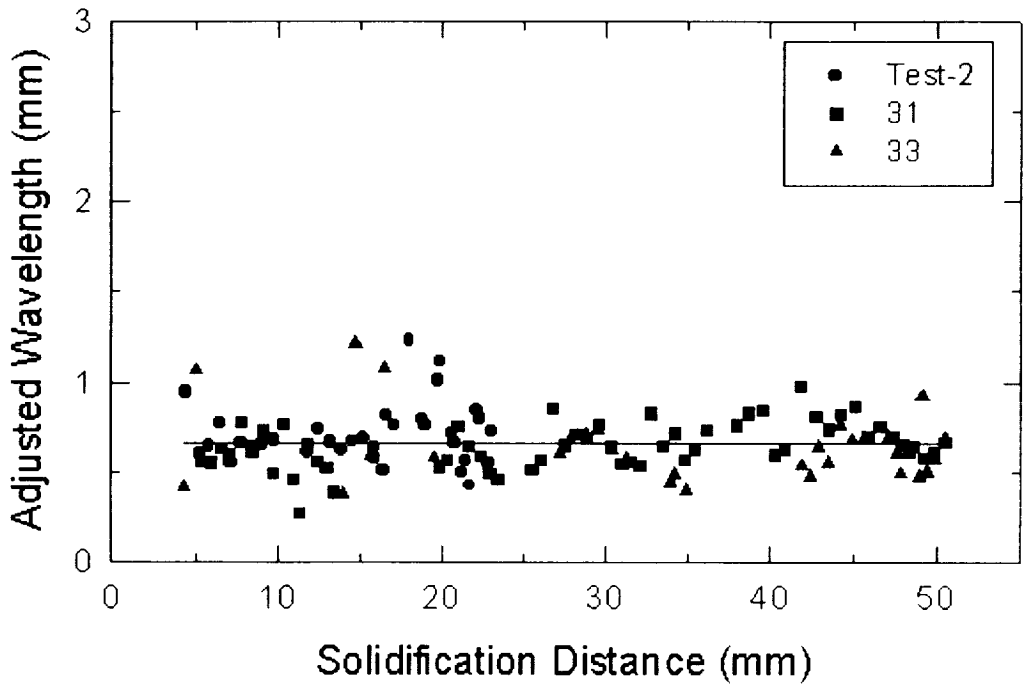

Figure 7. Adjusted layer wavelengths measured parallel to the growth direction for Sn-1.0 wt.% Cd samples directionally solidified at 3.8 μm/sec (Samples Test-2, 31, and 33) with a linear regression fit to the data.

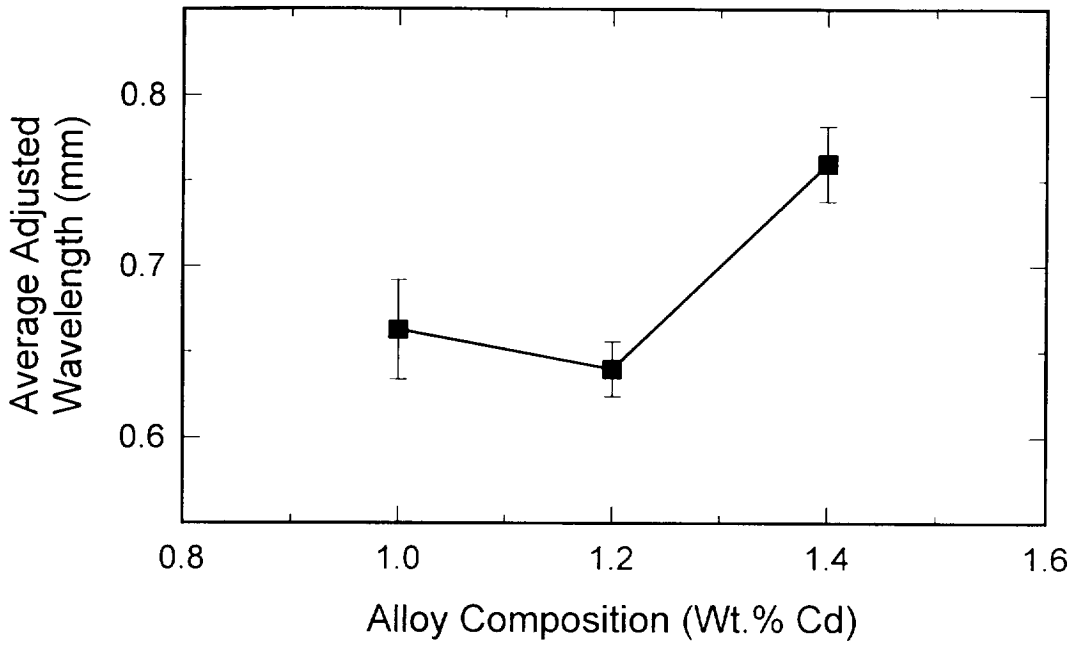

Figure 8. Average adjusted wavelengths as a function of alloy composition at a growth velocity of 3.8 μm/sec. Error bars represent 95% confidence limits.

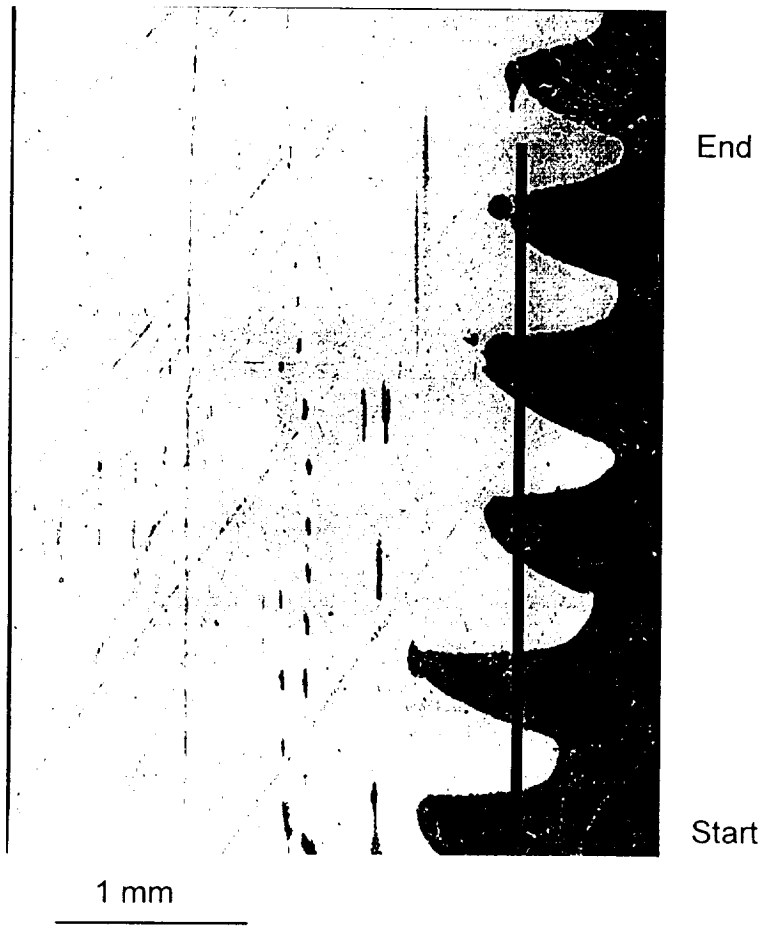

Figure 9. Optical micrographs of a longitudinal section near the center of a Sn-1.0 wt.% Cd rod directionally solidified at 3.8 μm/sec (Sample 31) showing a layered region in which phase compositions were measured. The right side of the montage is at the perimeter of the sample rod, while the left side is closer to the center of the rod. The growth direction is upward. The starting and ending points are marked for the compositional profile shown in Figure 10.

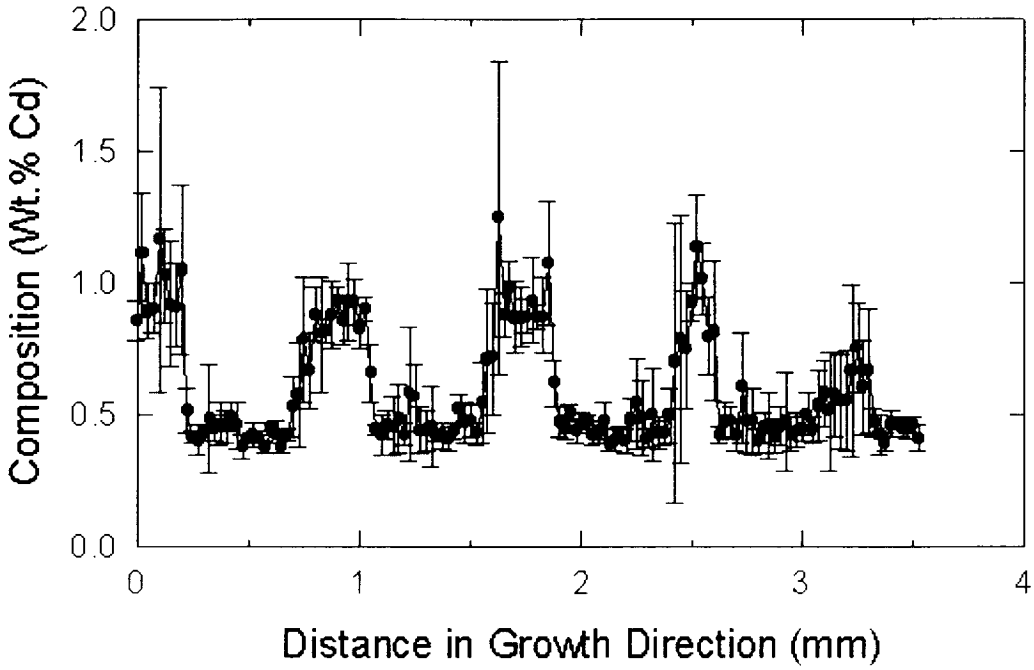

Figure 10. Compositional profile in the layered region obtained with an electron microprobe from a Sn-1.0 wt.% Cd sample directionally solidified at 3.8 μm/sec (see Sample 31 in Figure 9). Error bars represent 95% confidence limits.

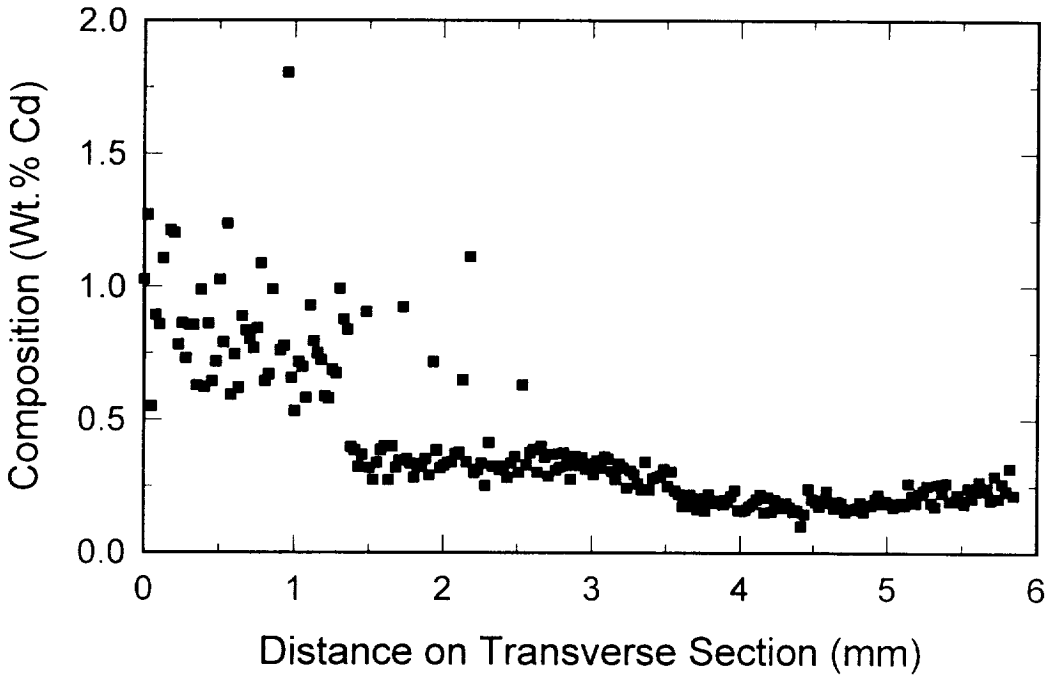

Figure 11. Compositional profile measured with an electron microprobe along a diameter of the transverse section given in Figure 4 for a Sn-1.0 wt.% Cd sample directionally solidified at 3.8 μm/sec (Sample 33). The profile starts in the β phase (higher Cd content) and progresses into the α phase.

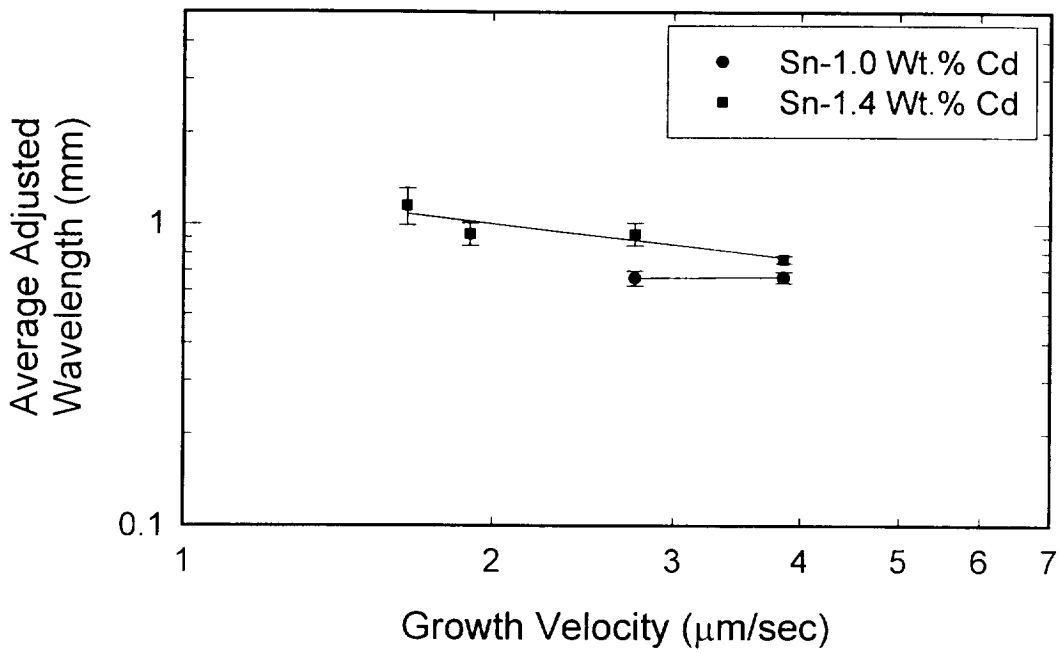

Figure 12. Average adjusted wavelengths as a function of growth velocity for the Sn-1.0 and -1.4 wt.% Cd alloys with linear regression fits to the data. Error bars represent 95% confidence limits.

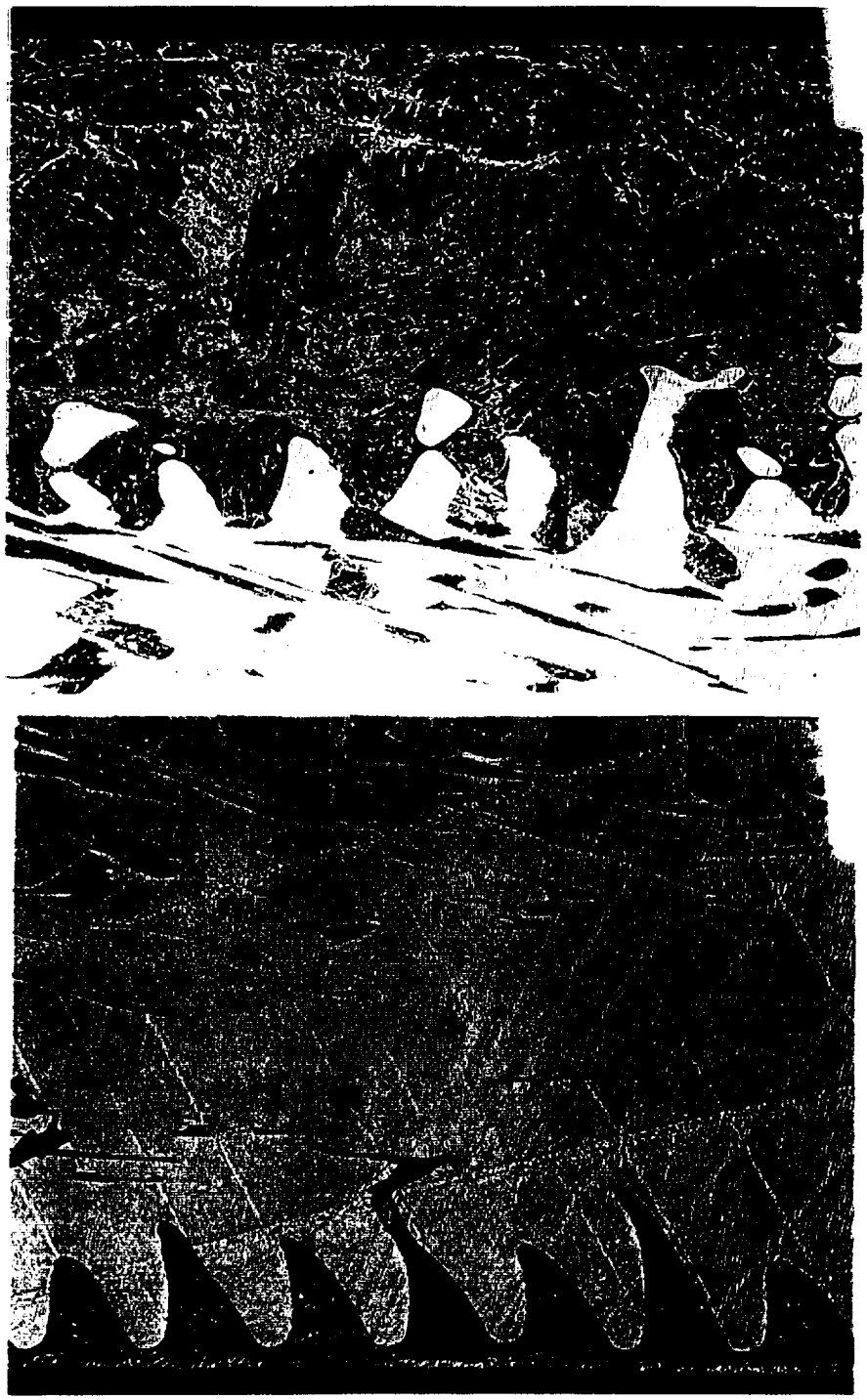

Figure 13. Optical micrographs of a longitudinal section near the center of a Sn-1.2 wt.% Cd rod directionally solidified at 3.8 μm/sec (Sample 32), showing layers that formed near the wall (left side of montage) and layers that formed closer to the center of the sample rod. The growth direction is upward.

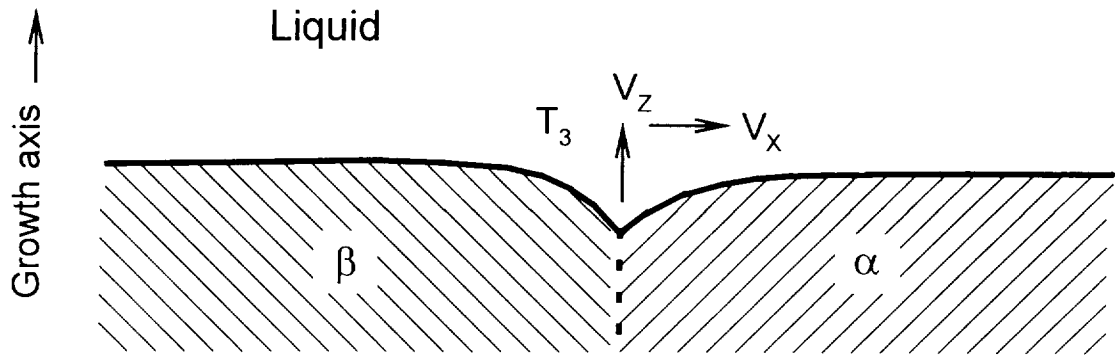

Figure 14. Schematic representation in two dimensions of the layered region near the three phase (α, β, and liquid) junction showing parameters specific to the junction: velocity in the x direction (V_x), velocity in the z direction (V_z), and temperature (T_3).

The Influence of Imposed Oscillations on the Formation of Layered Microstructures during Directional Solidification in Peritectic Systems

Introduction

The layered microstructures that can form in peritectic systems during plane front directional solidification are usually described as alternating layers of primary solid and peritectic solid oriented perpendicular to the growth direction. A variety of layer formation mechanisms have been proposed and cited, some based on factors inherent to directional solidification in the vicinity of the peritectic isotherm [1-10] and others based on perturbations to growth caused by external factors [11-13]. However, experimental work is still needed to elucidate the specific path of layer development during solidification for given cases and to separate intrinsic effects from disturbances in the growth conditions.

Recent research has focused on solidification of Sn-Cd alloys during whic

The Influence of Imposed Oscillations on the Formation of Layered Microstructures during Directional Solidification in Peritectic Systems

Introduction

The layered microstructures that can form in peritectic systems during plane front directional solidification are usually described as alternating layers of primary solid and peritectic solid oriented perpendicular to the growth direction. A variety of layer formation mechanisms have been proposed and cited, some based on factors inherent to directional solidification in the vicinity of the peritectic isotherm [1-10] and others based on perturbations to growth caused by external factors [11-13]. However, experimental work is still needed to elucidate the specific path of layer development during solidification for given cases and to separate intrinsic effects from disturbances in the growth conditions.

Recent research has focused on solidification of Sn-Cd alloys during which growth conditions were maintained at certain levels and external influences were minimized as much as possible [Sections III and IV and Reference 10]. For this alloy system in which longitudinal macrosegregation was not detected during solidification upward, the layered regions of the sample did not fill the entire sample cross section. As a consequence, the α phase and β phase were continuous in the three dimensional sample, so that nucleation was not required for each successive layer. The layered microstructures appeared to be consistent with oscillatory motion of the three phase junction between the primary solid, peritectic solid, and the liquid during solidification. This oscillatory motion could have been achieved by a lateral component to the velocity of the three phase junction in addition to the vertical component. The velocity of the three phase junction, both lateral and vertical, and the junction temperature are interrelated in a complex way through the imposed growth velocity and temperature gradient, the solute distribution in the liquid, and the corresponding phase equilibrium requirements. If the temperature of the three phase junction shifts, the vertical component of the junction velocity would vary from the imposed growth velocity, which would in turn affect the solute distribution in the liquid. The experimental results from the study of the Sn-Cd system could not confirm whether the temperature at the three phase junction remained constant or whether it varied. However, these results suggested that changing the junction temperature by external means could provide useful information about layer development. In order to better define the active layer formation mechanism and to examine the influence of external factors on layered microstructures, a complementary series of Sn-Cd alloys were directionally solidified with an oscillating furnace temperature.

Materials and Experimental Procedure

The Sn-Cd system was selected for the directional solidification experiments, partly because the solute element Cd is more dense in the liquid state than Sn, which should minimize density-driven convective flows when solidification occurs upward. Longitudinal macrosegregation was not detected at a growth velocity of 3.8 μm/sec in previously reported work [10]. The peritectic region of interest in the Sn-Cd phase diagram is shown in Figure 1. At

the peritectic temperature of 223°C, the compositions of the alloys studied (see Table I) fall between the primary α composition and the liquid composition. It should be noted that the peritectic β phase undergoes a eutectoid transformation during cooling to room temperature; the resultant two-phase mixture of α and (Cd) will be referred to as β for clarity.

Alloys rods were produced in 100 g batches by melting Sn and Cd of 99.99% purity in fused silica crucibles that were evacuated and back-filled with Ar (see Section III and Reference 10 for more procedural details). These rods were swaged to approximately 5 mm to fit into 6 mm ID fused silica crucibles for directional solidification. In the directional solidification apparatus (see Reference 15 for a complete description), samples are solidified upward by moving a furnace and cooling chamber assembly upward at the desired growth velocity relative to a stationary crucible under an Ar atmosphere. The temperature gradient in the liquid ahead of the solid-liquid interface was approximately 17°C/mm for these experiments. After rapidly solidifying for the first 20 mm of the sample rod to establish sufficient material in the cold zone for effective heat transfer, samples were directionally grown for at least 30 mm of the remaining 100 mm length followed by quenching to preserve the solid-liquid interface shape. For the samples listed in Table I, the solidification conditions employed were such that the solid-liquid interfaces were macroscopically flat and planar (see examples of quenched interfaces in Sections III and IV and Reference 10). Some of the samples were directionally solidified in the presence of externally induced temperature oscillations, which were produced by a non-optimized temperature controller on the furnace. The plot in Figure 2 shows these temperature oscillations as measured by a thermocouple placed in the liquid zone of a Sn-Cd sample not far from the solid-liquid interface when the furnace and cooling chamber assembly were stationary. The amplitude of the recorded temperature oscillation is on the order of 0.25°C, and the period is approximately 140 seconds.

After directional solidification, the composition of each alloy batch was measured from a slice of the unmelted section of the sample using inductively coupled plasma-atomic emission spectrometry (see Table I). The procedure determined Cd contents with 95% confidence limits of better than ±0.1 wt.% Cd. The directionally solidified portions of the sample rods were sectioned, mounted, ground, and polished using standard techniques and etched with a solution of 5% nitric acid in lactic acid. Layer wavelengths were measured from longitudinal sections near the rod centers along lines drawn parallel to the growth direction through the layered regions. To adjust these measurements for layers missing from a given longitudinal view, the wavelengths which were greater than twice the average were excluded from the data and the process iterated until the average remained unchanged. This process was usually repeated no more than once; all wavelengths reported in the results were checked following this procedure.

Results

The microstructures that formed in Sn-Cd alloys directionally solidified with an essentially constant furnace temperature are described in detail in Sections III and IV and Reference 10; the relevant points can be summarized as follows. Regularly layered microstructures were observed at a growth velocity of 3.8 μm/sec for alloy compositions of 1.0, 1.2, and 1.4 wt.% Cd (see Table I). Repetitive layers also formed for an alloy composition of 1.0

wt.% Cd at a growth velocity of 2.8 μm/sec and for an alloy composition of 1.4 wt.% Cd at growth velocities of 2.8, 1.9, and 1.6 μm/sec. For alloys with Cd levels lower than 1.0 wt.% Cd or greater than 1.4 wt.% Cd, regular layers were not observed. Growth velocities higher than 3.8 μm/sec precluded layer formation because the solid-liquid interface was no longer planar. Growth velocities lower than 2.8 μm/sec for 1.0 wt.% Cd samples and 1.6 μm/sec for 1.4 wt.% Cd samples had planar solid-liquid interfaces but also did not produce regularly layered microstructures.

The samples listed in Table I provide a direct comparison between microstructures solidified with a nearly constant furnace temperature and those solidified in conjunction with furnace temperature oscillations. The influence of these temperature oscillations is most clearly illustrated by samples which did not exhibit regular layer formation. For an alloy composition of 1.4 wt.% Cd, directional solidification at 1.0 μm/sec with a constant furnace temperature produced large aligned grains of α and β (see Sample 28 in Figure 3a); externally imposed temperature oscillations produced small, regularly spaced variations in the position of the α-β boundary (see Sample 22 in Figure 3b). For an alloy composition of 0.8 wt.% Cd, only isolated layers formed at a growth velocity of 3.8 μm/sec (Sample 27), whereas the same alloy produced regular layers under the influence of repeated temperature variations (Samples 23 and 26).

The effect of imposed temperature oscillations on the regularly layered microstructures produced at a growth velocity of 3.8 μm/sec was more subtle. In the 1.0 wt.% Cd samples solidified with a constant furnace temperature, the layers occurred as a narrow region of phase boundary oscillation between a region of α and a region of β (see Sample 31 in Figure 4a). In the presence of furnace temperature oscillations, the arrangement of the phases stayed the same, but the oscillatory pattern appeared more uniform over longer distances (see Sample 24 in Figure 4b). In the 1.4 wt.% Cd samples solidified with a relatively invariant furnace temperature, the layered regions were radially adjacent to β regions, so that the β phase was continuous (see Sample 29 in Figure 5a). While occasional α ligaments joined adjacent α layers, electron backscatter diffraction analyses indicated that orientations were repeated in adjacent α layers, which strongly suggested that the α phase was interconnected in three dimensions as well [10]. Under the influence of external temperature variations, the α layers showed a much greater degree of connectivity in a two dimensional section (see Sample 30 in Figure 5b). This greater continuity of α in the two dimensional view might indicate that the movement of the three phase junction was more restricted. In the case of the 1.2 wt.% Cd alloy, the microstructure developed through a constant furnace temperature resembled the 1.0 wt.% Cd samples, while the microstructure formed with furnace temperature oscillations looked similar to the 1.4 wt.% Cd alloy solidified under the same conditions. These differences may in part be a sectioning effect.

Some of these microstructural observations can be correlated with the measured wavelengths. The plots in Figure 6 show the wavelengths determined for 1.0 wt.% Cd samples solidified at 3.8 μm/sec with a constant furnace temperature (Sample 31) and in the presence of furnace temperature oscillations (Sample 24). The wavelengths for Sample 31 exhibit a greater spread of values than those for Sample 24; the standard deviation of the values for Sample 31 is 0.13 while the standard deviation for Sample 24 is 0.08. For the 1.4 wt.% Cd samples solidified at 3.8 μm/sec, the spread in the wavelength values as shown in the plots of Figure 7 was not affected significantly by the induced temperature oscillations; the standard deviations are 0.19

and 0.18 for Samples 29 and 30, respectively. The apparent change in the arrangement of phases for this alloy composition caused by the furnace temperature variations could not be detected in the measured wavelength values. Comparing Figure 6 and 7, the arrangement of phases in the higher Cd alloy produced a much greater range of measured wavelengths than in the lower Cd alloy.

The average adjusted wavelengths as a function of alloy composition at a growth velocity of 3.8 μm/sec are shown in Figure 8 for the cases of the nearly constant furnace temperature and the regularly varying furnace temperature. In both cases, the wavelength increased somewhat as the Cd content increased. From the 95% confidence limits, the values at an alloy composition of 1.4 wt.% Cd are the same for the two temperature conditions, and the wavelengths for the 1.0 and the 1.2 wt.% Cd alloys are only slightly different. An average oscillation period can be calculated for each average wavelength using the growth velocity; these numbers are reported in Table II. While the period for the 0.8 wt.% Cd alloy is close to the furnace temperature oscillation period of 140 sec, all of the calculated values are greater than the measured temperature periodicity.

Discussion

This comparison of Sn-Cd samples directionally solidified with a nearly constant furnace temperature with samples grown with an oscillating furnace temperature provides a measure of the degree to which the external variations can affect the intrinsic phase oscillations. Changing the furnace temperature should alter the temperature gradient in the liquid and the temperature at the position of the solid-liquid interface. This shift would provide a driving force for the interface to change its relative position, which would in turn change the interface velocity and the solute distribution in the liquid ahead of the interface. The magnitude of these changes will depend upon the amplitude and period of the imposed oscillations with respect to the inherent oscillations. The amplitude of the temperature swings from the non-optimized controller was no greater than 0.25°C, while the period was approximately 140 sec. The amplitude of any inherent temperature changes was not determined, and the period of inherent layer formation varied with alloy composition but was greater than 140 sec for the cases listed in Table II. When the intrinsic tendency to form regular layers was not strong, the externally imposed temperature oscillations dominated layer formation. This type of relationship was observed in the 0.8 wt.% Cd samples grown at 3.8 μm/sec (Samples 23, 26, and 27) and the 1.4 wt.% Cd samples grown at 1.0 μm/sec (Samples 22 and 28). The period calculated for Sample 27 was 150 sec, the value closest to that of the imposed temperature oscillations. When the intrinsic tendency to form regular layers was strong, the externally imposed temperature oscillations merely exerted a small influence on layer formation. In this case, the layer periodicity was not affected to a significant degree by the external temperature variations. However, the spread of measured layer spacings in the lower Cd samples appeared to be reduced, and the α phase appeared to be more connected in the higher Cd samples, which suggested that the temperature oscillations were limiting the range of movement of the three phase junction.

These results show that the externally induced temperature variations could couple with the intrinsic phase oscillations, indicating that temperature changes can play a part in layer

formation. The extent to which the interface temperature varies in inherent layer development is still not clear. A quenched interface from one of the samples grown with furnace temperature oscillations (Sample 24) is shown in Figure 9. In this particular instance, the curved β phase is clearly ahead of and growing over the α phase. The quenched interfaces observed in samples grown with a constant furnace temperature did not show such a pronounced difference in position or curvature between the two solids at the three phase junction (see examples in Sections III and IV and Reference 10). These differences in the appearance of the three phase junction most likely indicate a modified driving force or a change in the magnitude of the driving force for layer formation between the two furnace temperature conditions. Cyclic or step changes in imposed growth velocity should also affect layer formation and might be easier to put into practice and to interpret. An important point emphasized by the results of this study is the need to monitor growth parameters such as temperature in the hot zone and cold zone and smoothness of motion. If variations or perturbations fall into a certain amplitude and frequency range, they may alter layer formation, possibly in a fairly subtle manner. Changes in layered microstructures are difficult to discern unless a regular arrangement has first been achieved to serve as a basis for comparison.

Summary

This study compared the layered microstructures that formed in Sn-Cd alloys directionally solidified with a nearly constant furnace temperature with those that formed in conjunction with an oscillating furnace temperature. The amplitude and periodicity of the temperature oscillations were such that they coupled with the inherent phase oscillations, which suggests that temperature variations could be a part of intrinsic layer development. The externally induced temperature variations dominated the layer formation when the inherent tendency to form regular layers was low and appeared to affect the extent of the three phase junction motion when the inherent tendency to form regular layers was strong. Viewed from the opposite standpoint, these results indicate that layer formation in systems where longitudinal macrosegregation is not significant can be quite sensitive to variations in growth conditions or to external perturbations.

Acknowledgments

The authors would like to thank R. Trivedi of Ames Laboratory-U. S. Department of Energy and the Department of Materials Science and Engineering at Iowa State University for the use of equipment. J. T. Wheelock of the Materials Preparation Center at Ames Laboratory prepared the initial Sn-Cd rods. R. J. Hofer and C. A. Kamman (MPC) performed the compositional analyses. H. E. Sailsbury (MPC) was responsible for metallographic preparation of the samples and micrographs. This work was supported by the National Aeronautics and Space Administration under NASA Grant #NAG8-963 and was performed at Ames Laboratory. Ames Laboratory is operated for the U. S. Department of Energy by Iowa State University under contract No. W-7405-ENG-82.

References

1. W. J. Boettinger: *Metall. Trans.*, 1974, vol. 5, pp. 2023-2031 .
2. A. P. Titchener and J. A. Spittle: *Acta Metall.*, 1975, vol. 23, pp. 497-502.
3. H. D. Brody and S. A. David: in *Solidification and Casting of Metals*, The Metals Society, London, 1979, pp. 144-151.
4. M. Hillert: in *Solidification and Casting of Metals*, The Metals Society, London, 1979, pp. 81-87.
5. D. J. Larson, R. G. Pirich, and W. R. Wilcox, Annual Report on Contract NAS8-32998, Marshall Space Flight Center, 1981.
6. B. C. Fuh: Ph.D. Dissertation, Iowa State University, Ames, IA, 1984.
7. B. F. Oliver and B. Kad: *J. Less-Common Met.*, 1991, vol. 168, pp. 81-90.
8. J. H. Lee and J. D. Verhoeven: *J. Cryst. Growth*, 1994, vol. 144, pp. 353-366.
9. R. Trivedi: *Metall. and Mater. Trans. A*, 1995, vol. 26A, pp. 1583-1589.
10. K. L. Zeisler-Mashl and T. A. Lograsso: Accepted October 1996 for publication in *Metall. and Mater. Trans. A*.
11. N. J. W. Barker and A.Hellawell: *Met. Sci.*, 1974, vol. 8, pp. 353-356.
12. A. Ostrowski and E. W. Langer: in *Solidification and Casting of Metals*, The Metals Society, London, 1979, pp. 139-143.
13. J. W. Rutter, M. G. Julien, and G. R. Purdy: *Mater. Sci. and Technol.*, 1995, vol. 11, pp. 1233-1240.
14. J. Dutkiewicz, L. Zabdyr, Z. Moser, and J. Salawa: *Bull. Alloy Phase Diagrams*, 1989, vol. 10, pp. 223-229.
15. J. T. Mason: *An Apparatus for Directional Solidification*, IS-4817, UC-37, 1982.

Table I. Description of Directionally Solidified Sn-Cd Samples

Sample Number	Nominal Comp in Wt.% Cd (Meas. Comp.)	Average Velocity (μm/sec)	Fraction Solid	Phase Description from Longitudinal Section
• 23	0.8	3.8	0.5	Layers of α and β between α and β
• 26	0.8 (0.8)	3.8	1.0	Layers of α and β between α and β
27	0.8	3.8	0.6	α with some isolated β layers at edges
• 24	1.0 (1.0)	3.8	0.6	Layers of α and β between α and β
• Test-1	1.0	3.8	0.3	Layers of α and β between α and β
Test-2	1.0	3.8	0.3	Layers of α and β between α and β
31	1.0 (1.0)	3.8	0.5	Layers of α and β between α and β
33	1.0 (1.0)	3.8	0.5	Layers of α and β between α and β
• 25	1.2	3.8	0.6	Layers of α and β between α and β
32	1.2 (1.2)	3.8	0.5	Layers of α and β between α and β
• 22	1.4	1.0	0.5	α and β with sinusoidal boundary
28	1.4	1.0	0.5	α and β, not layers
• 30	1.4 (1.4)	3.8	0.6	α and β layers adjacent to β
11	1.4 (1.6)	3.8	0.5	α and β layers adjacent to β
14	1.4 (1.3)	3.8	0.4	α and β layers adjacent to β
15	1.4	3.8	1.0	α and β layers adjacent to β for first ≈50 mm
21	1.4 (1.4)	3.8	0.4	α and β layers adjacent to β
29	1.4	3.8	0.5	α and β layers adjacent to β

- Samples which were directionally solidified with furnace temperature oscillations

Table II. Oscillation Periods Calculated for Layered Samples Grown at 3.8 μm/sec

Alloy Composition (Wt.% Cd)	Period with Constant Furnace Temp. (sec)	Period with Varying Furnace Temp. (sec)
0.8	---	150
1.0	170	160
1.2	170	180
1.4	200	200

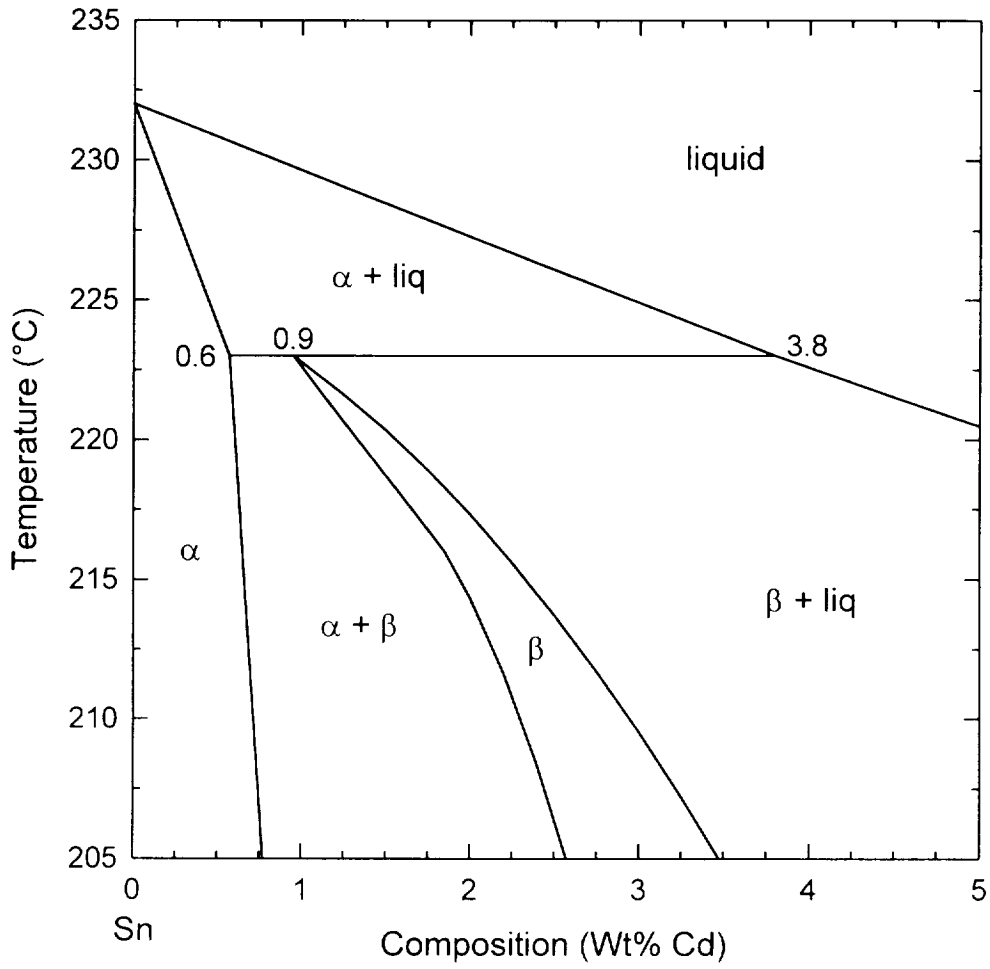

Figure 1. Section of the Sn-Cd phase diagram containing the peritectic reaction drawn from Reference 14.

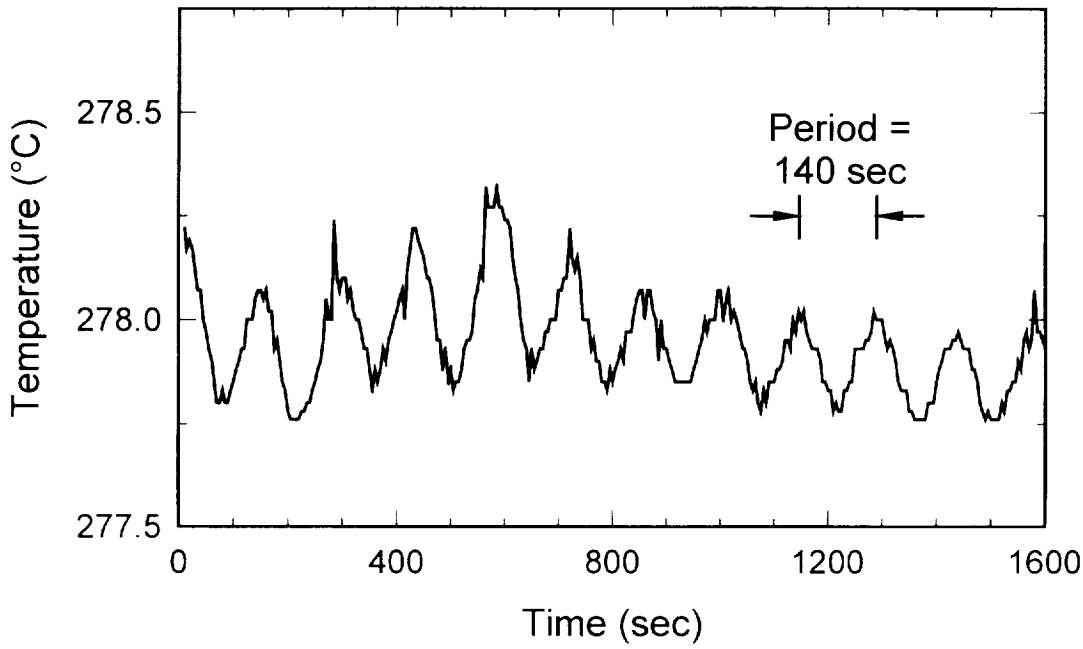

Figure 2. Temperature oscillations produced by a non-optimized temperature controller on the furnace and measured by a thermocouple immersed in a Sn-Cd sample at a growth velocity of zero.

a)

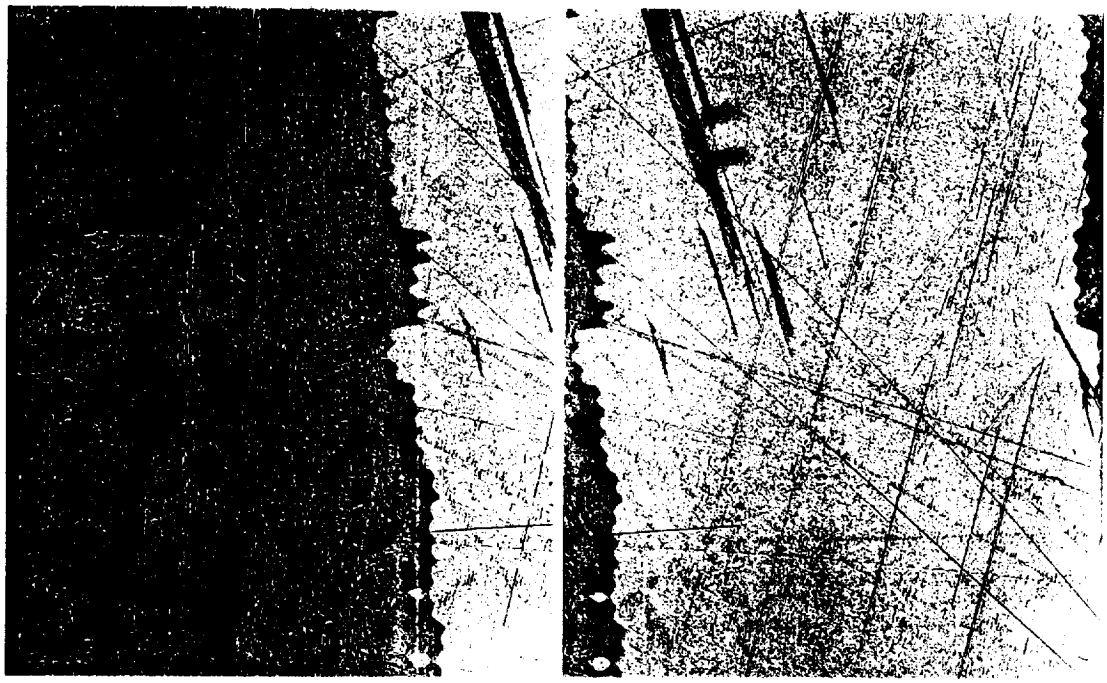

b)

Figure 3. Optical micrographs of longitudinal sections near the centers of Sn-1.4 wt.% Cd rods directionally solidified at 1.0 μm/sec, showing the arrangement of phases which developed a) with a nearly constant furnace temperature in Sample 28 and b) with repetitive variations in the furnace temperature in Sample 22. The light phase is α, and the mottled microconstituent is β which has transformed into a two-phase mixture during cooling. The micrographs are oriented so that the growth direction is upward.

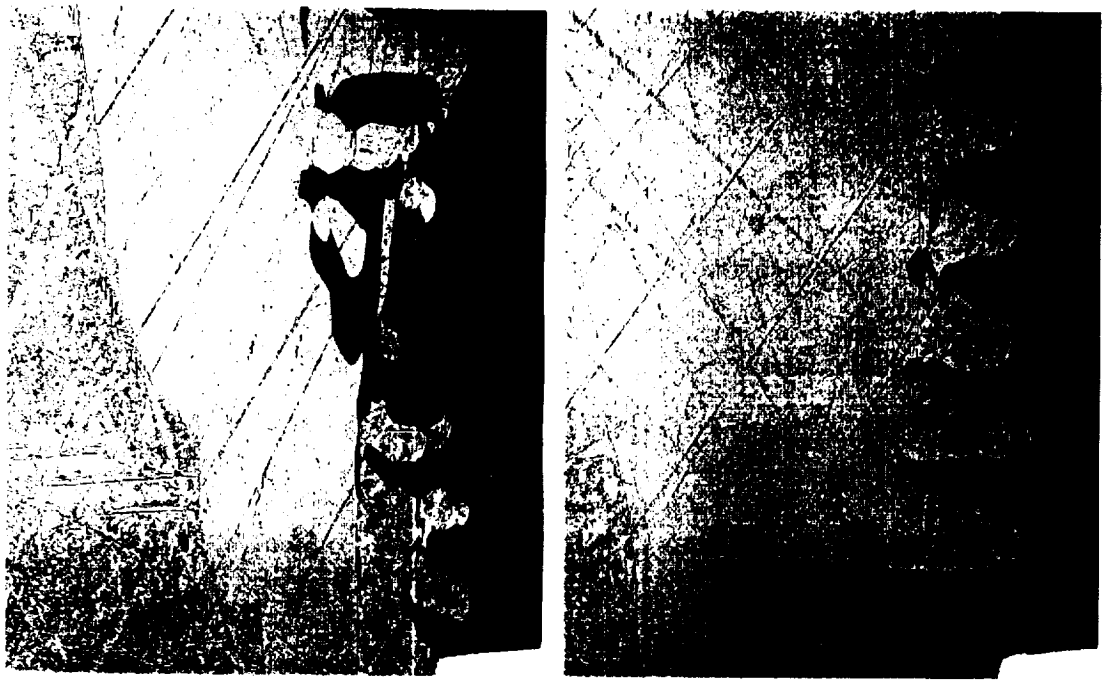

a)

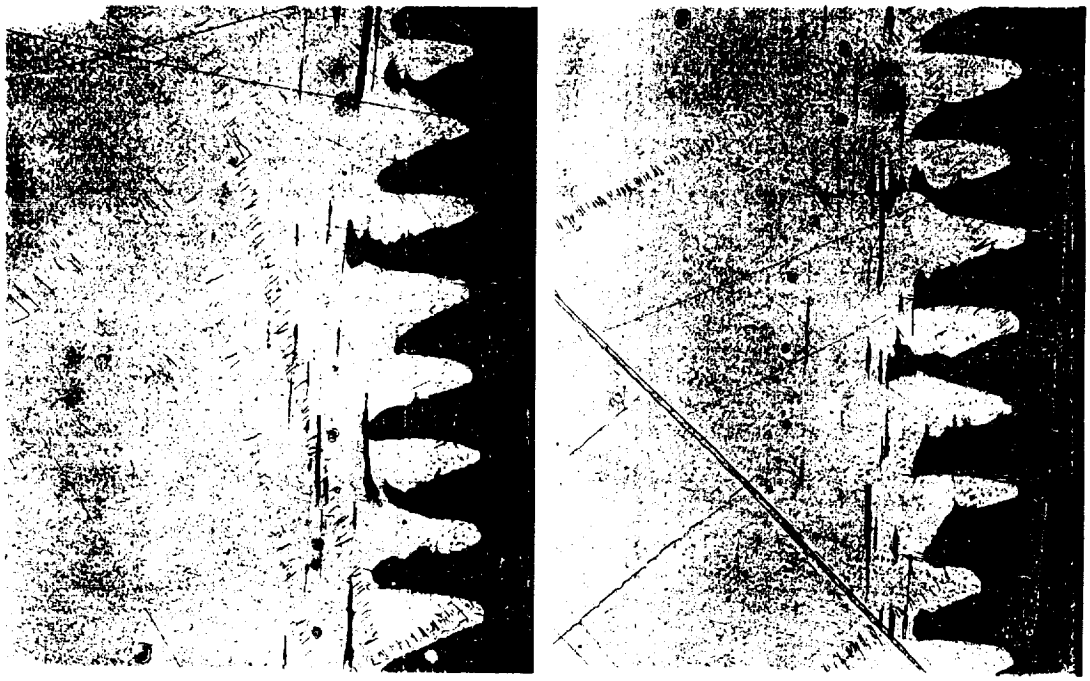

b)

Figure 4. Optical micrographs of longitudinal sections near the centers of Sn-1.0 wt.% Cd rods directionally solidified at 3.8 μm/sec, showing the arrangement of phases which developed a) with a nearly constant furnace temperature in Sample 31 and b) with repetitive variations in the furnace temperature in Sample 24. The growth direction is upward.

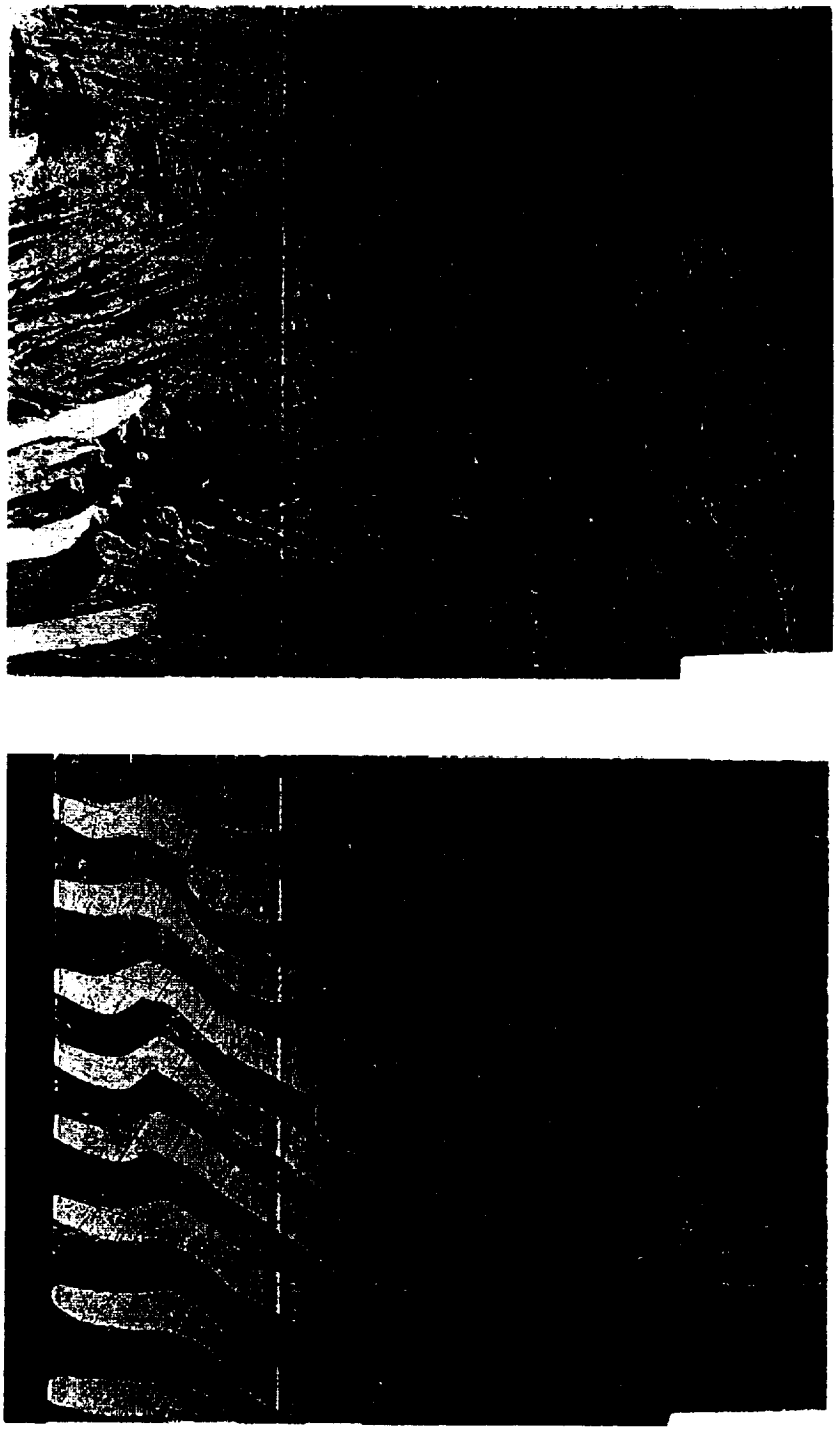

a)

Figure 5. Optical micrographs of longitudinal sections near the centers of Sn-1.4 wt.% Cd rods directionally solidified at 3.8 μm/sec, showing the arrangement of phases which developed a) with a nearly constant furnace temperature in Sample 29 and b) with repetitive variations in the furnace temperature in Sample 30. The growth direction is upward.

Figure 5. (continued)

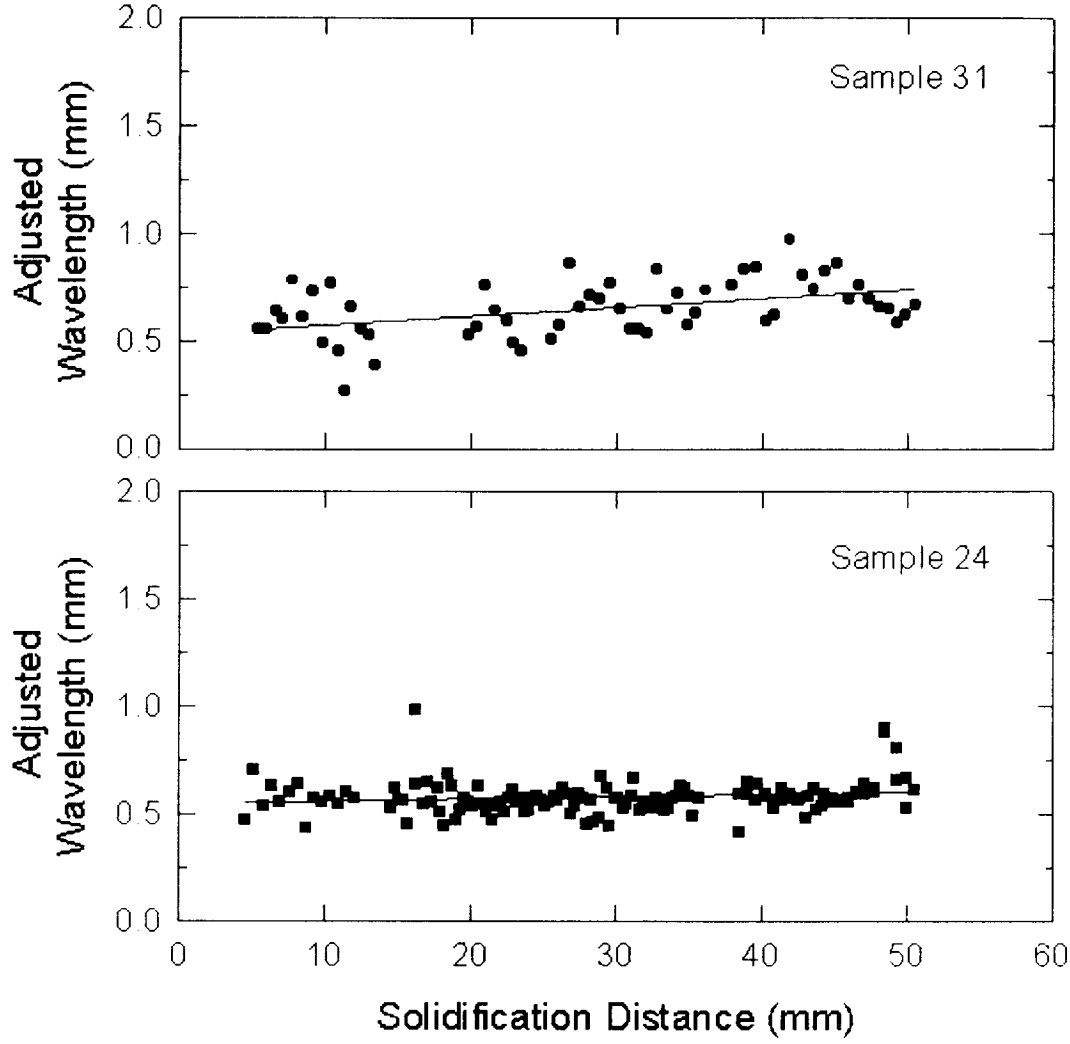

Figure 6. Adjusted layer wavelengths measured parallel to the growth direction for Sn-1.0 wt.% Cd samples directionally solidified at 3.8 μm/sec with a linear regression fit to the data. Sample 31 was grown with a nearly constant furnace temperature, and Sample 24 was grown with an oscillating furnace temperature.

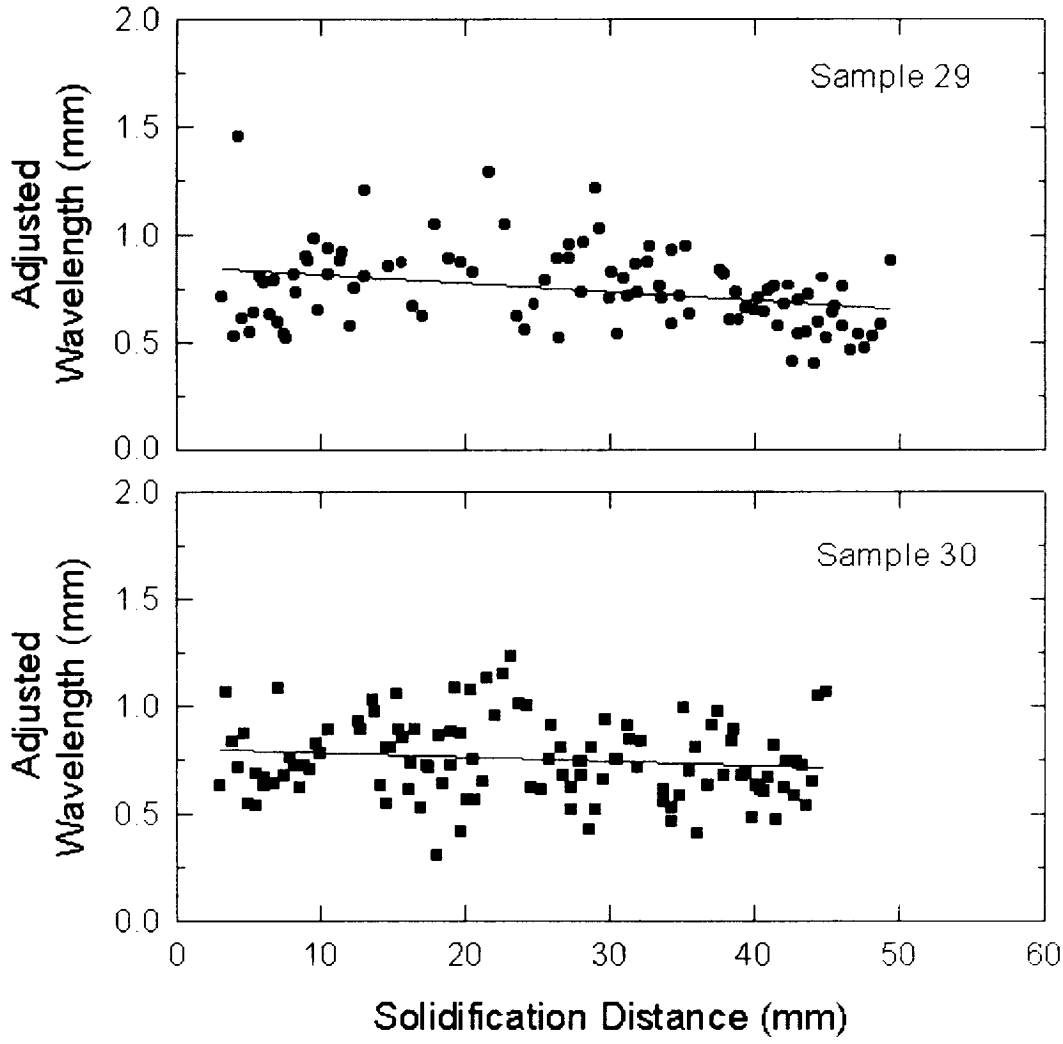

Figure 7. Adjusted layer wavelengths measured parallel to the growth direction for Sn-1.4 wt.% Cd samples directionally solidified at 3.8 μm/sec with a linear regression fit to the data. Sample 29 was grown with a nearly constant furnace temperature, and Sample 30 was grown with an oscillating furnace temperature.

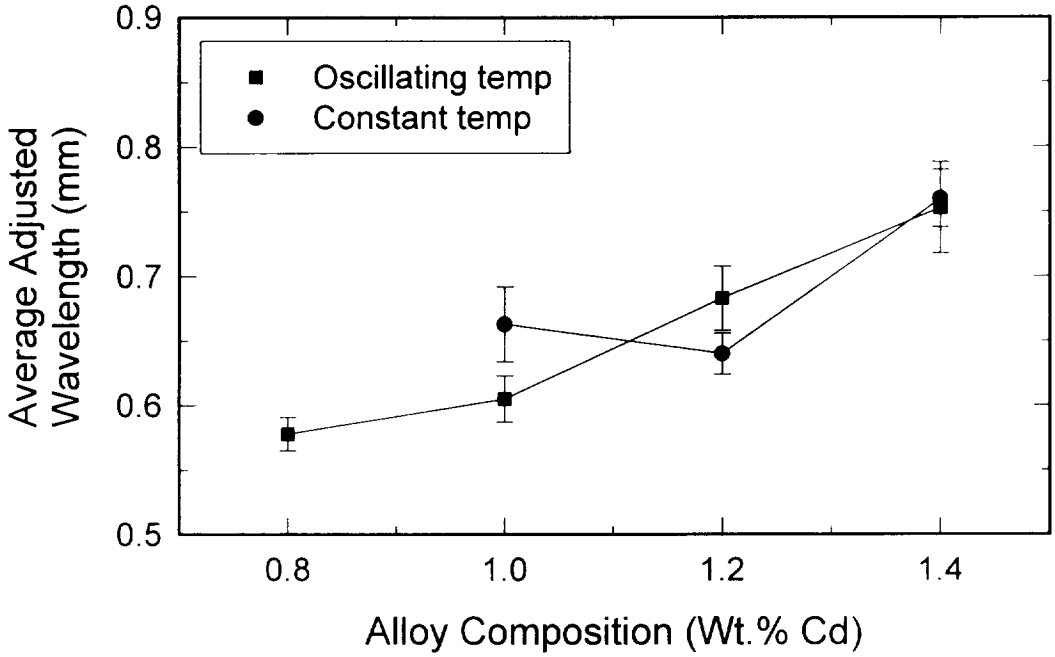

Figure 8. Average adjusted wavelengths as a function of alloy composition at a growth velocity of 3.8 μm/sec for a nearly constant furnace temperature and for a regularly varying furnace temperature. Error bars represent 95% confidence limits.

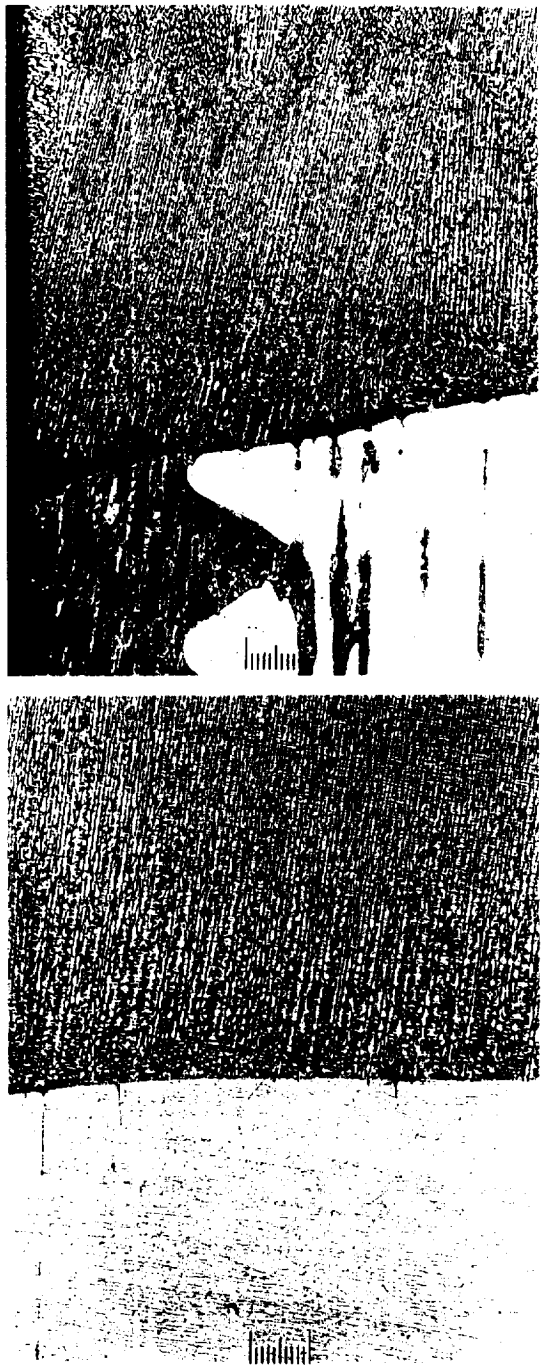

Figure 9. Optical micrographs of a longitudinal section near the center of a Sn-1.0 wt.% Cd rod that was directionally solidified at 3.8 μm/sec with an oscillating furnace temperature (Sample 24), showing the quenched interface.